

TA7

C6

CER 69/70/1A

COPY 2

UNSTEADY FLOW IN A STORM  
DRAINAGE SYSTEM

Engineering Sciences

FEB 5 1980

Branch Library

Part A  
THEORY AND ERROR CONSIDERATIONS

A. H. Barnes

U. S. Bureau of Public Roads  
Contract No. CPR-11-3584

Colorado State University  
Engineering Research Center  
June 1969

CER69-70AB1A

## TABLE OF CONTENTS

<u>Chapter</u>		<u>Page</u>
I	INTRODUCTION . . . . .	1
II	THEORETICAL CONSIDERATIONS . . . . .	5
III	GEOMETRIC RELATIONSHIPS . . . . .	18
IV	METHODS OF SOLUTION . . . . .	42
V	COMPUTER SOLUTION . . . . .	58
VI	EFFECT OF VARIATIONS IN COMPUTATIONAL PARAMETERS . . . . .	77
VII	EFFECTS OF HYDRAULIC PARAMETERS ON THE COMPUTED HYDROGRAPH . . . . .	87

## LIST OF FIGURES

<u>Figure</u>		<u>Page</u>
1	Continuity relationship definition sketch . . . . .	6
2	Unsteady - flow relationship definition sketch . . . . .	9
3	Circular cross-section parameters definition sketch . . . . .	19
4	Geometry of the circular cross-section variation with depth . . . . .	21
5	Geometry of circular cross-section relative error in parameter versus relative error in depth . . . . .	24
6	Relationship of circular and elliptical cross-sections definition sketch . . . . .	25
7	Percent difference in area versus eccentricity and depth . . . . .	27
8	Percent error in area at 0.2 x dia. depth for physical pipe . . . . .	31
9	Effect of bottom irregularities definition sketch . . . . .	34
10	A(x,t) plane in which the solutions along $\xi_+$ and $\xi_-$ are initially known . .	47
11	Network of characteristics by the method of grids of characteristics . . . . .	59
12	Network of characteristics by the method of specified intervals . . . . .	61
13	Rectangular grid for the solution by the method of specified intervals $\Delta t$ and $\Delta x$ .	64
14	Hypothetical inflow hydrograph . . . . .	70
15	Upstream boundary conditions . . . . .	72
16	Downstream boundary conditions . . . . .	74
17	Effect of $\Delta x$ on hydrographs at various positions along the channel: (1) $\Delta x = 40.91'$ , (2) $\Delta x = 20.45'$ (3) $\Delta x = 10.23'$ , (4) $\Delta x = 5.12'$ . . . . .	80



U18401 0575316

LIST OF FIGURES - (Continued)

<u>Figure</u>		<u>Page</u>
18	Relationship between $N$ and $x$ and time required for CDC 6600 computer . . .	82
19	Characteristics of depth-hydrograph . . . . .	83
20	Effect of friction coefficient, $f$ , at various positions along the channel (1) $f = 0.010$ , (2) $f = 0.012$ , (3) $f =$ $0.014$ , (4) $f = f(R_e)$ . . . . .	89

LIST OF TABLES

<u>Table</u>		<u>Page</u>
1	Physical pipe geometry . . . . .	29
2	Theoretical effect of bottom irregularity on water surface profile . . . . .	38
3	Physical pipe slope deviations . . . . .	41
4	Difference in $D_{PK}$ computed from various sizes of $\Delta x$ (in percent of channel diameter). . . . .	85
5	Difference in $T_{PK}$ computed from various sizes of $\Delta x$ (in percent of $t_p$ ) . . . . .	85
6	$D_{PK}$ /channel diameter, in percent along the channel with various values of $f$ . . . . .	91
7	$T_{PK}/t_p$ in percent along the channel with various values of $f$ . . . . .	93
8	Difference in $D_{PK}$ computed from $f$ as the function of Reynolds number and various values of $f$ (in percent of channel diameter) . . . . .	94
9	Difference in $T_{PK}$ computed from $f$ as the function of Reynolds number and various values of $f$ (in percent of $t_p$ ) . . . . .	94

## Chapter I

### INTRODUCTION

The theoretical prediction of the shape of the longitudinal free water-surface for open-channel flow has long been the goal of many investigators. Mathematically, the various shapes have been precisely defined for given sets of invariant boundary conditions. The validity of these theoretical predictions of the physical system depends upon the completeness of the theoretical description, and a knowledge of the physical constants affecting the flow.

If the variation of each physical factor or parameter could be expressed in simple mathematical form, the effect of the corresponding profile could likewise be determined. However, a given physical system does not, in general, lend itself to simple mathematical analyses.

The effort described therein proposes to provide some insight into the variability of experimentally observed parameters and their effect on predicted versus observed water surface profiles.

#### 1. Definitions

The problem area to be discussed pertains to that portion of open-channel flow phenomena defined as:

(a) free-surface in which the unbounded water surface is at a constant atmospheric pressure;

(b) unsteady, in which the discharge rate at a given location varies with time; by slope (mild or steep)

and the region (1, 2, or 3). Other slopes (adverse, horizontal, critical) exist in theory as well as to a limited extent in practice.

## 2. Delineation of Problem

The basic problem of this research effort is that of determining how well the mathematical model agrees with the physical model of free-surface, unsteady, gradually-varied flow. Exact agreement could not be anticipated due to the variabilities in geometry and fluid dynamic parameters from the constant values assumed in the mathematical model.

## 3. Limits of Study

The study is restricted to the mild and steep slope flow regime in the first and second region in which the discharges vary gradually with respect to time. This assumption infers that the vertical accelerations are negligible as compared to those in the direction of flow. Thus, the vertical pressure distributions may be assumed as varying linearly.

The hydraulic factors influencing the results were limited to the physical system available for the experimental observations. The hydraulic roughness was limited to the hydraulically smooth surface region. The velocities and corresponding velocity distributions were limited to the available slopes and the boundary roughness.

If in a channel of given cross-sectional shape of infinite length, the discharge were held constant, the

depth of flow would eventually, in time and space, assume a limiting value. This depth is the direct result of the boundary drag or channel roughness and is referred to as normal depth. It will be noted from the definition that normal depth, in the physical sense, never exists except in the transition from one depth to another.

The mechanical energy contained within a moving mass may be expressed as the sum of the potential and kinetic energies. This energy relative to the channel bottom for a given discharge assumes different values depending on the depth and consequent velocity. For a derivable condition of minimum energy, the flow will take place at a determinable depth. This depth is defined as critical depth.

The relative magnitudes of normal depth and critical depth for a given channel and discharge determine one characteristic of the flow. If the normal depth is greater than the critical, the velocity is in subcritical regime and the slope is referred to as a "mild" slope. If the normal depth is less than the critical, the velocity is greater in the subcritical regime and the slope is referred to as being "steep"

Since the normal and critical depths and the channel bottom define three regions in which the free-surface may exist, it is convenient to label these regions as 1, 2, and 3. One being furthest from the bottom, 2 being between normal and critical depth, and 3 being nearest the bottom.



The mathematical development of the theoretical expression explaining the physical phenomena of unsteady free-surface flow has been accomplished by numerous investigators. The earliest (1871) presentation of the basic equations is attributed to Jean-Claude Barre de Saint-Venant. These equations express the conservation of matter and momentum. Their derivation may proceed along several parallel lines of reasoning each of course with the same end result. For the reader acquainted with these developments, the following section may be omitted. It is included herein for completeness and for those readers desiring another author's viewpoint.

## Chapter II

## THEORETICAL CONSIDERATIONS

1. Continuity Relationship

The conservation of matter requires that the mass which moves into a control volume must move out and/or be accounted for by a change in storage or density. In the following it will be assumed that the mass is incompressible and that the difference between the inflow and outflow changes the amount in storage.

Figure 1 presents the definition of terms in which the area and velocity are functions of both position (x) and time (t).

$$\begin{aligned} \text{Inflow 1} = & \left( V - \frac{\partial V}{\partial x} \right) \left( A - \frac{\partial A}{\partial x} \frac{dx}{2} \right) \rho dt = VA - V \frac{\partial A}{\partial x} \frac{dx}{2} - \\ & - A \frac{\partial V}{\partial x} \frac{dx}{2} + \frac{\partial V}{\partial x} \frac{\partial A}{\partial x} \left( \frac{dx}{2} \right)^2 \end{aligned}$$

$$\text{Inflow 2} = q \rho \quad dx dt$$

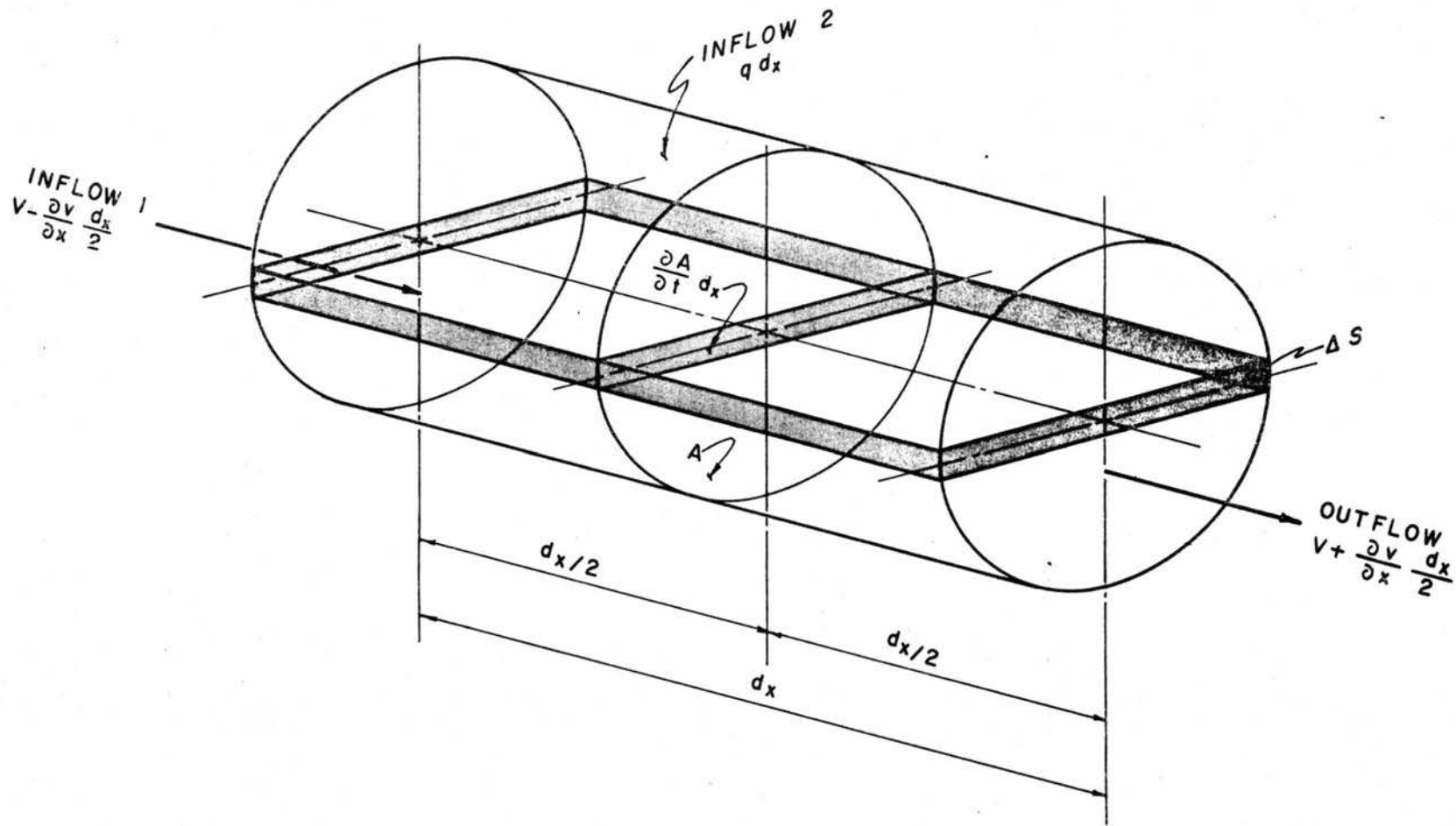
$$\begin{aligned} \text{Outflow} = & \left( V + \frac{\partial V}{\partial x} \frac{dx}{2} \right) \left( A + \frac{\partial A}{\partial x} \frac{dx}{2} \right) dt = VA + V \frac{\partial A}{\partial x} \frac{dx}{2} + \\ & + A \frac{\partial V}{\partial x} \frac{dx}{2} + \frac{\partial V}{\partial x} \frac{\partial A}{\partial x} \left( \frac{dx}{2} \right)^2 \end{aligned}$$

$$\text{Change in mass storage} = \frac{\partial A}{\partial t} dt \rho dx$$

since,

$$\text{Inflow 1} + \text{Inflow 2} - \text{Outflow} - \text{Change in storage} = 0$$

$$V \frac{\partial A}{\partial x} + A \frac{\partial V}{\partial x} + \frac{\partial A}{\partial t} dt - q = 0 \quad (1)$$



CONTINUITY RELATIONSHIP

DEFINITION SKETCH

FIG. 1

which can be simplified to

$$\frac{\partial (AV)}{\partial x} + \frac{\partial A}{\partial t} - q = 0 \quad (2)$$

Equation (2) thus represents the complete differential equation of continuity for unsteady flow of an incompressible fluid in an open channel.

The first term represents the distance rate of change of discharge along the direction of motion. The second term represents the change of cross-sectional area with time. The third term is the constant lateral inflow rate. For the purposes of this investigation, the distributed lateral inflow  $q$  was zero. Performing the indicated operations the following form of the continuity equation is that which will be used in subsequent calculation

$$\frac{A}{B} \frac{\partial V}{\partial x} + V \frac{\partial y}{\partial x} + \frac{\partial y}{\partial t} = 0 \quad (3)$$

## 2. Momentum Relationship for Unsteady Flow

The mathematical representation of the dynamics of unsteady flow, in a prismatic open-channel may be developed by application of Newton's second law of motion which in one form states:

$$F = \frac{d}{dt} (mv) \quad (4)$$

The sum of all forces acting on an element of flow is equal to the time rate of change of the momentum

(mass times velocity) in the same direction. For the application of interest this may be expressed as:

$$\iiint_{c.v.} \rho dA \vec{V} = \oint_{c.s.} \vec{V} (\vec{V} \cdot d\vec{A}) + \frac{\partial}{\partial t} \iiint_{c.v.} \vec{V} (\rho dv) \quad (5)$$

The left side of equation (5) represents the sum of all forces acting on an incremental element volume of flow integrated over the volume. Referring to figure 2, with the positive direction in the direction of flow:

$$\begin{aligned} \int_A \rho dA &= \int_A (dF_1 + dF_{f2} + dW \sin \theta - dF_{f1} - dF_2) \\ &= \int_A (dF_1 - dF_2) + \int_A dW \sin \theta + \int_A (dF_{f1} - dF_{f2}) \end{aligned} \quad (6)$$

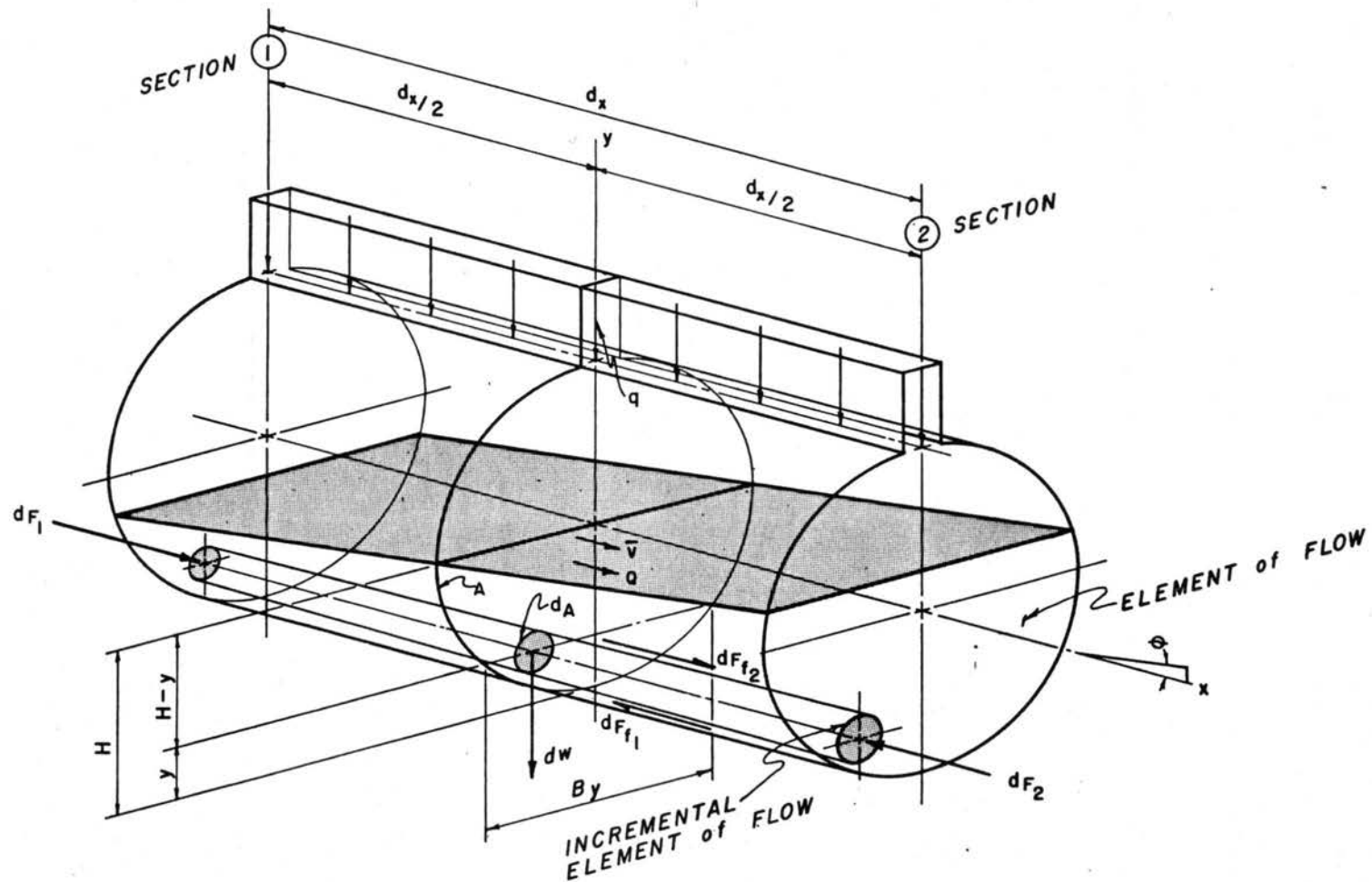
$\int_A (dF_1 - dF_2)$  represents the net pressure force on the total element of flow of area  $A$  and length  $dx$ , and may be expressed as:

$$\int_A (dF_1 - dF_2) = K \omega \frac{\partial y}{\partial x} A dx \quad (7)$$

in which  $K$  represents the ratio of the combined pressure effects of curvilinear flow and vertical acceleration to the hydrostatic pressure,  $\omega$  is the specific weight of the fluid.

---

<sup>1</sup>Shames, I. H., Mechanics of fluids, McGraw Hill Co.



UNSTEADY - FLOW RELATIONSHIP  
DEFINITION SKETCH

FIG. 2

The  $\iiint dW \sin \theta$  is the component of the weight of the total elemental volume ( $A dx$ ) in the direction of flow, such that:

$$\iiint^A dW \sin \theta = \omega \sin \theta dx A \quad (8)$$

The resistance to motion of the incremental element is represented by  $dF_{f1} - dF_{f2}$ . Since the shear resistance acting on one incremental element is equal and opposite to that on the adjacent element, the summation of all resistance forces will result in the shear resistance at the fixed boundaries. The total shear resistance to motion may then be expressed in terms of the conditions of flow as:

$$\int_A (dF_{f1} - dF_{f2}) = dF_f = \omega S_f dx A \quad (9)$$

in which  $S_f$  is the slope of the friction gradient.

Equation (6) may now be restated as:

$$K \omega \frac{\partial y}{\partial x} dx A + \omega \sin \theta dx A - \omega S_f dx A = \omega dx A \left( \frac{\partial y}{\partial x} + \sin \theta - S_f \right) \quad (10)$$

The first term of the right side of equation (5) expresses the force to accelerate the elemental mass of the base flow. This term may be expanded as follows:

$$\oint_{\text{c.s.}} \vec{V} (\rho \vec{V} \cdot d\vec{A}) = \frac{\partial}{\partial x} (\rho V^2 A) dx + V (\rho \frac{\partial V}{\partial t} B dx) \quad (11)$$

Since:

$$B \frac{\partial V}{\partial t} = \frac{\partial A}{\partial t}$$

$$\oint_{\text{c.s.}} \vec{V} (\rho \vec{V} \cdot d\vec{A}) = \frac{\partial}{\partial x} (\rho V^2 A) dx + V (\rho \frac{\partial A}{\partial t}) dx \quad (12)$$

After performing the indicated differentiation and collecting terms,

$$\oint_{\text{c.s.}} \vec{V} (\rho \vec{V} \cdot d\vec{A}) = V \rho dx (2A \frac{\partial V}{\partial x} + V \frac{\partial A}{\partial x} + \frac{\partial A}{\partial t}) \quad (13)$$

Rewriting the equation of continuity equation (3)

$$V \frac{\partial A}{\partial x} + \frac{\partial A}{\partial t} = -A \frac{\partial V}{\partial x}$$

Thus,

$$\begin{aligned} \oint_{\text{c.s.}} \vec{V} (\rho \vec{V} \cdot d\vec{A}) &= \rho A V \frac{\partial V}{\partial x} dx \\ &= \frac{\rho}{2} A \frac{\partial (V^2)}{\partial x} dx \end{aligned} \quad (14)$$

The second term of the right of equation (5) expresses the rate of change of momentum within the control volume. Since the velocity representation of the control volume is assumed independent of position, the integration and differentiation with time may be interchanged such that,



$$\frac{\partial}{\partial t} \iiint_{c.v.} V^x (\rho \, d v) = \rho \frac{\partial V}{\partial t} A \, dx \quad (15)$$

For the general case of unsteadiness due in part to lateral inflow, an additional term representing the momentum change of the lateral inflow must be provided. If the lateral inflow is uniformly distributed with respect to  $x$ , this term will be:

$$\Delta M_q = \rho \, q \, V \, dx \quad (16)$$

in which  $q$  is the lateral inflow rate per unit length and  $V$  is the mean relative velocity of the final mass flow to the initial lateral velocity in the  $x$  direction.

Rewriting equation (5) in its expanded form from equations (10), (14), (15), and (16),

$$\begin{aligned} \omega \, dx \, A \left( K \frac{\partial y}{\partial x} + \sin \theta - S_f \right) = \\ \frac{\rho}{2} A \frac{\partial (V^2)}{\partial x} \, dx + \rho \frac{\partial V}{\partial t} A \, dx + \rho q V \, dx \end{aligned} \quad (17)$$

Introducing the velocity distribution factors  $\alpha$  and  $\beta$  to relate the mean of the energy and momentum terms to the mean velocity, and dividing by  $\omega \, dx \, A$ , equation (17) becomes

$$K \frac{\partial y}{\partial x} + \sin \theta - S_f = \frac{\beta}{g} \frac{\partial V}{\partial t} + \frac{\alpha}{2g} \frac{\partial V^2}{\partial x} + \frac{qV}{gA} \quad (18)$$

Equation (18) is the general equation for unsteady free-surface flow in a prismatic channel. Each term may be physically identified as a ratio of a force gradient per unit cross-sectional area to the unit weight of liquid flowing. The terms have the following significance:

- |   |  |
|---|--|
| $K \frac{\partial y}{\partial x}$               | - force gradient due to change of depth in direction of flow         |
| $\sin \theta$                                   | - force gradient due to slope of channel bottom                      |
| $S_f$   | - force gradient due to resistance to flow due to boundary roughness |
| $\frac{\beta}{g} \frac{\partial V}{\partial t}$ | - force gradient due to temporal (local) inertia of the flow         |
| $\frac{\alpha}{2g} \frac{V}{x}$                 | - force gradient due to the convective inertia of the flow           |
| $\frac{qV}{gA}$                                 | - force gradient due to the inertia of the lateral inflow.           |

### 3. Discussion of Variables

The two equations of unsteady flow relate two independent variables (position and time) to two dependent variables (depth and velocity). The parameters describe the geometry and the hydraulic characteristics of the system.

These parameters are listed below:

- I. Geometric
  - A. Diameter (for circular pipe)
  - B. Depth
    - 1. Area
    - 2. Wetted perimeter
    - 3. Hydraulic radius
    - 4. Mean depth
    - 5. Top surface width
  - C. Channel slope
- II. Hydraulic
  - A. Hydraulic resistance (friction factor)
  - B. Velocity distribution factors
  - C. Pressure coefficient
- 4. Cross-section Geometry

The geometry of a prismatic channel is the primary factor for modification of a flood wave. The non-linearity of these quantities is the primary cause for a lack of general closed solutions to the partial differential equations. Hence the need for analog or digital solutions of these equations.

5. Slope of Channel Bottom.

The channel-bottom slope as expressed in the sine of  $\theta$  differs from slope as expressed as the tangent of  $\theta$  by less than 0.1 percent for all angles up to a slope of 4 percent. The use of tangent of  $\theta$  or slope alone is thus justified.

## 6. Hydraulic Resistance

The resistance to flow is of secondary importance to that of geometry in the influence on the passage of a flood wave. The evaluation of this term depends on empirical relations and thus cannot be precisely predicted for a given condition of flow.

Theoretical analyses of the equations of unsteady flow have depended on the use of the Chezy coefficient of roughness. This is probably due to convenient form in the integration process. For the study presented here, it was decided that the Darcy-Weisbach friction factor would be more appropriate since it would accommodate for variations of depth and velocity.

Little is known regarding the coefficient of friction for unsteady flow. Experimental observations do not permit direct evaluations of resistance for unsteady flow. Thus for this study, the same friction coefficient was used as would be used for the same conditions of steady uniform flow.

## 7. Velocity Distribution Factors

The velocity distribution factors beta and alpha are both greater than one. As discussed later, these values are approximately 1.01 and 1.03, respectively. These values have been shown to vary with depth of flow in a circular cross section.

### 8. Pressure Coefficient.

Equation (18) was developed by means of Newton's second law of motion applied only in the direction of the mean velocity.

The effect of vertical acceleration, and acceleration due to curvilinear motion in both the vertical and horizontal directions are considered to be of second order magnitude as compared to the accelerations in the direction of flow. These residual effects are encompassed in the pressure distribution coefficient (K). The pressure coefficient will take on values compared to unity depending on the time rate of change of the area at the specified cross section and the curvature of the stream lines as represented by the second derivative of the depth with position. The following table indicates the magnitude of K relative to 1.

	$\frac{\partial A}{\partial t} < 0$	$\frac{\partial A}{\partial t} = 0$	$\frac{\partial A}{\partial t} > 0$
$\frac{\partial^2 y}{\partial x^2} < 0$	$K < 1$	$K < 1$	$K < \text{or} > 1$
$\frac{\partial^2 y}{\partial x^2} = 0$	$K < 1$	$K = 1$	$K > 1$
$\frac{\partial^2 y}{\partial x^2} > 0$	$K > \text{or} < 1$	$K > 1$	$K > 1$

For sufficiently small rates of change of area with time, and small curvature of streamlines, the pressure coefficient term may be taken as unity.

### 9. Conclusion

As a consequence of the preceding discussion of the relative effects of the various terms in the basic equations, the two equations are presented in their simplified form. These forms are the working equations for subsequent solution and comparison with observed data.

The continuity of matter is expressed as:

$$\frac{A}{VB} \frac{\partial V}{\partial x} + \frac{\partial y}{\partial x} + \frac{1}{V} \frac{\partial y}{\partial t} = 0 \quad (19)$$

The continuity of momentum is simplified to

$$\frac{V}{g} \frac{\partial V}{\partial x} + \frac{1}{g} \frac{\partial V}{\partial t} + \frac{\partial y}{\partial x} = S_o - S_f \quad (20)$$

These partial-differential equations are first order, non-linear, non-homogeneous, and hyperbolic in form. Because of this form, their solution will depend upon an independent initial condition and two independent boundary conditions. With these conditions the dependent variables will be defined at each position and instant of time.

The method of solution is developed in the next section.

## Chapter III

## GEOMETRIC RELATIONSHIPS

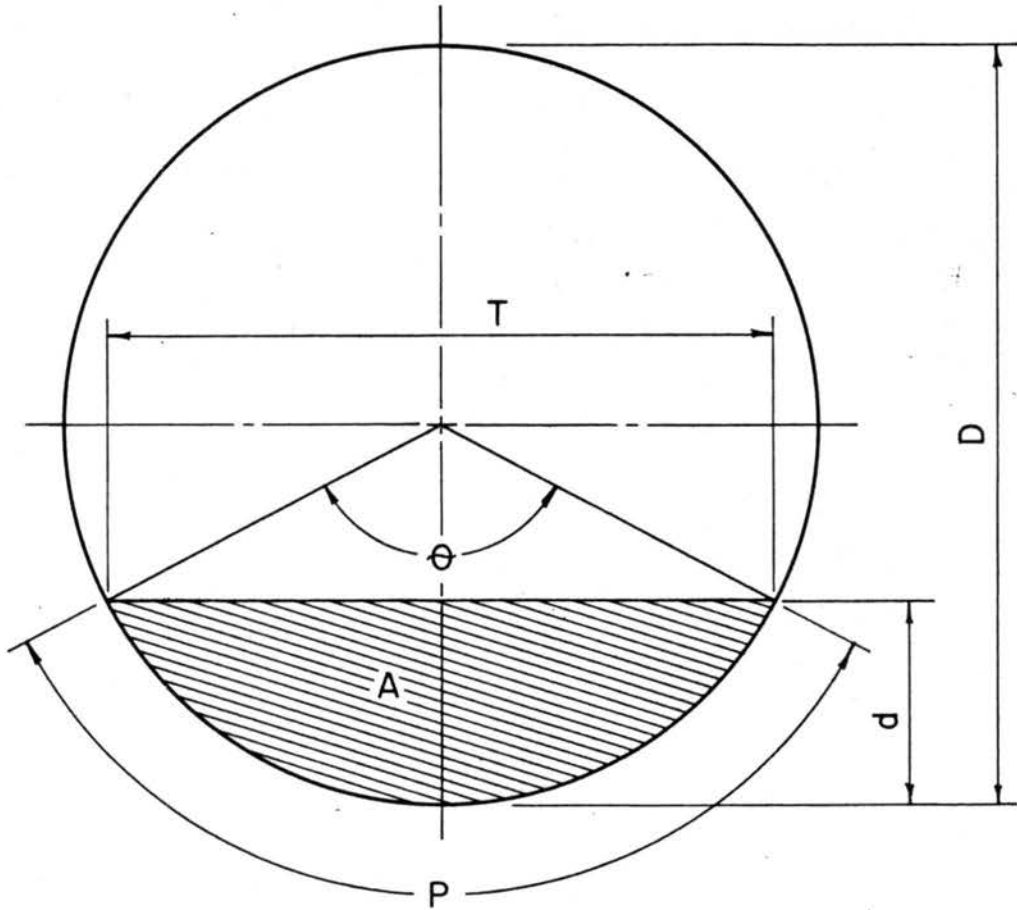
The errors due to geometric irregularities incurred in the prediction of the characteristics of flow in an open channel are a function of the depth of flow. The analysis of observed data is influenced also by the error in the observed depth. The evaluation of these errors and their relative significance is developed in the following discussion.

1. Characteristics of Circular Cross-Section

Referring to figure 3, the geometric properties of circular cross-section which influence the flow of a free-surface liquid are defined as follows:

- 1.- Diameter,  $D$
- 2 - Depth,  $d$
- 3 - Central Angle,  $\theta$
- 4 - Wetted perimeter,  $P$
- 5 - Surface width,  $B$
- 6 - Area,  $A$
- 7 - Hydraulic depth,  $d_* = \frac{A}{B}$
- 8 - Hydraulic radius,  $R = \frac{A}{P}$
- 9 - Section factor (from the Darcy-Weisbach equation)  $Z = A^2R = \frac{A^3}{P}$

Each of these parameters may be expressed as the ratio of its value at a specific depth to that at the upper



CIRCULAR CROSS-SECTION PARAMETERS  
DEFINITION SKETCH

FIG. 3



limit of depth equal to the diameter. Figure 4 displays these variations as a function of the depth-diameter ratio. It is interesting to note that the hydraulic radius and the section factor maximize at values greater than one. This fact infers that the theoretical maximum discharge would occur at less than full depth for the same energy slope. The usual theory based on atmospheric pressure of the free surface does not necessarily apply at this depth in practice, hence, prediction of flow at depth ratios near one must be based on additional considerations.

Errors in Parameters as a Function of Errors in  
Depth

The error in each of the dependent parameters can be expressed in terms of the relative error in the depth as follows:

1. Wetted perimeter defined as

$$P = \frac{D}{2} \theta \quad (21)$$

becomes

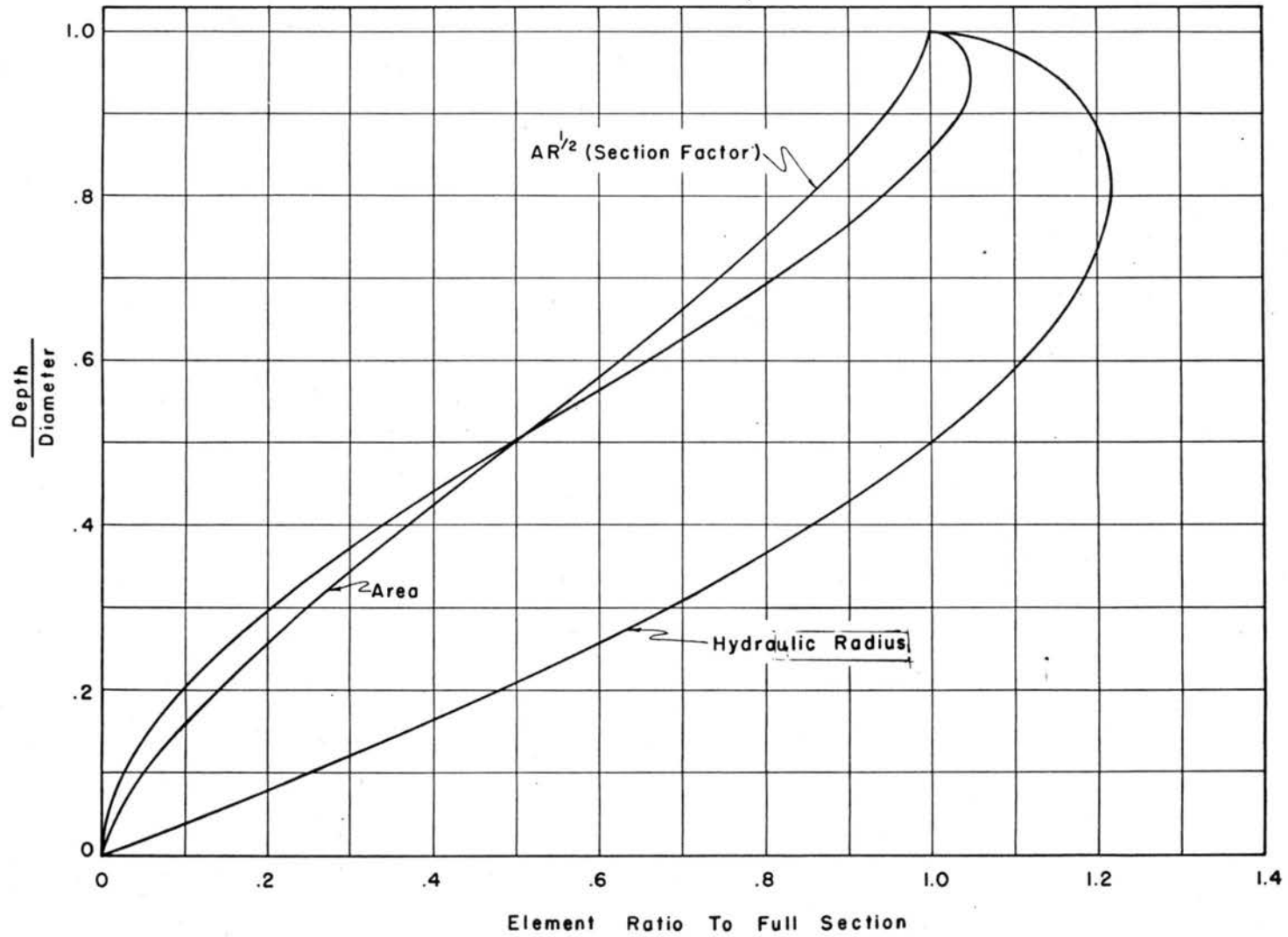
$$\frac{dP}{P} = \frac{d\theta}{\theta} \quad (22)$$

in which

$$\theta = 2 \cos^{-1} \left( 1 - \frac{2d}{D} \right) \quad (23)$$

and

$$\frac{d\theta}{\theta} = \frac{1}{\left( \frac{D}{d} - 1 \right)^{1/2} \cos^{-1} \left( 1 - \frac{2d}{D} \right)} \left( \frac{dd}{D} \right) \quad (24)$$



GEOMETRY OF THE CIRCULAR CROSS-SECTION  
 VARIATION WITH DEPTH

FIG. 4

2. Surface width defined as

$$B = D \sin \frac{\theta}{2} \quad (25)$$

becomes

$$\frac{dB}{B} = \frac{1}{\left(\frac{D}{d}-1\right)^{1/2} \tan \frac{\theta}{2}} \frac{dd}{d} \quad (26)$$

3. Area defined as

$$A = \frac{D^2}{8} (\theta - \sin \theta) \quad (27)$$

becomes

$$\frac{dA}{A} = \frac{1 - \cos \theta}{1 - \frac{\sin \theta}{\theta}} \left(\frac{d\theta}{\theta}\right) \quad (28)$$

4. Hydraulic depth defined as

$$d_* = \frac{A}{B} \quad (29)$$

becomes

$$\frac{dd_*}{d_*} = \frac{dA}{A} - \frac{dB}{B} \quad (30)$$

5. Hydraulic radius defined as

$$R = \frac{A}{P} \quad (31)$$

becomes

$$\frac{dR}{R} = \frac{dA}{A} - \frac{dP}{P} \quad (32)$$

6. Section factor defined as

$$Z = A^2 R \quad (33)$$

becomes

$$\frac{dZ}{Z} = 2 \frac{dA}{A} + \frac{dR}{R} \quad (34)$$

These relative errors, represented in equations (22), (24), (26), (28), (30), (32) and (34) being functions of depth are plotted as ratios of the relative depth error in figure 5. It may be seen that the relative error in all parameters except wetted perimeter and hydraulic depth become less for increasing depth for a given relative depth error. The significance of these curves will be demonstrated in the calculation of roughness values and Reynold's numbers.

#### Errors in Parameters as a Function of Ellipticity

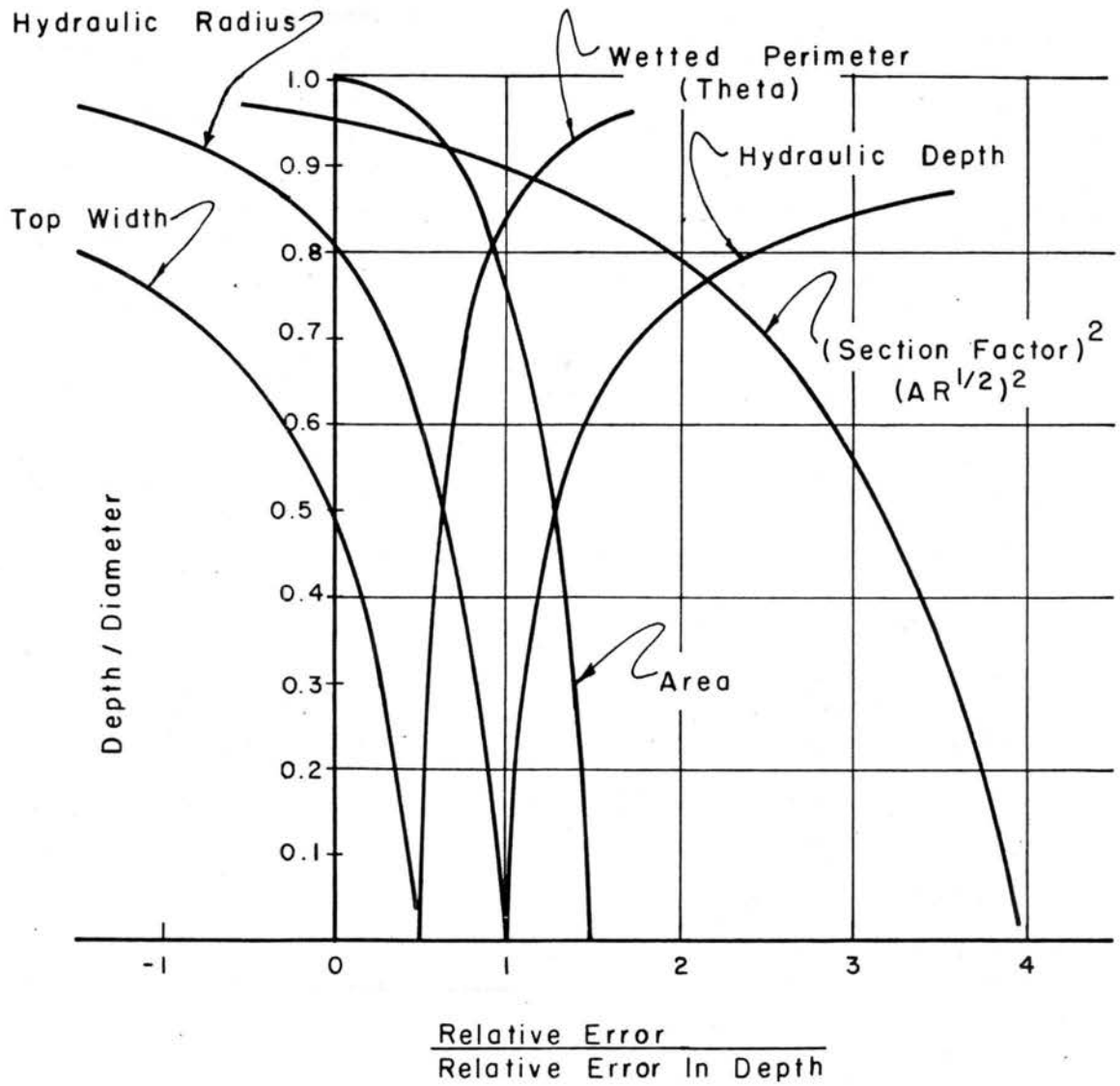
Since no physical "circular" pipe possesses the mathematically defined circular shape, it is of interest to determine the effect of a departure from the ideal shape.

As a systematic approximation, an elliptical shape was assumed. The parameters describing the departure from the flow area in a circular cross section are then the eccentricity and the direction of the principal axes. The eccentricity is defined as

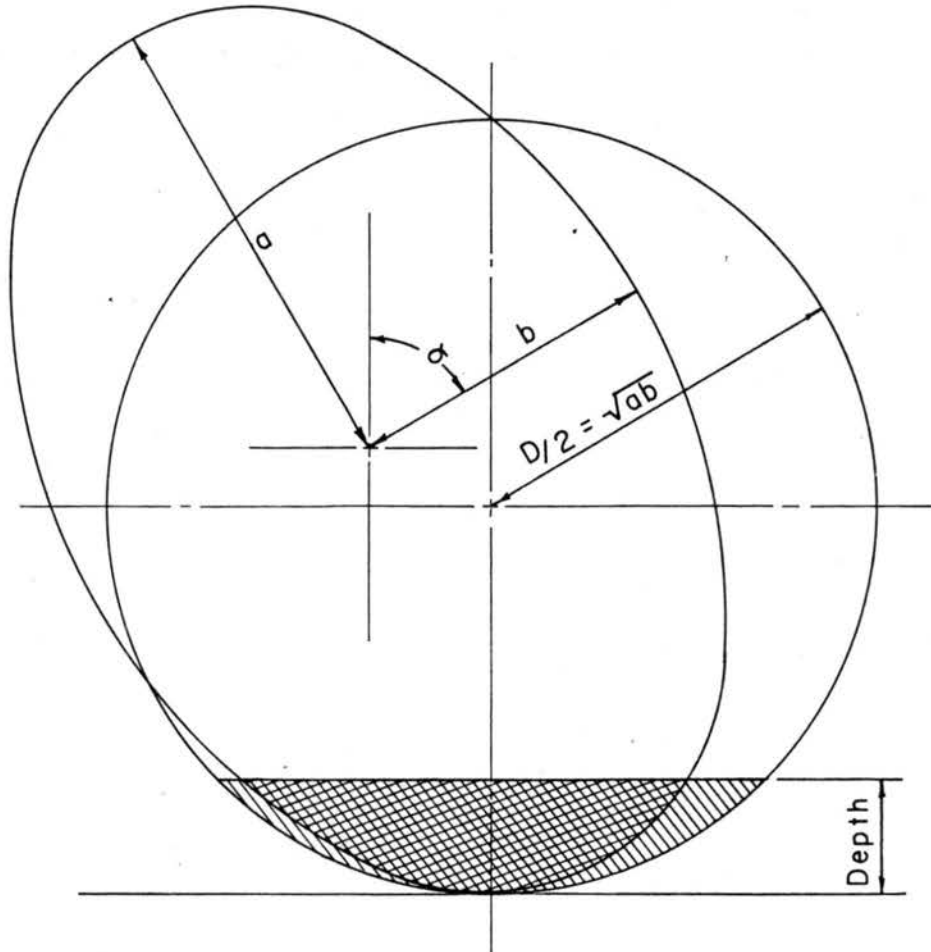
$$e = \sqrt{1 - \left(\frac{b}{a}\right)^2} \quad (35)$$


in which "a" and "b" are the major and minor semi-diameter, respectively. The direction of the principal axes defined here as the angle ( $\alpha$ ) that the minor axis makes with the vertical as shown in figure 6.

In order to compare the circular segment with an elliptical segment, the percentage difference between



GEOMETRY OF CIRCULAR CROSS-SECTION  
 RELATIVE ERROR IN PARAMETER  
 VERSUS  
 RELATIVE ERROR IN DEPTH  
 FIG. 5



ACS - CIRCULAR SEGMENT - 

AES - ELLIPTIC SEGEMENT - 

$$\% \text{ DIFF.} = \frac{\text{ACS} - \text{AES}}{\text{ACS}} \times 100$$

$$e = \sqrt{1 - \left(\frac{a}{b}\right)^2}$$

RELATIONSHIP OF CIRCULAR AND ELLIPTICAL  
CROSS-SECTIONS  
DEFINITION SKETCH

FIG. 6

the two areas was computed for a range of depths up to the center of the ellipse. The eccentricity was varied in increments of 0.05 up to 0.30 and for values of alpha ranging from 0 to  $\frac{\pi}{2}$  in increments of  $\pi/10$ . For all eccentricities, the area of the complete ellipse was made equal to that for the complete circle.

The result of these calculations are shown in figure 7 as percent difference in area between the circular and elliptical segments as a function of eccentricity for various values of alpha with depth relative to the center of the ellipse as a parameter.

These calculations indicate

(1) that the relative error in area increases with increased eccentricity;

(2) that the relative error in area decreases with increasing depth;

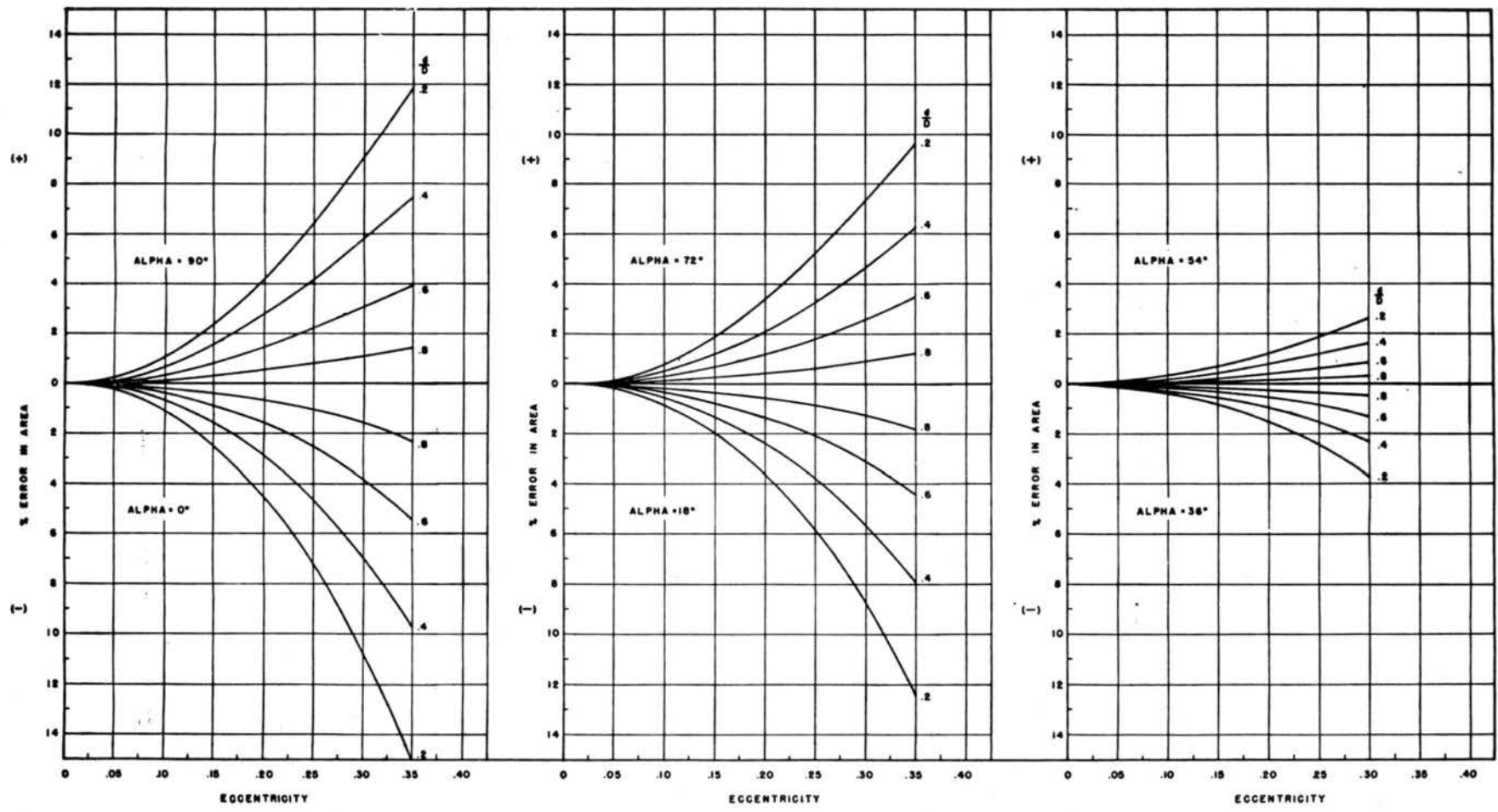
(3) that the relative error in area maximizes at the vertical and horizontal positions of the principal axes and is a minimum at an angular position of  $45^\circ$  with the horizontal.

The relationship of these geometric properties of an ellipse to the physical situation will be discussed in the following section.

#### Characteristics of the Physical Pipe

##### I. Measurements and calculations

The steel pipe used as an open channel for the data analyzed herein was nominally 3 feet in diameter



PERCENT DIFFERENCE IN AREA  
 VERSUS  
 ECCENTRICITY AND DEPTH

FIG. 7



1/2 inch thick rolled plate with a longitudinal welded joint. The 20 foot sections were butt-welded together and supported on steel rails at approximately 20 foot spacing, not necessarily at the pipe joints. As a result of the manufacturing process, handling, field welding, and the method of support it is not to be expected that the pipe would be perfectly circular or possess a straight line invert profile. The total length of the pipe was approximately 822 ft.

Measurements were made of the inside diameter of the pipe at 60° intervals to the nearest 0.001 inch. These measurements were made at cross sections spaced at 40-feet before the inside of the pipe was painted, after painting similar measurements were made at 20-ft intervals. An ellipse was fitted to the three measured diameters at each section and its orientation determined.

#### Results and Discussions

The result of the above calculations are presented in Table 1, Pipe Geometry. The differences between the means of each of the parameters for the two surveys are not significant on the 5 percent level. This would indicate (1) that the painting of the pipe had no effect on the internal geometry; and (2) that doubling the number of stations did not improve, significantly, ones knowledge of the geometry.

Accepting an average area of 968.41 sq. in. (6.725 sq. ft.) the mean diameter for the pipe is then

TABLE 1. PHYSICAL PIPE GEOMETRY

	Stations	Maximum	Units of inches		Standard Deviation
			Mean	Minimum	
Major Axis	40	17.869	17.617	17.538	0.175
	84	17.913*	17.604	17.554	0.047
Minor Axis	40	17.626	17.516	17.435	0.0375
	84	17.680	17.510	17.430	0.031
Eccentricity	40	0.176	0.1021	0.046	0.0310
	84	0.175	0.0993	0.051	0.0244
Alpha	40	165.58	84.84	13.71	46.5
	84	160.37	82.94	7.78	49.43
Area	40	989.5	969.47	965.3	3.84
	84	994.9*	968.4	964.1**	3.94
Wetted Perimeter	40	111.51	110.373	110.13	0.2769
	84	111.82*	110.314	110.07**	0.2167
Hydraulic Radius	40	8.87	8.7785	8.76	0.0183
	84	8.89	8.7742	8.75*	0.0181

\* Occurred at same section

\*\* Occurred at same section

2.9262 feet. This figure has been used for the pipe diameter for all subsequent calculations.

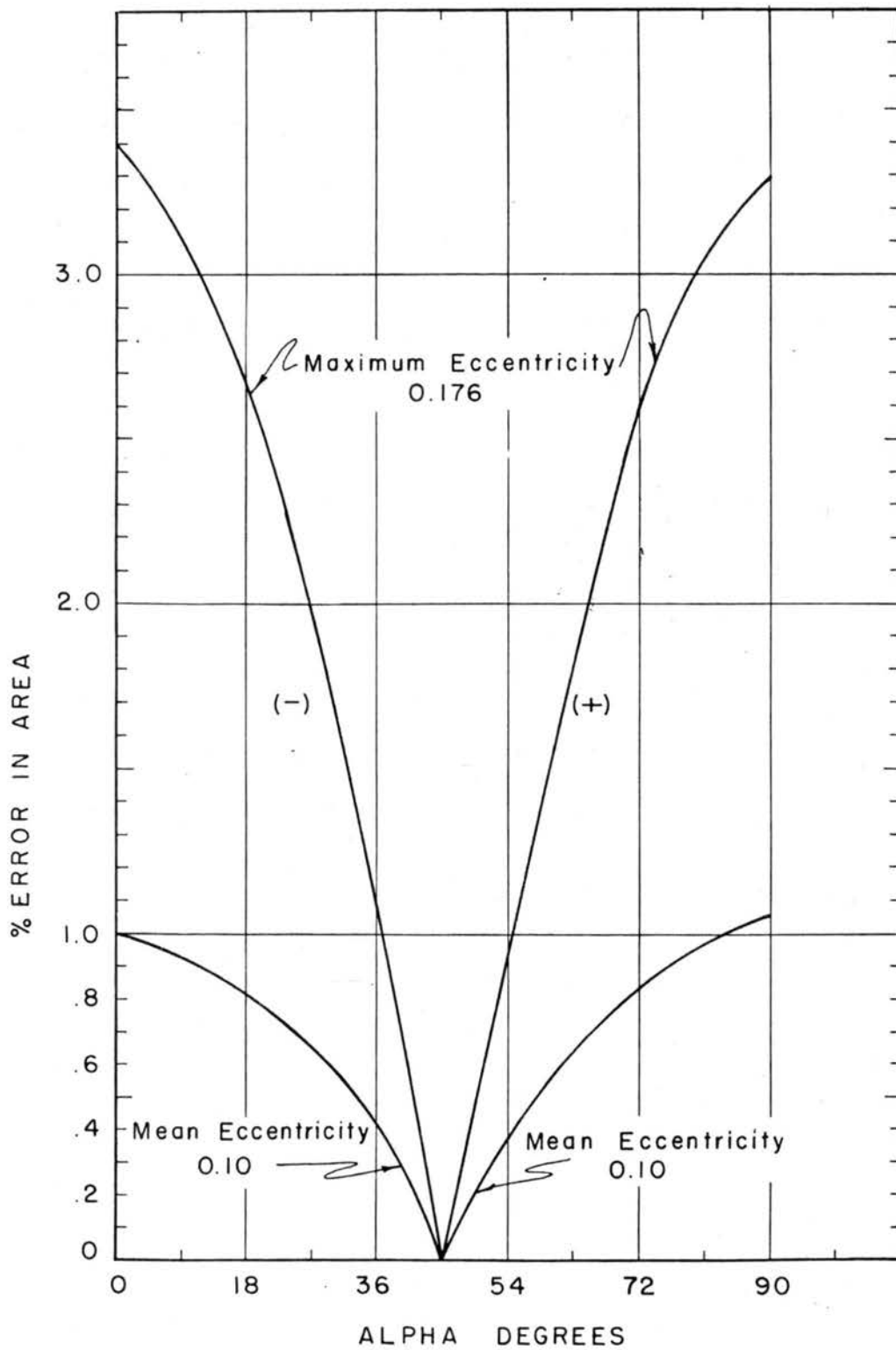
The eccentricity and the angle alpha for the observed geometry of the pipe serve as a means to estimate the possible error in subsequent hydraulic calculations. Referring to figure 7, the percent difference between the circular and elliptical segments for the maximum and mean eccentricity at a depth ratio of 0.2 was determined and in turn plotted in figure 8 as a function of the angle alpha.

As may be seen from this plot, the error in area becomes a maximum at an angular position of zero and 90 degrees. For the mean eccentricity for the pipe of this depth ratio the maximum error is 1.1 percent. For the mean alpha angle of about 85 degrees, the maximum error for the mean eccentricity is approximately 1 percent.

For depth ratios greater than 0.2 the relative error becomes less. For larger eccentricities, the relative error becomes larger at an increasing rate. For smaller alpha angles, the relative error decreases through zero at approximately 45 degrees to an absolute value equal to the maximum at zero degrees.

### Conclusions

In view of the interrelated effects of depth, eccentricity, and alpha, it appears that an error in the computation of the flow area by assuming a circular cross section instead of an approximated ellipse, may range



PERCENT ERROR IN AREA AT 0.2 x DIA. DEPTH  
FOR PHYSICAL PIPE

FIG. 8

from zero to 3 percent with 1 percent as being representative.

## 2. Errors Due to Vertical Displacements of a Circular Cross-Section

General - The deviations of a given solid boundary from a mathematical straight alignment may be identified in three broad regions,

(1) The surface irregularities which contribute directly to viscous shear and consequent hydraulic roughness

(2) Misalignments of the mean boundary which occur gradually over an appreciable distance. These may be considered as unintentional, but unavoidable in a given physical situation.

(3) Intentional changes in boundary direction either horizontally or vertically to alter the direction of flow.

Surface irregularities and intentional boundary realignments may in general be readily accounted for as to their effect on surface profiles. However, the unavoidable gradual boundary misalignments are generally ignored or assumed to introduce negligible effect on the surface profile. Based on the energy conversions relating to such changes in cross-sectional area, the foregoing assumptions are probably justified. The energy transfers are small, by definitions, and may well be masked by the uncertainty of the mean turbulent energy loss as well as

its time variability. Thus, the depths computed from any commonly used formula represent only the time-distance mean values.

In order to estimate the effect of vertical misalignments of the channel section on the water surface elevations, the following analysis was made.

Theory - It is to be expected that gradual vertical misalignments of an open channel boundary will be reflected in a change of surface profile. This effect may be idealized and subsequently quantitized by considering a sinusoidal channel bottom profile.<sup>1</sup> (See fig. 9).

At any section the total energy is

$$E = z + y + \frac{v^2}{2g}$$

upon differentiation,

$$\frac{dE}{dx} = \frac{dz}{dx} + \frac{dy}{dx} + \frac{v}{g} \frac{dv}{dx}, \text{ or}$$

(36)

$$-S_f = -S_b + \frac{dy}{dx} + \frac{v}{g} \frac{dv}{dx}$$

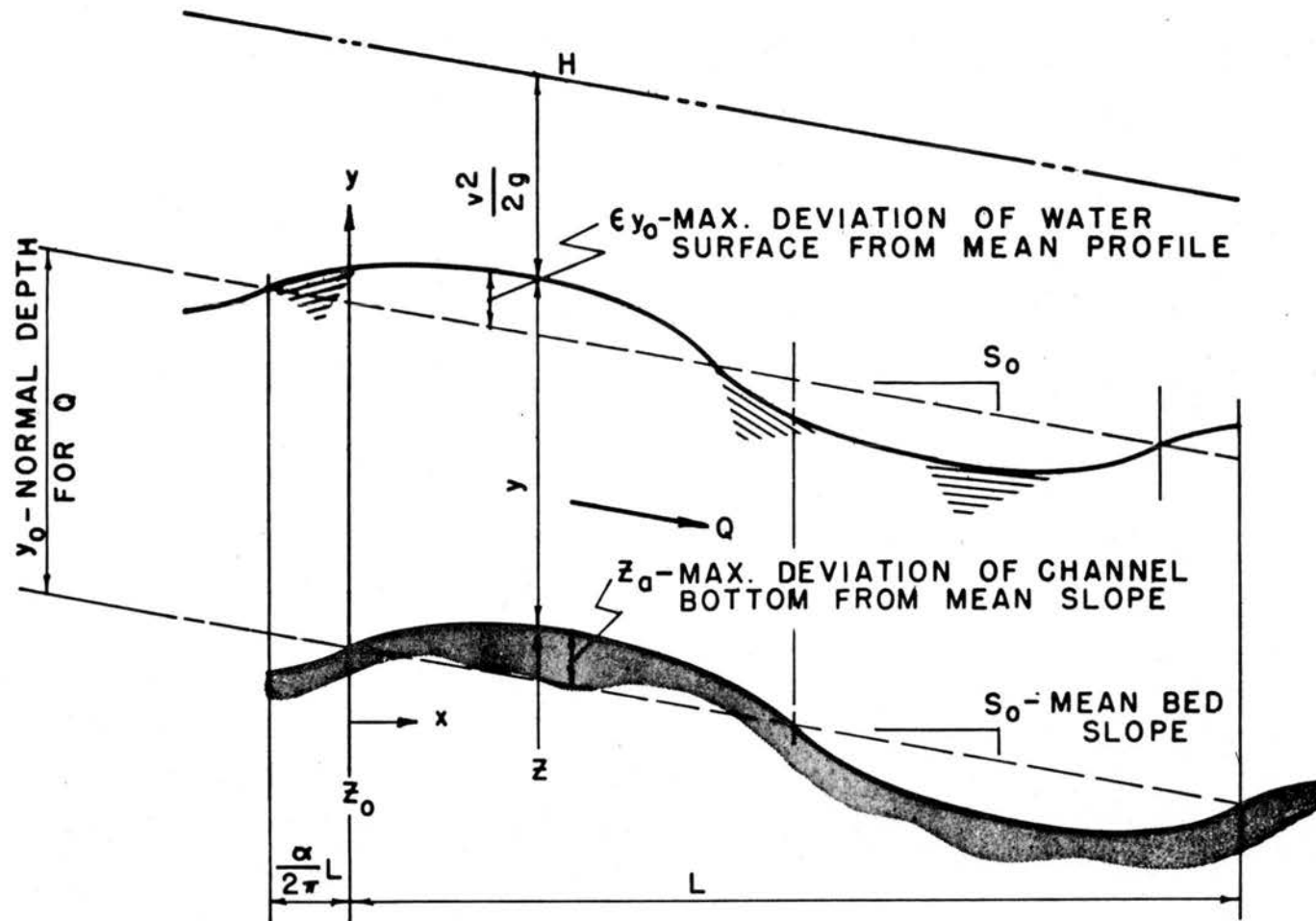
In which,  $S_f$  is the rate of energy loss which may be represented by

$$S_f = \frac{f}{8g} \frac{v^2}{R} = \frac{f}{8g} \frac{Q^2}{A^2R}$$

$$= \left(\frac{A_0}{A}\right)^3 \left(\frac{R_0}{R}\right) S_0 \quad (37)$$

---

<sup>1</sup> Proc. of 1st Australasia Conference on Hydraulics and Fluid Mechanics, J. M. Henderson



EFFECT OF BOTTOM IRREGULARITIES  
 DEFINITION SKETCH

FIG. 9

Since

$$z = z_o - x S_o + z_a \sin \frac{2\pi y}{L}$$

$$-S_b = \frac{dz}{dx} = -S_o + \frac{2\pi}{L} z_a \cos \frac{2\pi x}{L} \quad (38)$$

and

$$\frac{v}{g} \frac{dv}{dx} = - \frac{Q^2 T}{g A^3} \frac{dy}{dx} = - F_o^2 \frac{dy}{dx}$$

$$= F_o^2 \left( \frac{A_o}{A} \right)^3 \left( \frac{T}{T_o} \right) \frac{dy}{dx} \quad (39)$$

In which,  $F_o$  is the Froude Number corresponding to a uniform slope  $S_o$ .

After substitution of equations (37), (38), and (39) into equation (36) and solving,

$$\frac{dy}{dx} = \frac{1}{1 - F_o^2 \left( \frac{A_o}{A} \right)^3 \left( \frac{T}{T_o} \right)} \left\{ S_o \left[ 1 - \left( \frac{A_o}{A} \right)^3 \left( \frac{R_o}{R} \right) \right] - \frac{2\pi z_a}{L} \cos \frac{2\pi x}{L} \right\} \quad (40)$$

Equation (40) then is the differential equation of the depth resulting from a sinusoidally varying bottom of amplitude  $z_a$  in length  $L$ . A solution to this equation may be found if the geometry ratios can be expressed in terms of the depth ratios ( $y/y_o$ ). It is not possible to express the geometry of a circular section as a simple continuous function of the depth-normal depth ratio. It



is possible however, to achieve a solution if the depth ratio is expressed as:

$$\frac{y}{y_0} = 1 + \epsilon \sin \left( \frac{2\pi y}{L} - \alpha \right) \quad (41)$$

in which  $\epsilon$  is the ratio amplitude to  $y_0$  and  $\alpha$  is the phase angle for the depth wave. Then,

$$\frac{dy}{dx} = \frac{2\pi y_0}{L} \epsilon \cos \left( \frac{2\pi y}{L} - \alpha \right) \quad (42)$$

From equations (40) and (42), expanding the cosine of the sum, and equating the coefficients of the unknown phase angle  $\alpha$ ; the value of  $\alpha$  may be determined as

$$\alpha = \tan^{-1} \left[ \frac{-3 S_0 L}{2 y_0 (1 - F_0^2)} \right] \quad (43)$$

The amplitude of the depth wave  $y_0$  can now be evaluated from,

$$\epsilon = - \frac{2 z_a \sin \alpha}{3 S_0 L} \quad (44)$$

Equations (43) and (44) relate those quantities required to estimate the effect of periodic channel irregularities to corresponding changes in depth of flow.

Calculations and Results - Equations (43) and (44) were solved for various combinations of:

- (a) channel slope
- (b) wave length of channel irregularity
- (c) amplitude of channel irregularity

## (d) normal depth

The Darcy-Weisbach friction factor was taken as a constant 0.012.

Table 2 presents the results of these calculations. The results indicate, as would be expected, that for a Froude number greater than one, the depth wave is practically in phase with the bottom wave. The slight difference is due to the resistance. For a Froude number less than one the depth wave is out of phase with the bottom wave by essentially  $\pi$ . Again the slight difference is due to the resistance.

It is to be noted that the amplitude of the depth wave is unchanged for various lengths of the bottom wave (other parameters unchanged). The amplitude of the depth wave compared to the bottom wave ranges from approximately one for low Froude numbers to approximately 3 for Froude numbers close to one.

Significance to Physical Observations - The channel invert was aligned as carefully as possible to a constant uniform slope. This was accomplished by first adjusting the pipe to a predetermined position on the supporting rails. All leveling was done with a self-leveling level with an optical micrometer with a least count of 0.001 inches. The invert elevations were observed at 45 positions approximately 20 feet apart. A least-square determination of the slope and the deviations at each position was then made. If the deviations displayed

TABLE 2. THEORETICAL EFFECT OF BOTTOM IRREGULARITY  
ON WATER SURFACE PROFILE

Slope	Froude No.	$z_a$ - ft.	L - ft.	$\alpha$ - Rad.	$\epsilon y_0$ - ft.
.0100	2.582	.01	20	6.266	.002
			40	6.249	.002
			60	6.232	.002
			80	6.216	.002
		.02	20	6.266	.004
			40	6.249	.004
			60	6.232	.004
			80	6.216	.004
		.03	20	6.266	.005
			40	6.249	.005
			60	6.232	.005
			80	6.216	.005
		.04	20	6.266	.007
			40	6.249	.007
			60	6.232	.007
			80	6.216	.007
.001	.816	.01	20	3.170	.030
			40	3.198	.030
			60	3.227	.030
			80	3.255	.030
		.02	20	3.170	.060
			40	3.198	.060
			60	3.277	.060
			80	3.255	.060
		.03	20	3.170	.090
			40	3.198	.090
			60	3.227	.090
			80	3.255	.090
		.04	20	3.170	.120
			40	3.198	.120
			60	3.227	.120
			80	3.255	.120
.0001	.258	.01	20	3.142	.011
			40	3.143	.011
			60	3.144	.011
			80	3.145	.011
		.02	20	3.142	.021
			40	3.143	.021
			60	3.144	.021
			80	3.145	.021

Table 2. Con't. Theoretical effect of bottom irregularity on water surface profile

Slope	Froude No.	$z_a$ - ft.	L - ft.	$\alpha$ - Rad.	$\epsilon y_0$ - ft.
		.03	20	3.142	.032
			40	3.143	.032
			60	3.144	.032
			80	3.145	.032
		.04	20	3.142	.043
			40	3.143	.043
			60	3.144	.043
			80	3.145	.043

a consistent or excessive trend in a given length, that portion of the pipe was readjusted, and the elevations redetermined.

Due to unavoidable irregularities in successive sections of the pipe and the method of joining sections, it was impossible to completely eliminate all deviations from mean slope. Table 3 presents the results of mean slope determinations and the corresponding maximum and root-mean-square deviations from the least square fit.

From these results it may be concluded that the invert profile could be characterized by an undulating bottom with approximately 0.01 feet amplitude and a 20 feet to 40 feet wave length.

Equations (43) and (44) were solved as the case for an infinitely wide channel with a sinusoidal bottom. This case may be considered as a limiting case for a circular cross section flowing partially full if one considers the radius to remain constant and the centerline of the section to vary sinusoidally about the mean slope. Thus, the entire section may be considered as changing position vertically rather than only the invert or radius to vary sinusoidally.

Conclusions - On consideration of the results of Table 2 in predicting the effect on the observed water surface profile, it may be concluded that for the slopes used the observed depths may deviate from the ideal by 0.01 to 0.03 feet on the average. Based on the maximum

deviations the water depth may differ from the ideal by 0.03 to 0.09 feet.

TABLE 3. PHYSICAL PIPE SLOPE DEVIATIONS

Slope	Max. Deviation - ft.	Root-Mean-Square Deviation - ft.
.0000052	+.0188	.0116
.0000157	+.0182	.0135
.0000303	+.0214	.0099
.0001325	+.0195	.0099
.0005197	+.0347	.0117
.0010101	+.0279	.0119
.0074578	-.0240	.0133
.0200690	+.0375	.0141

## Chapter IV

## METHODS OF SOLUTION

The solution to a previously stated equation for unsteady open-channel flow may be categorized in numerous ways. One way would be to consider integration of these equations in closed form as contrasted with the finite difference solution.

The solutions of these equations by means of direct integration is obviously most impracticable if not impossible. This is due in part to the non-linear characteristics of the equation and the fact that they are most commonly applied to channels of arbitrary shape. There have been solutions for these equations for the infinitely wide channel and for boundary resistance expressed as relatively simple functions of the depth and velocity.

It is conceivable that a continuous solution of these equations could be made by means of an electronic analog computer. Although this was not done in this study, it presents an interesting possibility. The difficulties of such a solution would involve the generation of geometric parameters and again boundary resistance as continuous analog functions. This perhaps could be overcome by the use of a hybrid computer.

The final possible method of solution depends upon consideration of finite differences of distance and time. These assume that the variations in the dependent variables

which occur during the short intervals of time is comparable to the variations taking place in the continuous function. The methods available for this type of solution include the semigraphical solution as was done by Akers and numerical methods as have been investigated by numerous researchers. Numerical solutions may be accomplished in various manners, however the use of the electronic digital computer is obviously the most convenient and accurate.

Numerical procedures utilizing a digital computer are likewise numerous depending upon the type of problem and the individual who develops the procedure. Several methods were attempted during the course of this study. These methods depend upon various mesh patterns in the time-space domain. The methods which were used and subsequently discarded were those defined by Richtmyer<sup>(1)</sup>. These methods are termed diffusing, leap-frog and Lax-Wendroff. These methods perform satisfactorily within certain ranges of flow characteristics. They inherently produced instabilities when the flow changed from sub- to super-critical flow or vice versa. This is due to the changing pattern of zone of dependence and region of influence as described by Yevjevich.

Following the successful solutions utilizing the method of characteristics, it was decided to utilize this computational procedure throughout the study. The description of this procedure as used in this study follows.

---

(1) A survey of Difference Methods for Non-Steady Fluid Dynamics, R. D. Richtmyer, NCAR Technical notes 63-2



## Method of Characteristics

### Introduction

The equations of unsteady free-surface flow equations (19) and (20) form a system of quasi-linear partial differential equations of the first order and of a hyperbolic type. The discussion of why the system of the equations of unsteady free-surface flow is called a system of quasi-linear partial differential equations of the first order and of a hyperbolic type, is found on pages 53 and 57.

Various possible methods to integrate these two partial differential equations were discussed by Yevjevich (1961; 1964). One of these methods is called the method of characteristics. This method was first proposed by Massau (1889) for integrating the two partial differential equations of unsteady flow in channels by graphical procedure. This method has been also widely used for the solution of a variety of problems in physics and mechanics, and they can be found in Courant and Friedrichs (1948), Crandall (1956), and Dwczarek (1964).

The solution of the method of characteristics by hand calculation or graphical with hand or desk calculator is extremely laborious and time consuming. As a result, in the period before the advent of electronic computers, a variety of schemes of the solution by this method were proposed. The details of various schemes can be found in Yevjevich (1964). In general, solutions of

the method of characteristics may be performed by two ways: graphical method and digital computer. A digital computer gives several advantages. It does not only do the tedious computation which is done by the graphical method, but it also gives the solution for the complete system of equations without simplification and approximation. This permits a significant increase in accuracy.

The purpose of this study was to use a digital computer to solve the equations of unsteady free-surface flow by the method of characteristics. In this section, the method of characteristics is described for a system of two quasi-linear partial differential equations of the hyperbolic type with two dependent and two independent variables.

General form of the equations of unsteady free-surface flow

The general form of the equations of unsteady free-surface flow is written in a system of quasi-linear partial differential equations of hyperbolic type with two dependent variables  $V$  and  $y$ , and two independent variables  $x$  and  $t$ .

$$A_1 \frac{\partial V}{\partial x} + B_1 \frac{\partial V}{\partial t} + C_1 \frac{\partial y}{\partial x} + D_1 \frac{\partial y}{\partial t} + E_1 = 0 \quad (45)$$

$$A_2 \frac{\partial V}{\partial x} + B_2 \frac{\partial V}{\partial t} + C_2 \frac{\partial y}{\partial x} + D_2 \frac{\partial y}{\partial t} + E_2 = 0 \quad (46)$$

where  $V$  is the velocity,  $y$  is the depth,  $x$  is the distance along the channel,  $t$  is the time, and  $A_1$ ,  $A_2$ , ...,  $E_2$  are coefficients which are the functions of variables  $V$ ,  $y$ ,  $x$  and  $t$ .

Equations (45) and (46) are comparable to equations (19) and (20), respectively, with the following conditions

$$A_1 = \frac{A}{VB}; \quad B_1 = 0; \quad C_1 = 1; \quad D_1 = \frac{1}{V}; \quad E_1 = 0$$

$$A_2 = \frac{\alpha V}{g}; \quad B_2 = \frac{\beta}{g}; \quad C_2 = 1; \quad D_2 = 0; \quad E_2 = S_f - S_o.$$

The general form of the equations of unsteady free-surface flow was used exclusively in this section as well as in the next. This is because, first, the general form is compact and easy to treat in mathematical derivation. For instance, in the derivation of the characteristic equations, the general form is easier to deal with than the actual unsteady flow equations. Second, if the general form was considered and treated once, then any change in the boundary conditions of the flow, such as lateral in flows, does not require a new mathematical consideration, but only to equate properly the coefficients between the two systems.

#### Mathematical properties of the equations

Consider a certain region in the  $(x, t)$  place, say on the curves  $\xi_+$  or  $\xi_-$  in figure 10. If the

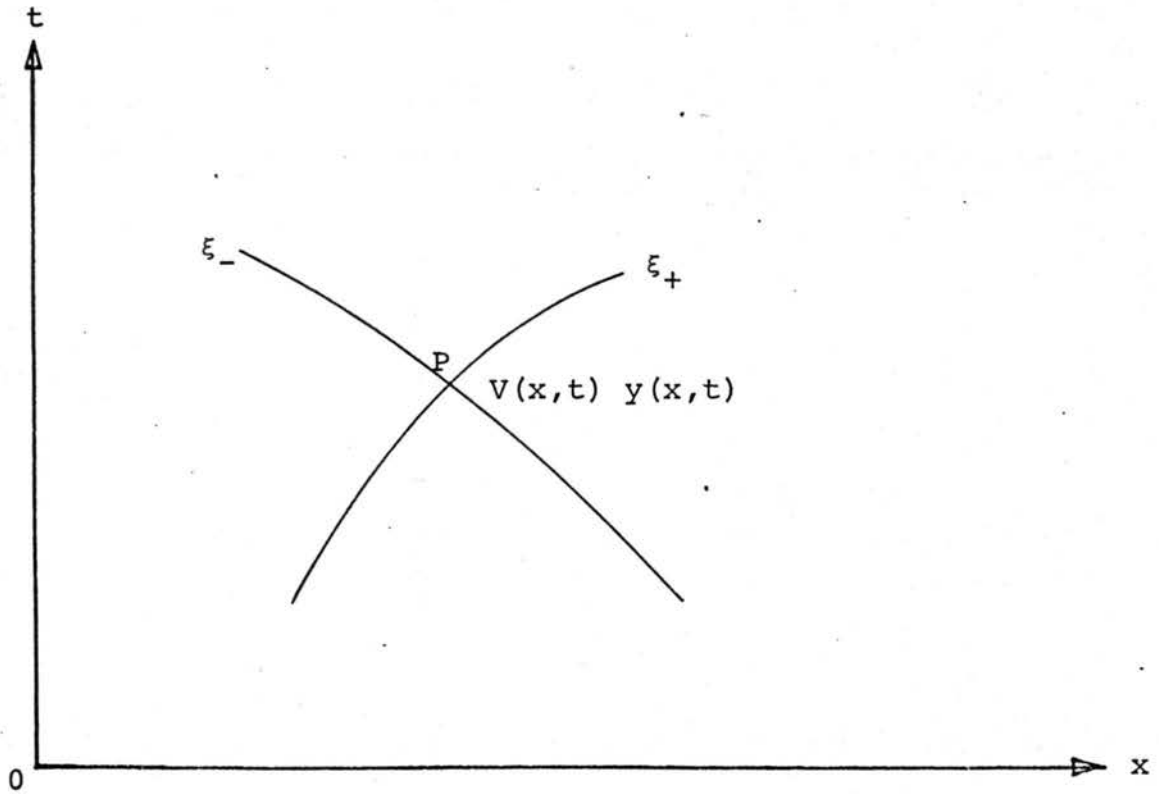


Fig. 10 -  $A(x,t)$  plane in which the solutions along  $\xi_+$  and  $\xi_-$  are initially known

$V$  and  $y$  are continuous; then  $\frac{\partial V}{\partial x}$ ,  $\frac{\partial V}{\partial t}$ ,  $\frac{\partial y}{\partial x}$ , and  $\frac{\partial y}{\partial t}$  have finite values and a unique solution of the equations (45) and (46) exists on the curves  $\xi_+$  or  $\xi_-$ . Therefore, if the values of  $V$  and  $y$  and their derivatives are known along curve  $\xi_+$ ; then the derivatives  $\frac{\partial V}{\partial x}$ ,  $\frac{\partial V}{\partial t}$ ,  $\frac{\partial y}{\partial x}$ , and  $\frac{\partial y}{\partial t}$  at any point of curve  $\xi_+$  being at the distance  $x$  and the time  $t$ , are known and the derivatives  $\frac{\partial V}{\partial x}$ ,  $\frac{\partial V}{\partial t}$ ,  $\frac{\partial y}{\partial x}$ , and  $\frac{\partial y}{\partial t}$  at the point  $P$  can be computed then the velocity  $V$  and the depth  $y$  along the curve  $\xi_+$  can be determined. Since the solution along curve  $\xi_+$  is known, their derivatives are also known.

$$\frac{\partial V}{\partial S'} = \frac{\partial V}{\partial x} \frac{\partial x}{\partial S'} + \frac{\partial V}{\partial t} \frac{\partial t}{\partial S'} \quad (47)$$

$$\frac{\partial D}{\partial S'} = \frac{\partial D}{\partial x} \frac{\partial x}{\partial S'} + \frac{\partial D}{\partial t} \frac{\partial t}{\partial S'} \quad (48)$$

where  $S'$  is the differential element along curve  $\xi_+$ . Therefore, in the additions to equations (45) and (46), there are two more equations which can be written from equations (47) and (48)

$$dV = \frac{\partial V}{\partial x} dx + \frac{\partial V}{\partial t} dt \quad (49)$$

$$dy = \frac{\partial y}{\partial x} dx + \frac{\partial y}{\partial t} dt \quad (50)$$

where;

$$dV = \frac{\partial V}{\partial S'} ds'$$

$$dy = \frac{\partial y}{\partial S'} ds'$$

$$dx = \frac{\partial x}{\partial S'} ds'$$

$$dt = \frac{\partial t}{\partial S'} ds'$$

The four equations (45), (46), (49) and (50) with four unknowns  $\frac{\partial V}{\partial x}$ ,  $\frac{\partial V}{\partial t}$ ,  $\frac{\partial y}{\partial x}$  and  $\frac{\partial y}{\partial t}$ , can be written into a single matrix equation

$$\begin{bmatrix} A_1 & B_1 & C_1 & D_1 \\ A_2 & B_2 & C_2 & D_2 \\ dx & dt & 0 & 0 \\ 0 & 0 & dx & dt \end{bmatrix} \begin{bmatrix} \frac{\partial V}{\partial x} \\ \frac{\partial V}{\partial t} \\ \frac{\partial y}{\partial x} \\ \frac{\partial y}{\partial t} \end{bmatrix} = \begin{bmatrix} -E_1 \\ -E_2 \\ dV \\ dy \end{bmatrix} \quad (51)$$

Solving equation (51), the derivative  $\frac{\partial V}{\partial x}$  can be determined.

$$\frac{\partial V}{\partial x} = \frac{\begin{vmatrix} -E_1 & B_1 & C_1 & D_1 \\ -E_2 & B_2 & C_2 & D_2 \\ dV & dt & 0 & 0 \\ dy & 0 & dx & dt \end{vmatrix}}{\begin{vmatrix} A_1 & B_1 & C_1 & D_1 \\ A_2 & B_2 & C_2 & D_2 \\ dx & dt & 0 & 0 \\ 0 & 0 & dx & dt \end{vmatrix}} = \frac{\Delta_1}{\Delta} \quad (52)$$

Similarly, for the other derivatives

$$\frac{\partial V}{\partial t} = \frac{\Delta_2}{\Delta} \quad (53)$$

$$\frac{\partial y}{\partial x} = \frac{\Delta_3}{\Delta} \quad (54)$$

$$\frac{\partial y}{\partial t} = \frac{\Delta_4}{\Delta} \quad (55)$$

where  $\Delta_2$ ,  $\Delta_3$  and  $\Delta_4$  are appropriate determinants.

From inspection of the equations (52), (53), (54) and (55), a unique solution along the curve  $\xi_+$  exists only if the direction of curve  $\xi_+$  is such that the determinant  $\Delta \neq 0$ . When the direction of curve

$\xi_+$  is such that the determinant  $\Delta = 0$ , then there is no unique solution along the curve  $\xi_+$ . It is initially assumed that in the region of  $(x, t)$  plane the first derivatives of  $V$  and  $y$ ,  $\frac{\partial V}{\partial x}$ ,  $\frac{\partial V}{\partial t}$ ,  $\frac{\partial y}{\partial x}$ ,  $\frac{\partial y}{\partial t}$ , have finite values. Equations (52), (53), (54) and (55) were rewritten in the form for the purpose of mathematical inspection of the equations.

$$\Delta \frac{\partial V}{\partial x} = \Delta_1$$

$$\Delta \frac{\partial V}{\partial t} = \Delta_2$$

$$\Delta \frac{\partial y}{\partial x} = \Delta_3$$

$$\Delta \frac{\partial y}{\partial t} = \Delta_4$$

(56)

From inspection of the equation (56), if the determinant  $\Delta$  vanishes along curve  $\xi_+$  then the determinants  $\Delta_1$ ,  $\Delta_2$ ,  $\Delta_3$  and  $\Delta_4$  must also vanish. Therefore, on curve  $\xi_+$  there exist

$$\frac{\partial V}{\partial x} = 0$$

$$\frac{\partial V}{\partial t} = 0$$

$$\frac{\partial y}{\partial x} = 0$$

$$\frac{\partial y}{\partial t} = 0$$

(57)



In the case determinant  $\Delta$  in the equations (52), (53), (54), and (55) vanishes,

$$\Delta = \begin{vmatrix} A_1 & B_1 & C_1 & D_1 \\ A_2 & B_2 & C_2 & D_2 \\ dx & dt & 0 & 0 \\ 0 & 0 & dx & dt \end{vmatrix} = 0 \quad (58)$$

Expanding equation (58),

$$\begin{aligned} (A_1 C_2 - A_2 C_1) dt^2 - \{(A_1 D_2 - A_2 D_1) + (B_1 C_2 - B_2 C_1)\} dx dt \\ + (B_1 D_2 - B_2 D_1) dx^2 = 0 \end{aligned} \quad (59)$$

The following notation is introduced in order to simplify the algebra and the computer program coding.

$$[xy] = x_1 y_2 - x_2 y_1$$

Equation (59) then becomes

$$[AC] \left(\frac{dt}{dx}\right)^2 - \left\{ [AD] + [BC] \right\} \frac{dt}{dx} + [BD] = 0 \quad (60)$$

If the direction of curve  $\xi_+$  at P in the (x, t) plane of figure 10 is such that it has a slope satisfying equation (60); then the derivatives of B and y along the curve  $\xi_+$ ,  $\frac{\partial V}{\partial x}$ ,  $\frac{\partial V}{\partial t}$ ,  $\frac{\partial y}{\partial x}$ ,  $\frac{\partial y}{\partial t}$  are not

uniquely determined by the values of  $V$  and  $y$  along the curve. Such direction of curve  $\xi_+$  is called a characteristic direction, and the curve  $\xi_+$  is called a characteristic curve or, simply, characteristics.

Equation (60) is in a quadratic form of the slope  $\frac{dt}{dx}$ . Therefore, there are two solutions of  $\frac{dt}{dx}$ .

$$\left(\frac{dt}{dx}\right)_+ = \frac{[AD] + [BC] + \sqrt{([AD] + [BC])^2 - 4[AC][BD]}}{2[AC]} \quad (61)$$

$$\left(\frac{dt}{dx}\right)_- = \frac{[AD] + [BC] - \sqrt{([AD] + [BC])^2 - 4[AC][BD]}}{2[AC]} \quad (62)$$

The notations for the two characteristics are introduced such that

$$\xi_+ = \left(\frac{dt}{dx}\right)_+ \quad \text{and} \quad \xi_- = \left(\frac{dt}{dx}\right)_- \quad (63)$$

In this case, if equation (60) has two real solutions, then the system of equation (51) is called a system of equations of the hyperbolic type, for two complex solutions it is called the elliptic type and for one real solution it is called the parabolic type.

As previously mentioned, if the determinant  $\Delta$  vanishes, then the determinants  $\Delta_1$ ,  $\Delta_2$ ,  $\Delta_3$  and  $\Delta_4$  must also vanish. Therefore, for example  $\Delta_4 = 0$

$$\begin{vmatrix} A_1 & B_1 & C_1 & -E_1 \\ A_2 & B_2 & C_2 & -E_2 \\ dx & dt & 0 & dV \\ 0 & 0 & dx & dy \end{vmatrix} = 0 \quad (64)$$

Expanding the equation (64)

$$\left\{ [AC] \frac{dt}{dx} - [BC] \right\} \frac{dy}{dx} + [AB] \frac{dV}{dx} + \left\{ [AE] \frac{dt}{dx} - [BE] \right\} = 0 \quad (65)$$

where  $\left(\frac{dt}{dx}\right)_+$  obtained from equation (61) is substituted into equation (65), it becomes an ordinary differential equation for  $V$  and  $y$  along the characteristic  $\xi_+$

$$\left\{ [AC] \xi_+ - [BC] \right\} \frac{dy}{dx} + [AB] \frac{dV}{dx} + \left\{ [AE] \xi_+ - [BE] \right\} = 0 \quad (66)$$

Similarly, another ordinary differential equation for  $V$  and  $y$  along the characteristic  $\xi_-$  can be obtained by substituting  $\left(\frac{dt}{dx}\right)_-$  of equation (62) into equation (65).

$$\left\{ [AC] \xi_- - [BC] \right\} \frac{dy}{dx} + [AB] \frac{dV}{dx} + \left\{ [AE] \xi_- - [BE] \right\} = 0 \quad (67)$$

Now there are two ordinary differential equations (66) and (67) with two unknowns  $V$  and  $y$ . The solution can be obtained by solving these two equations simultaneously.

No new relationships are obtained by using the determinants  $\Delta_1$ ,  $\Delta_2$  and  $\Delta_3$  being zero. In other words, the two ordinary differential equations (66) and (67) can be obtained by the relationship of any one of  $\Delta_1$ ,  $\Delta_2$ ,  $\Delta_3$  and  $\Delta_4$  being zero.

In summary, a procedure of solving a quasi-linear partial differential equations with two dependent and two independent variables is: First, the characteristic direction at a point in the  $(x, t)$  plane, at which the dependent variables  $V$  and  $y$  are known, is computed. For example, in figure 10 the velocity  $V$  and the depth  $y$  are known at the point  $P$  of the coordinates  $(x, t)$ . The characteristic direction at the point  $P$  can be determined from the characteristic equations (61) and (62), since they are the functions of the coefficients of the partial differential equations and the dependent variables  $V$  and  $y$  at that point. Second, the two ordinary differential equations (66) and (67) are simultaneously solved along the two characteristic curves. In this way, the values of the dependent variables  $V$  and  $y$  along the two characteristic curves are obtained. This procedure is called the method of characteristics.

#### Characteristics of the Equations of Unsteady Free-Surface Flow

In comparison of equations (19) and (20) of unsteady free-surface flow with the general form, equations

(45) and (46), a system of four equations of four unknowns  $\frac{\partial V}{\partial x}$ ,  $\frac{\partial V}{\partial t}$ ,  $\frac{\partial y}{\partial x}$ , and  $\frac{\partial y}{\partial t}$  was written from equation (51).

$$\begin{bmatrix} \frac{A}{VB} & 0 & 1 & \frac{1}{V} \\ \frac{V}{g} & \frac{1}{g} & 1 & 0 \\ dx & dt & 0 & 0 \\ 0 & 0 & dx & dt \end{bmatrix} \begin{bmatrix} \frac{\partial V}{\partial x} \\ \frac{\partial V}{\partial t} \\ \frac{\partial y}{\partial x} \\ \frac{\partial y}{\partial t} \end{bmatrix} = \begin{bmatrix} 0 \\ S_o - S_f \\ dV \\ dD \end{bmatrix} \quad (68)$$

The two characteristic directions at a point in the  $(x, t)$  plane with the values of the two dependent variables  $V$  and  $y$  are known, were written from equations (61) and (62) respectively.

$$\left(\frac{dt}{dx}\right)_+ = \frac{1}{V + \sqrt{gA/B}} = \xi_+ \quad (69)$$

$$\left(\frac{dt}{dx}\right)_- = \frac{1}{V - \sqrt{gA/B}} = \xi_- \quad (70)$$

The two ordinary differential equations for  $V$  and  $y$  along the characteristics  $\xi_+$  and  $\xi_-$  were written from equations (66) and (67) respectively.

$$\left\{ \left(\frac{A}{VB} - \frac{V}{g}\right) \xi_+ + \frac{1}{g} \right\} \frac{dy}{dx} + \left(\frac{A}{VBg}\right) \frac{dV}{dx} + \frac{A}{VB} (S_o - S_f) \xi_+ = 0 \quad (71)$$

$$\left\{ \left(\frac{A}{VB} - \frac{V}{g}\right) \xi_- + \frac{1}{g} \right\} \frac{dy}{dx} + \left(\frac{A}{VBg}\right) \frac{dV}{dx} + \frac{A}{VB} (S_o - S_f) \xi_- = 0 \quad (72)$$

The system of the equations of unsteady free-surface flow, which is in a form of a single matrix, equation (68), is called quasi-linear because the equations are linear with respect to the derivative of the highest order, in this case it is the first order. And it is called the hyperbolic type because there are two real solutions of characteristics which obtained from equations (69) and (70). This is proved by the inspection of the term under the square-root in equations (69) and (70) which is always positive. Thus, there are two real solutions of characteristics in equation (68).

## Chapter V

## COMPUTER SOLUTION

This section deals with: (1) Procedure of solving the two characteristic equations and the two ordinary differential equations by numerical methods. This includes the general concept of arranging the two characteristic directions for computation and the methods of integrating the two differential equations along the characteristic directions by finite differences, and (2) Details of computer solution of the selected method from several possible methods.

Methods of Characteristics for Obtaining a Numerical Solution

Generally speaking, there are two approaches of solving the set of equations (69), (70), (71), and (72) by the method of characteristics on a computer.

The first is called the method of grids of characteristics. This includes establishing the initial characteristic curves which are known from the initial condition. The receding characteristic curves emanate from it. In figure 11 the initial characteristic curve  $\xi_0$  is known from the inflow hydrograph and is drawn from  $x = 0$  and  $t = 0$ . By introducing the values of the dependent variables  $V$  and  $y$  along the initial characteristic curve,  $\xi_0$ , at the appropriate points in the computation scheme, the values of  $V$  and  $y$  at successive points being functions of the independent variables  $x$ , and  $t$  are

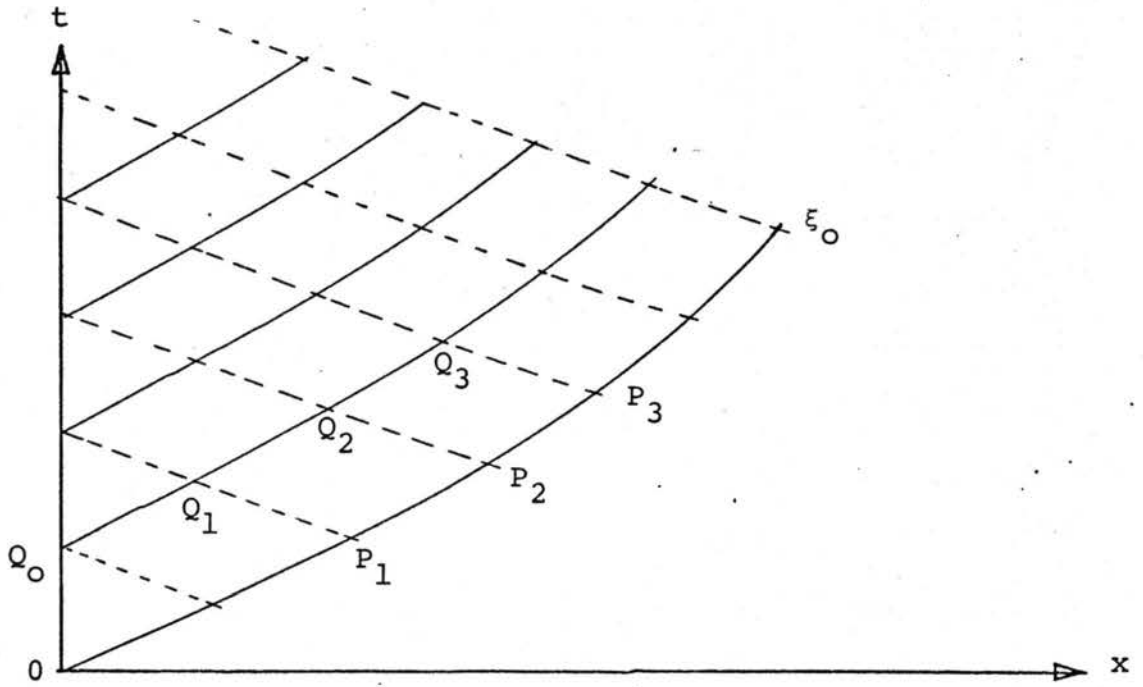


Fig. 11 - Network of characteristics by the method of grids of characteristics



obtained. For example, the values of the depths and velocities at points  $Q_1$ ,  $Q_2$  and  $Q_3$  in figure 11, are obtained from the values of the depths, velocities and the coordinates  $(x, t)$  of the points  $Q_0$ ,  $P_1$ ,  $P_2$ , and  $P_3$  respectively.

In the same manner, all values of the dependent variables  $V$  and  $y$  as functions of the independent variables  $x$  and  $t$  can be computed.

The second method is called the method of specified intervals of the independent variables. With this approach the dependent variables  $V$  and  $y$  are known functions of the independent variables  $x$  and  $t$ , either being as given initial conditions or as the results of previous stages of computations. For example, it is assumed that  $V$  and  $y$  are known along the distance  $x$  at the time  $t$ . Figure 12 represents rectangular grids in  $(x, t)$  plane with intervals  $\Delta x$  and  $\Delta t$  in  $x$  and  $t$  coordinates respectively. In this case,  $V$  and  $y$  at points  $M_0$ ,  $A_0$ ,  $B_0$ , ...,  $N_0$  are known, then the values of  $V$  and  $y$  at the time  $t + \Delta t$  and particularly at points  $M_1$ ,  $A_1$ ,  $B_1$ , ...,  $N_1$  can be computed from the set of equations (69), (70), (71), (72) and the boundary conditions. In this manner,  $V$  and  $y$  at the time  $t + 2\Delta t$  at various points along the distance  $x$  can be computed. This process can be continued as far as desired.

In this study, method of grids of characteristic is referred to as the first method and method of specified

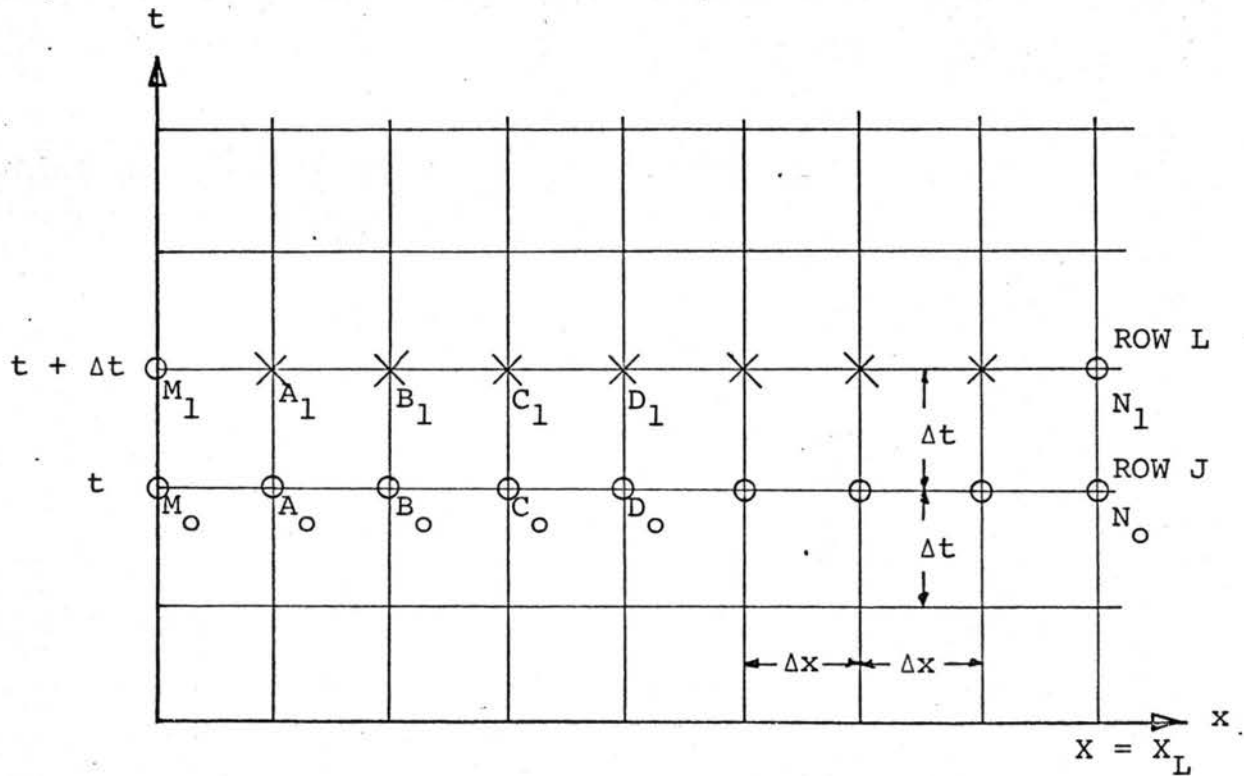


Fig. 12 - Network of characteristics by the method of specified intervals

intervals of the independent variables is referred to as the second method. The second method was selected and used in this study because the values of  $x$  and  $t$  at  $M_1, A_1, B_1, \dots, N_1$  of the second method are exactly known, and only the values of  $V$  and  $y$  at  $M_1, A_1, B_1, \dots, N_1$  have to be determined. For the first method it would be impracticable to arrange the computation in such a way that the points of intersection of characteristic lines occur at the values of  $x$  and  $t$  on rectangular grids. Furthermore, for the study of unsteady free-surface flow, the second method has the advantage that it gives results directly in the form which is most likely needed and useable, such as, the hydrograph at each position along the channel and also the water surface profile at any given time. From the point of view of computer programming, the arrangement of the steps of computation for the second method appears to offer advantages over the first method. Since the values of the dependent variables at the time  $t$  in the second method are known at the predetermined points and the only information needed to be stored in the computer is the values of dependent variables at the time  $t+\Delta t$ . Therefore, this method needs only computer storage of two time lines as indicated in figure 12. Values of the dependent variables  $V$  and  $y$  of row  $J$  are known and stored while the values of  $V$  and  $y$  of row  $L$  are computed for the first time interval. After completion

of the first time interval, the values of  $V$  and  $y$  of row  $L$  are stored for the next computation at the second time interval, and the values of  $V$  and  $y$  of row  $J$  are printed out and replaced by row  $L$ .

#### Numerical solution

This section includes the details of solving the equations of unsteady free-surface flow by the method of characteristics with specified time interval,  $\Delta t$ , and specified distance interval. In this method,  $V$  and  $y$  at a point  $P$  on the  $(x, t)$  plane of figure 13 can be computed from the initial conditions or previous values of  $V$  and  $y$  at points  $A$ ,  $B$  and  $C$  with the following assumptions:

(a)  $\Delta t$  is sufficiently small that the parts of the characteristics between  $P$  and  $R$  and between  $P$  and  $S$  are considered straight lines.

(b) The slope of  $PR$  at  $P$  is the positive characteristic direction of point  $C$ ,  $(\xi_+)_C$ ; and the slope of  $PS$  at  $P$  is the negative characteristic direction of point  $C$ ,  $(\xi_-)_C$ .

Since  $x_p$  and  $t_p$  are known, the depth at point  $P$ ,  $y_p$  and the velocity at point  $P$ ,  $V_p$  are to be computed. The computation proceeds as follows:

(1) The  $x$ -coordinates of  $R$  and  $S$  are determined from the relationships of  $(\xi_+)_C$ ,  $(\xi_-)_C$  and the geometry.

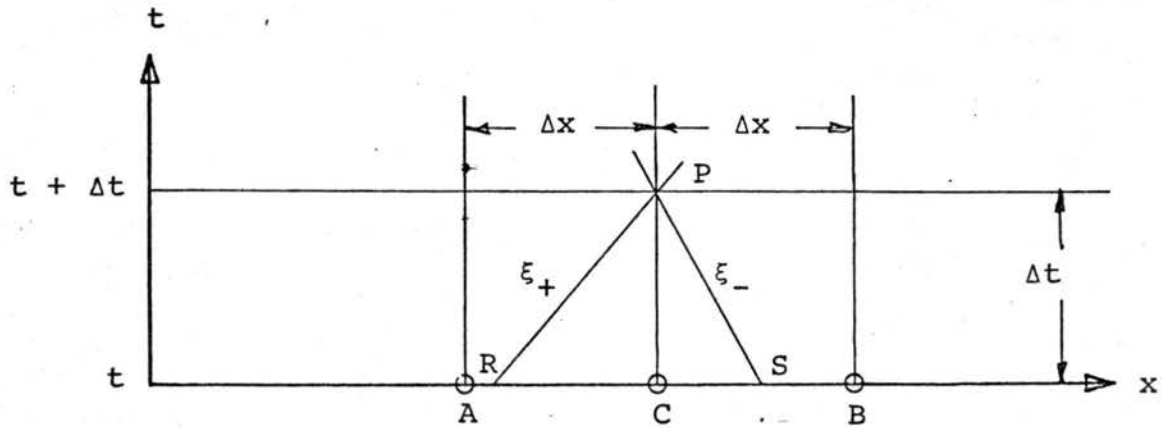
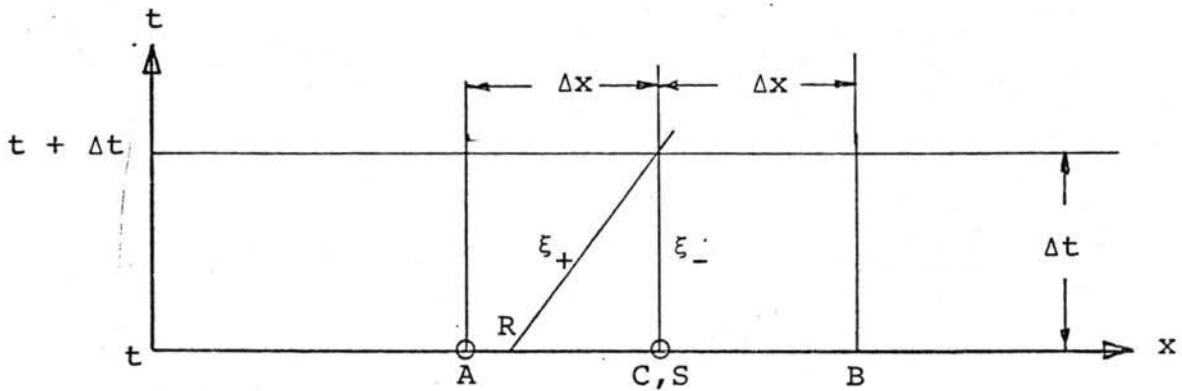
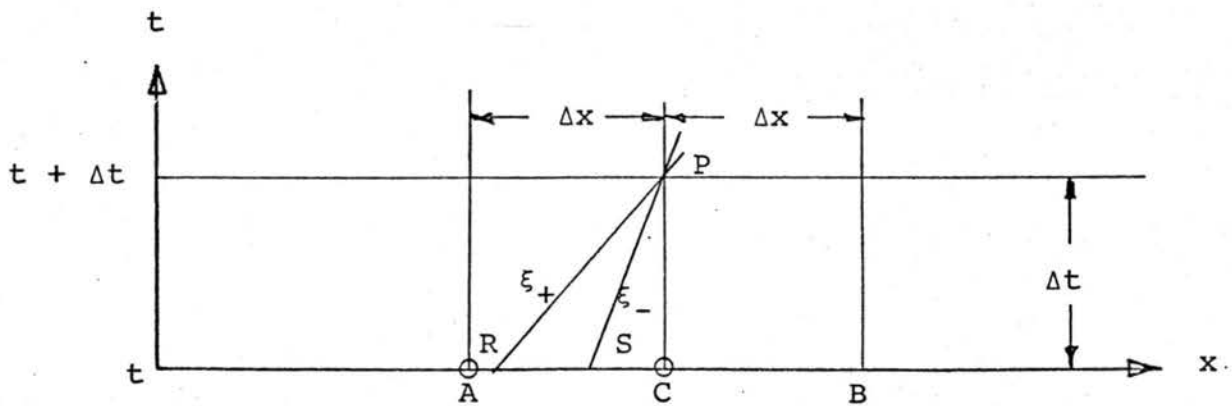
(a)  $V < \sqrt{gA/B}$ (b)  $V = \sqrt{gA/B}$ (c)  $V > \sqrt{gA/B}$ 

Fig. 13 - Rectangular grid for the solution by the method of specified intervals  $\Delta t$  and  $\Delta x$

$$t_P - t_R = (\xi_+)_C (x_P - x_R) \quad (73)$$

$$t_P - t_S = (\xi_-)_C (x_P - x_S) \quad (74)$$

where  $(\xi_+)_C$  and  $(\xi_-)_C$  are to be computed from equations (69) and (70), respectively

(2) The values of  $V_R$ ,  $V_S$ ,  $y_R$  and  $y_S$  are determined from the method of interpolation from the application of Taylor's expansion,

$$f(x+h) = f(x) + hf'(x) + \frac{h^2}{2!} f''(x) + \dots + \frac{h^{n-1}}{n!} f^{(n-1)}(x) + o(h^n) \quad (75)$$

in which in finite difference form:

$$f'(x) = \frac{f(x+h) - f(x)}{\Delta x} + o(h^2)$$

$$f''(x) = \frac{f(x+2h) - 2f(x+h) + f(x)}{\Delta^2 x} + o(h^3) \quad (76)$$

For the second order interpolation, the third and higher derivatives of equation (75) are neglected. By setting  $x = 0$  at point  $c$ , equation (75) becomes

$$V_R = V_C + \frac{V_B - V_A}{2\Delta x} (x_C - x_R) + \frac{V_B - 2V_C + V_A}{2\Delta^2 x} (x_C - x_R)^2 \quad (77)$$

$$V_S = V_C + \frac{V_B - V_A}{2\Delta x} (x_C - x_S) + \frac{V_B - 2V_C + V_A}{2\Delta^2 x} (x_C - x_S)^2 \quad (78)$$

$$Y_R = Y_C + \frac{Y_C - Y_A}{\Delta x} (x_C - x_R) + \frac{Y_B - 2Y_C + Y_A}{2\Delta^2 x} (x_C - x_R)^2 \quad (79)$$

$$Y_S = Y_C + \frac{Y_B - Y_A}{2\Delta x} (x_C - x_S) + \frac{Y_B - 2Y_C + Y_A}{2\Delta^2 x} (x_C - x_S)^2 \quad (80)$$

(3)  $V_P$  and  $y_P$  are obtained by solving simultaneously, the finite difference forms of equations (71) and (72).

$$F_{C+} (Y_P - Y_R) + G_{C+} (V_P - V_R) + S_{C+} (x_P - x_R) = 0 \quad (81)$$

$$F_{C-} (Y_P - Y_S) + G_{C-} (V_P - V_S) + S_{C-} (x_P - x_S) = 0 \quad (82)$$

in which

$$F_{C+} = [AC]_C (\xi_+)_C - [BC]_C$$

$$G_{C+} = [AB]_C$$

$$S_{C+} = [AE]_C (\xi_+)_C - [BE]_C$$

$$F_{C-} = [AC]_C (\xi_-)_C - [BC]_C$$

$$G_{C-} = [AB]_C$$

$$S_{C-} = [AE]_C (\xi_-)_C - [BE]_C$$

Solving equations (81) and (82) simultaneously,

$$Y_P = \frac{\begin{vmatrix} T_{C_+} & G_{C_+} \\ T_{C_-} & G_{C_-} \end{vmatrix}}{\begin{vmatrix} F_{C_+} & G_{C_+} \\ F_{C_-} & G_{C_-} \end{vmatrix}} \quad (83)$$

and

$$V_P = \frac{\begin{vmatrix} F_{C_+} & T_{C_+} \\ F_{C_-} & T_{C_-} \end{vmatrix}}{\begin{vmatrix} F_{C_+} & G_{C_+} \\ F_{C_-} & G_{C_-} \end{vmatrix}} \quad (84)$$

where

$$T_{C_+} = F_{C_+} Y_R + G_{C_+} V_R - S_{C_+} (x_P - x_R)$$

$$T_{C_-} = F_{C_-} Y_S + G_{C_-} V_S - S_{C_-} (x_P - x_S)$$

By this means velocities and depths at the time  $t+\Delta t$  for all points along the channel are obtained, except at the two boundary points, one being upstream and the other being downstream. These two points  $M_1$  and  $N_1$  in figure 12 can be computed from the given boundary conditions. The method of computation is described following the next section.



### Initial conditions

The necessary initial condition for the unsteady free-surface flow is that all velocities and depths of water along the channel must be known at a given time. In this study it was assumed that at the initial time, the discharge was constant throughout the reach. Thus the problem can be treated as a steady nonuniform flow. Velocities and depths along the channel are then determined by the computation of a conventional backwater or drawdown surface profile, depending on the downstream control. This procedure uses the standard step method described by Chow.

### Boundary conditions

The two governing equations for unsteady flow require two independent conditions relating velocity and depth at some location along the channel. One of these conditions is necessarily the discharge-time relationship existing at the inlet end to the section of channel under study. This relationship can be either expressed in a mathematical form or as discrete points of discharge at selected intervals of time.

The other condition which must be imposed on the problem is that of a discharge-versus-depth relationship at the downstream end as characterized by a control structure or critical depth at a free outfall. This is the condition which must exist for sub-critical flow of the base discharge.

If the base discharge is flowing in the super-critical range or is on a super-critical slope then the

boundary condition must be expressed at the inlet end. This function takes the form of a discharge versus depth relationship. This condition is somewhat difficult to visualize from a physical standpoint, however, it is a necessary condition in as much as the characteristic directions both have a positive slope and thus there can be no influence of downstream conditions on conditions upstream.

The following discussion presents a detailed analysis of these boundary conditions. It was of interest to investigate arbitrary inflow hydrographs for purposes of testing and verifying the computer program. This also provided for investigating the significance of variations in the hydraulic parameters.

(1) Upstream boundary conditions - The boundary condition at the upstream inlet is given by an inflow hydrograph,  $Q(t)$ . There is no limitation of the shape of the inflow hydrograph. A hypothetical hydrograph which has the function of Pearson Type III distribution with four parameters, was selected. The inflow  $Q$  at the time  $t$  which is designated by  $Q(t)$  may thus be described by:

$$Q(t) = Q_b + Q_o e^{-\frac{(t-t_p)}{(t_g-t_p)}} \left(\frac{t}{t_p}\right)^{t/(t_g-t_p)} \quad (85)$$

in which  $Q_b$  is the constant base inflow, (refer to fig. (14)),  $Q_o$  is the peak inflow,  $t_p$  is time from beginning of storm runoff to the peak discharge,  $t_g$  is time from

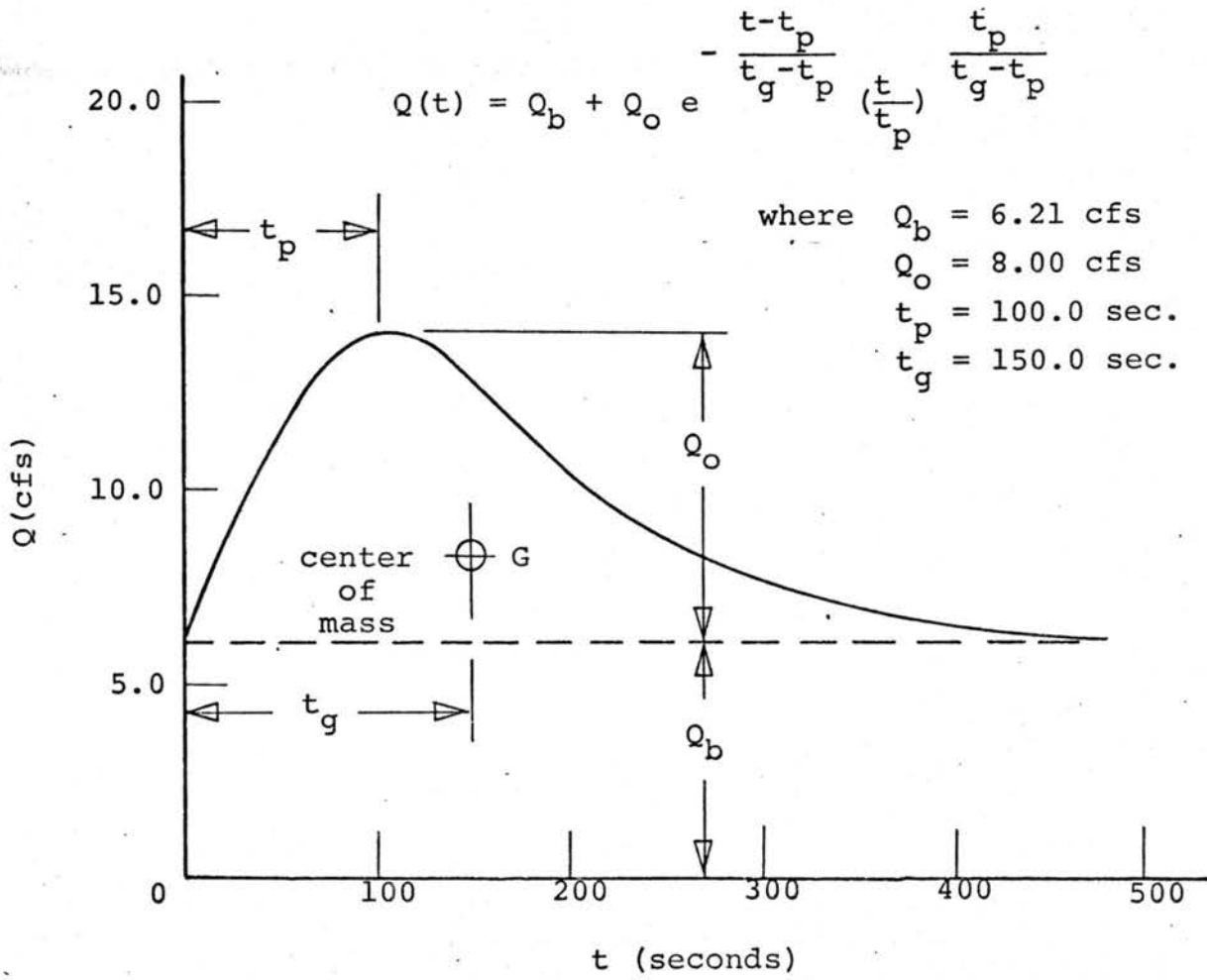


Fig. 14 - Hypothetical inflow hydrograph

beginning of storm runoff to the center of mass of storm runoff. One hydrograph with arbitrary values of  $Q_b$ ,  $Q_o$ ,  $t_p$  and  $t_g$  was used in this portion of the study. The shape and values of the parameters are shown in figure 14.

The depth and the velocity at the upstream boundary point P of figure 15 which is at  $x = 0$  and at the time  $t + \Delta t$ , can be computed from initial conditions at C and B, and the boundary conditions which are given by the inflow hydrograph,

$$AV = Q(t) \quad (86)$$

where A is the cross-section area and V is the velocity at P.

By having the same assumptions and procedure of computing velocities and depths at the other points along the channel which have been described under computational procedures, the initial conditions give the negative characteristic direction at point C. The relationship between the depth,  $y_p$ , and velocity,  $V_p$ , at point P, can be determined from equation (72). Substituting the boundary condition of equation (86) into equation (83), it gives

$$y_p = y_s - \frac{G_{C-} \left\{ \frac{Q(t)}{A} - V_s \right\} + S_{C-} (x_p - x_s)}{F_{C-}} \quad (87)$$

where A is the cross-section area at P which is a function of  $y_p$ .

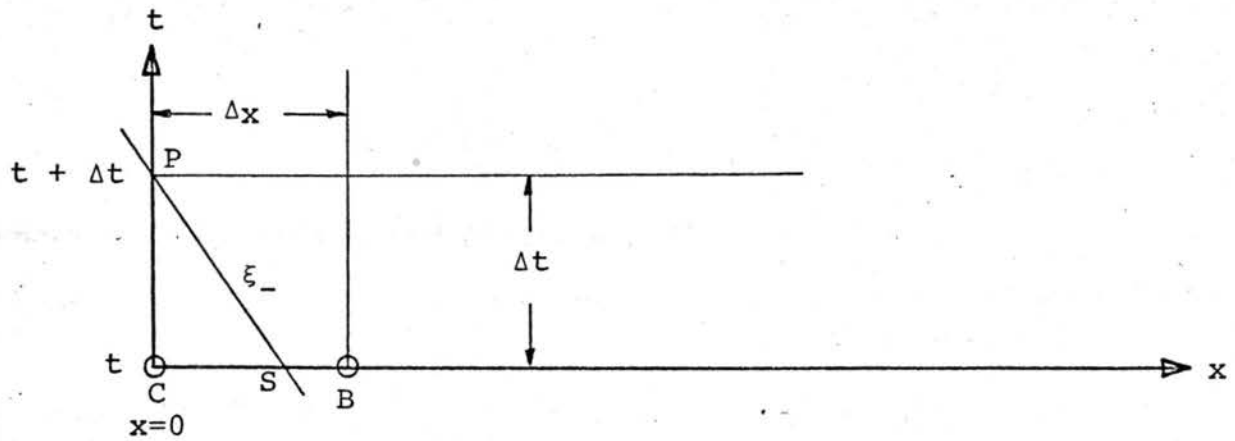
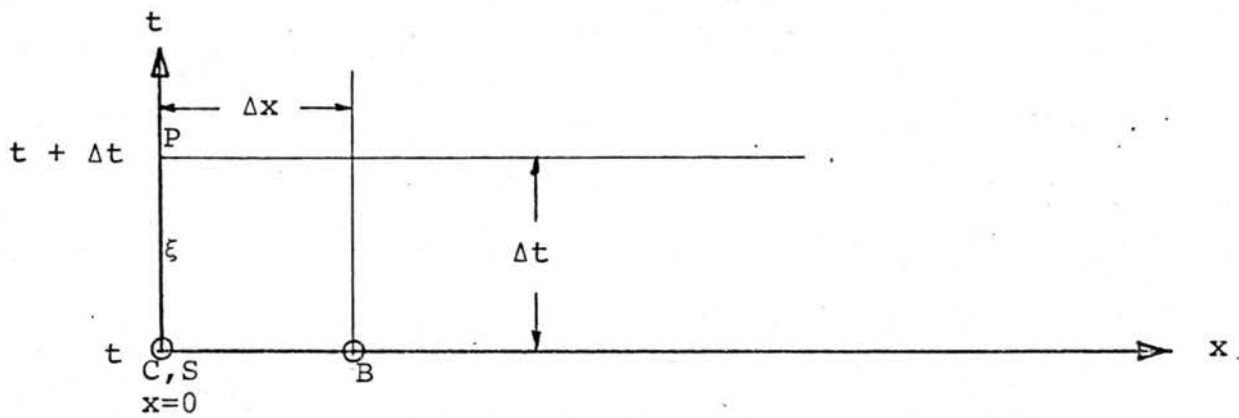
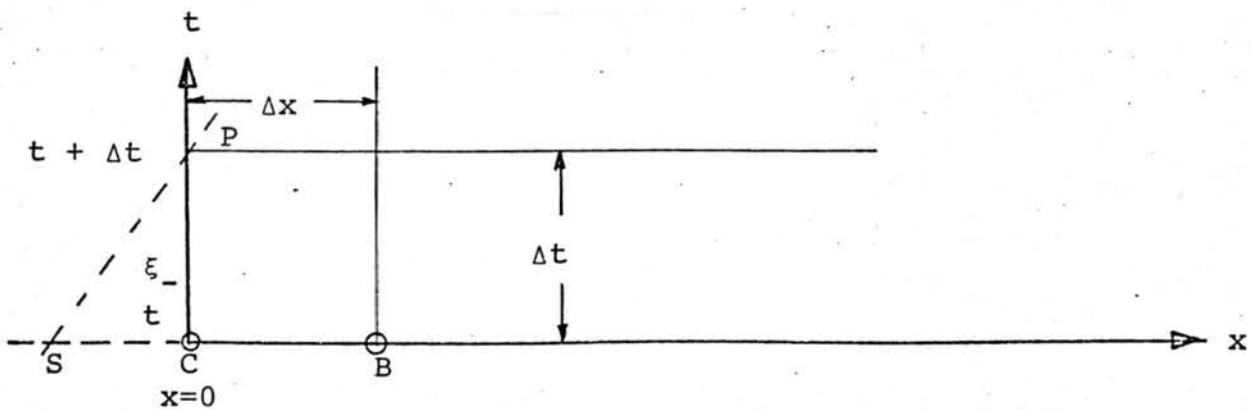
(a)  $v < \sqrt{gA/B}$ (b)  $v = \sqrt{gA/B}$ (c)  $v > \sqrt{gA/B}$ 

Fig. 15 - Upstream boundary conditions

Solving for  $y_p$  from equation (87) and substituting  $y_p$  into equation (84), then  $V_p$  can be determined. Since equation (84) is not linear in  $y_p$ , a Newton-Rhapson iteration was used for its solution.

(2) Downstream boundary conditions - The boundary conditions at downstream outlet may generally be given by a stage-discharge relationship. In this study, it was assumed a free outfall at the end of conduit. Therefore, there exists a critical flow at the downstream end. With the relationship

$$\frac{V}{\sqrt{g \frac{A}{B}}} = 1 \quad (88)$$

where  $A$  is the cross-section area and  $B$  is the top width at the downstream boundary.

Figure 16 shows the downstream boundary where critical depth occurs. For the free fall, it was assumed that the critical depth occurs at the distance 4.5 times critical depth from the end. This was also applied to the unsteady case, with the critical depth being computed from the base discharge,  $Q_b$ . Therefore, the distance,  $x_L$ , to the downstream boundary from the inlet is determined by

$$x_L = x_F - 4.5 d_c \quad (89)$$

where  $x_F$  is the total length of the channel and  $d_c$  is the critical depth for the discharge  $Q_b$ .

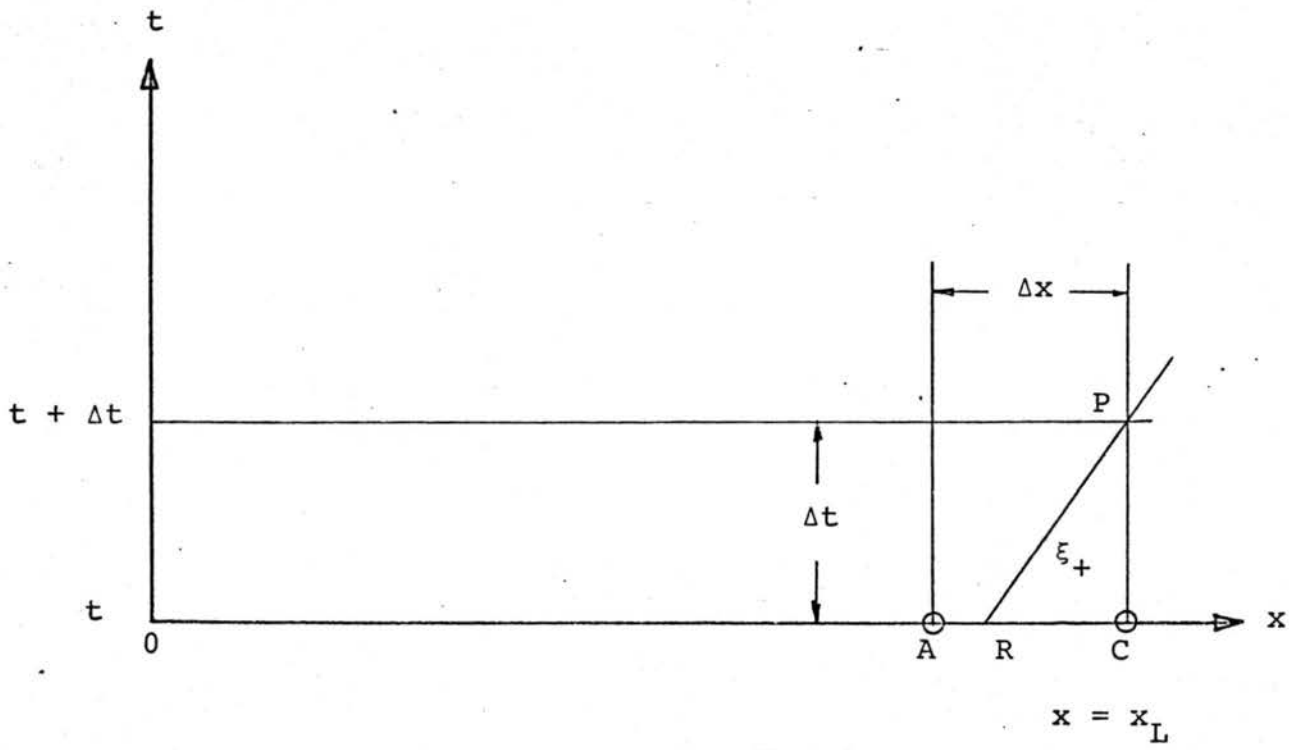


Fig. 16 - Downstream boundary conditions

The depth and the velocity at the downstream boundary point P and at the time  $t+\Delta t$ , can be computed from the initial conditions at A and C, and the boundary conditions which are given by equation (88).

By the same assumptions and procedure of computing velocities and depths at the other points along the channel, the initial conditions give the relationship between the depth,  $y_P$ , and the velocity,  $V_P$ , by equation (71). Substituting the boundary conditions of equation (88) into equation (83), results in

$$y_P = y_R - \frac{G_{C_+} \left( \sqrt{\frac{Ag}{B}} - V_R \right) + S_{C_+} (x_P - x_R)}{F_{C_+}} \quad (90)$$

where A is the cross-section area and B is the top width at P which both are the function of  $y_P$ .

Solving  $y_P$  from equation (90) and substituting  $y_P$  into equation (84),  $V_P$  can be determined. Since, equation (84) is not linear in  $y_P$ , a Newton-Raphson iteration was used for a solution.

#### Summary of the computation procedure

In solving the equations of unsteady free-surface flow (equations (19) and (20)) by the method of specified intervals the steps of computing velocity V and depth D at various times and positions along the channel are:

(1) Values of V and y at various positions along the channel for the steady-state condition of constant base flow,  $Q_b$ , are determined from a computation of the backwater curve.



- (2) The upstream boundary conditions are evaluated.
- (3) Values of  $V$  and  $y$  at the time  $t+\Delta t$  along the channel are computed from the known values of  $V$  and  $y$  at the time  $t$ .
- (4) The downstream boundary conditions are evaluated.
- (5) Steps (2), (3), and (4) are repeated as long as desired.

The details of the computation and the computer program are described in the Appendix.

## Chapter VI

## EFFECT OF VARIATIONS IN COMPUTATIONAL PARAMETERS

General

The discrepancy between a computed value and its observed value from a physical experiment is attributable to numerous sources of errors. These errors in general are the result of systematic and random errors in the observational system, and conceivable systematic errors in computational procedures. The random errors are a result of unavoidable accidental variations in physical systems. In general, one would not expect there to be random errors in the computational procedure. The discussion that follows will be concerned primarily with errors relating to the computational procedure.

Computational discrepancies emanating from this particular study are the result of;

1. The approximation of infinitesimal variations being represented by finite variations. This is a result of assuming in general, linear relationships versus the true curvilinear relationships. These are systematic. However, the propagation of this error is not readily determined since it may be positive or negative during different computations.

2. Computational errors resulting from truncation of numerical values. This is necessarily due to the limited precision of any discrete-element calculator.

3. Round off in the printed output. The printed output of any computed value from a digital computer differs from the internally generated number by the round-off of a number during conversion from the internally stored value to its printed output. The computer used for these calculations rounds off in a manner conventionally used by manual calculators.

It has been assumed that truncation and round-off errors due to the computational procedure is generally negligible as compared to those errors accompanying the finite difference approximation or the effect of physical parameters on a solution of the problem.

It is the purpose of the following discussion to present a notion as to the significance of the controllable variables in the solution of the unsteady flow equations. These are considered under the computational parameters of incremental length and incremental time interval during which the integration process proceeds.

The effect of variations in the hydraulic parameters of roughness and the velocity distribution coefficients is also discussed.

#### Effect of computation parameter $\Delta x$

The method of characteristics with specified intervals gives the complete numerical solution of the unsteady free-surface flow. The accuracy of the results depends on the size of the rectangular grids  $\Delta x$  and  $t$  of figure 12. In this section only the effect of  $\Delta x$

is discussed,  $\Delta t$  will be discussed in the next section.

If  $N$  is the number of intervals along the channel or space axis, and  $X_L$  is the length of the channel then

$$\Delta x = \frac{X_L}{N} \quad (91)$$

Since  $X_L$  was assumed to be fixed,  $N$  was arbitrarily selected as any even number, thus  $\Delta x$  was determined. The smaller  $\Delta x$ , presumably the more accurate are the results. It is also clear that the smaller  $\Delta x$ , the required computing time is greater. In compromising these two conditions to satisfy the purpose of this study, several values of  $N$  for a fixed  $X_L$  were studied.

Figure 17 shows the effect of the size of  $\Delta x$  on the depth-hydrographs at three positions along the channel. The upper figure is the depth-hydrograph at a position 50.0 feet downstream from the inlet for  $\Delta x$  of 40.91, 20.45, 10.23 and 5.12 feet corresponding to  $N$  values of 20, 40, 80, 160 respectively. The middle and lower figures are the depth-hydrographs at 410.0 feet from the inlet, and 771.7 feet from the inlet, respectively. From comparison of the depth-hydrographs of figure 17, with the given inflow discharge hydrograph of figure 14, it was found that:

(1) The critical portion of the channel for computing of the depth-hydrographs is near the outlet where

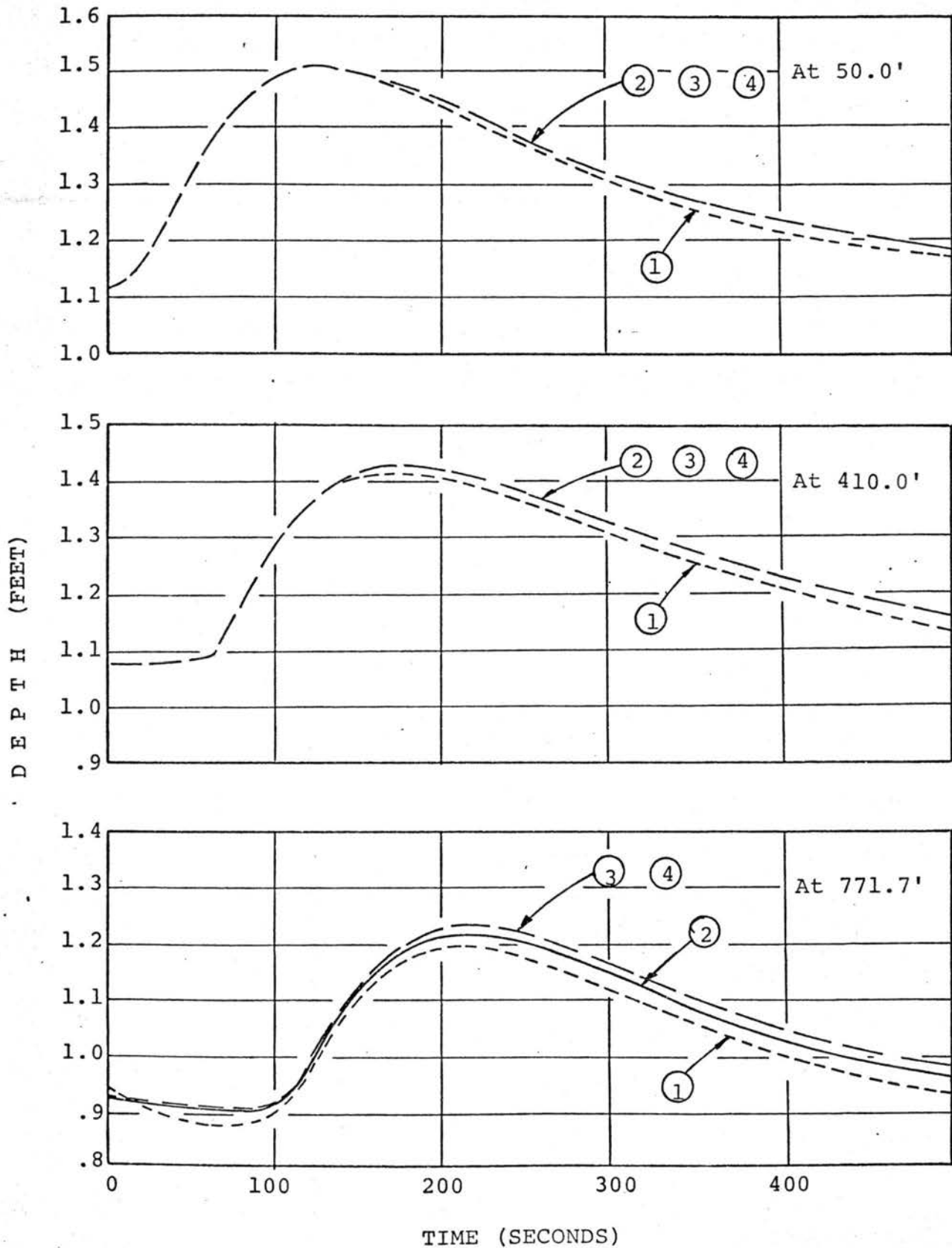


Fig. 17 - Effect of  $x$  on hydrographs at various positions along the channel: (1)  $\Delta x = 40.91'$ , (2)  $\Delta x = 20.45'$ , (3)  $\Delta x = 10.23'$ , (4)  $\Delta x = 5.12'$

there is the greatest curvature of the water surface profile. The maximum differences between the computed depths with  $\Delta x$  being 40.91 and 5.12 feet, are approximately 0.3, 0.6, 1.0 per cent of the channel diameter at 50.0, 410.0 and 771.7 feet from the inlet, respectively.

(2) There is no significant increase in accuracy of the order of 0.005 feet or 0.15 per cent of the channel diameter when  $\Delta x$  is less than 10.23 feet. Therefore,  $\Delta x$  equal to 10.23 feet, or  $N$  equal to 80, was selected in the computation for the other portions of this study.

As previously mentioned, the smaller the  $\Delta x$ , the more computing time is required. For this particular computer program, the relationship between the times required for the CDC 6600 computer and various  $\Delta x$  or  $N$  is shown in figure 18. This relationship is approximately a power function. This results from the fact that the number of computational locations in the  $x-t$  plane is proportional to the square of the  $x$ -positions, for a constant final time value.

The peak depth,  $D_{PK}$  and the time to peak depth  $T_{PK}$ , are two important parameters of describing a depth-hydrograph. These two parameters are defined and shown graphically in figure 19. The required accuracy of computed hydrograph at various positions along the channel can be measured by the percentage of the diameter of the channel for  $D_{PK}$ , and the inflow discharge-hydrograph parameter  $t_p$ , for  $T_{PK}$ .

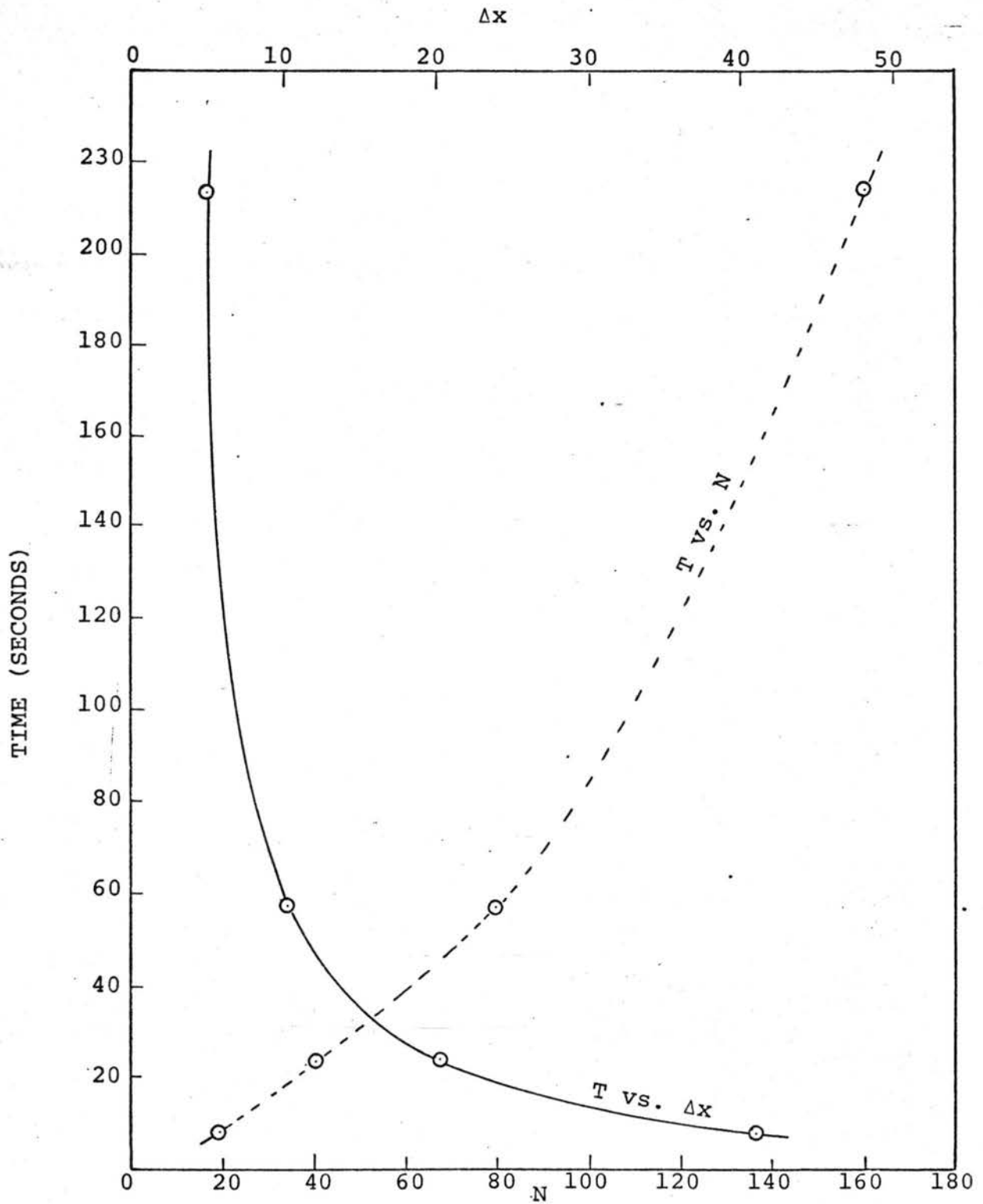


Fig. 18 - Relationship between  $N$  and  $\Delta x$  and time required for CDC 6600 computer

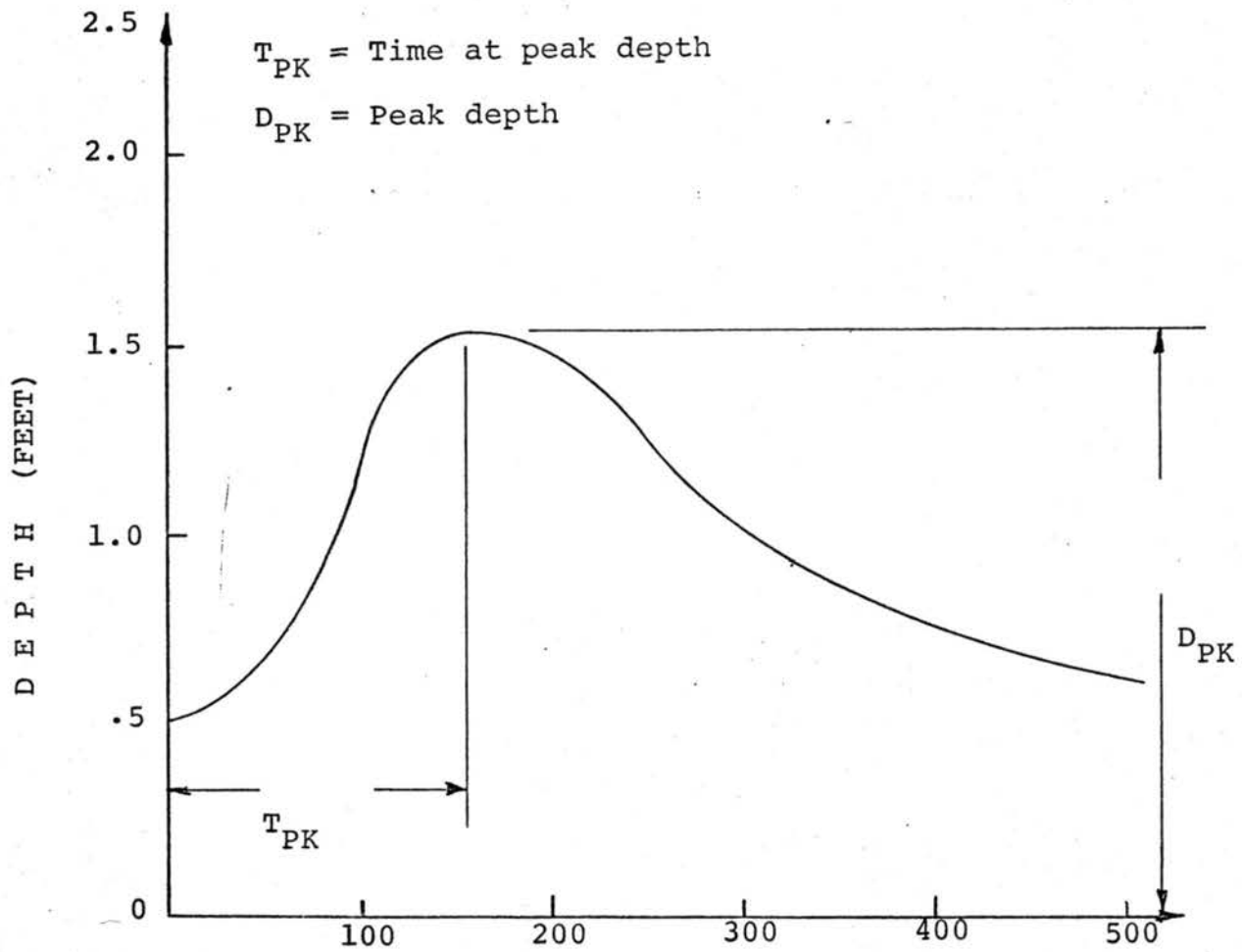


Fig. 19 - Characteristics of depth-hydrograph



From this criteria of defining an accuracy of a computed hydrograph, it was found that the percentage differences of  $D_{PK}$  to the diameter of the channel range from 0.0 to 2.1 along the channel for  $\Delta x$  from 40.91 to 5.12 feet. At the upstream there is no significant difference of  $D_{PK}$  to the diameter for different values of  $\Delta x$ . At the approximate middle of the channel there is 0.2% difference. At the downstream end, the difference was 2.1%. It was also found that there is no significant change of the percentages of  $D_{PK}$  to the diameter by reducing the sizes of  $\Delta x$  below 10.23 feet.

In using the other parameter,  $T_{PK}$ , for defining the accuracy of computed hydrographs of using different values of  $\Delta x$ , it was found that there is no significant difference of the percentages of  $T_{PK}$  to  $t_p$  on the order of 1.2 at the upstream, 2.0 at the middle, and 8.5 at the downstream. It was also found that there is no significant change of the percentages of  $T_{PK}$  to  $t_p$  (on the order 1.9) by reducing the size of  $\Delta x$  below 10.23 feet.

Tables 4 and 5 show respectively the difference in percentages of  $D_{PK}$  to the diameter of the channel with different values of  $\Delta x$ . These values at even distances (0, 50, 100, ... feet) were computed by linear interpolation from the values in the grid system of figure 12 therefore some error may have been introduced. However, the change in shape of depth-hydrograph due to varying  $\Delta x$  is

TABLE 4. DIFFERENCE IN  $D_{PK}$  COMPUTED FROM VARIOUS SIZES OF  $\Delta x$   
(in percent of channel diameter)

$\Delta x$	DISTANCE (Feet)																
(ft)	0	50	100	150	200	250	300	350	400	450	500	550	600	650	700	750	800
40.91	0	-0.02	-0.16	-0.04	-0.06	-0.08	-0.11	-0.16	-0.24	-0.31	-0.41	-0.50	-0.59	-0.70	-0.94	-1.43	-2.07
20.45	0	-0.01	-0.02	-0.02	-0.03	-0.04	-0.04	-0.06	-0.10	-0.13	-0.18	-0.22	-0.27	-0.39	-0.42	-0.66	-0.99
10.23	0	0	-0.01	0	-0.01	-0.01	-0.01	-0.02	-0.03	-0.04	-0.06	-0.08	-0.09	-0.11	-0.14	-0.23	-0.39

TABLE 5. DIFFERENCE IN  $T_{PK}$  COMPUTED FROM VARIOUS SIZES OF  $\Delta x$   
(in percent of  $t_p$ )

$\Delta x$	DISTANCE (Feet)																
(ft)	0	50	100	150	200	250	300	350	400	450	500	550	600	650	700	750	800
40.91	1.23	-0.09	0.18	0.14	-1.21	-0.36	-1.62	-2.04	-2.02	-1.81	-1.09	1.21	-0.96	-1.43	-8.47	-7.32	-3.48
20.45	-0.40	-0.09	0	0.14	0.05	-0.06	0	-0.40	-0.40	-1.81	-2.73	-0.42	-0.40	0	-3.58	-4.07	-2.04
10.23	0.41	0	0	0.14	0.05	0	0	-0.22	-0.40	0	-1.90	-0.24	-0.42	0	-1.49	-1.62	-0.41

considered to be small. Larger  $\Delta x$  produced lower and later peak depth.

Determination of computation parameter  $\Delta t$

The grid sizes of  $\Delta x$  and  $\Delta t$  in the computation scheme, figure , is limited by the characteristic lines  $\xi_+$  ,  $\xi_-$ , as shown in figure 13. The characteristic lines are expressed by equations (69) and (70).

$$\left(\frac{dt}{dx}\right)_+ = \frac{1}{V + \sqrt{gA/B}} = \xi_+$$

$$\left(\frac{dt}{dx}\right)_- = \frac{1}{V - \sqrt{gA/B}} = \xi_-$$

From figure 13, in order to have R on AC and S on CB for  $V < \sqrt{gA/B}$  and S on AC for  $V > \sqrt{gA/B}$  , for a given value of  $\Delta t$ ; the slope  $\xi_+$  and  $\xi_-$  must be minimum. This implies that V and A/B of equations (69) and (70) must be maximum. Therefore, the following two conditions must be considered.

- (1) Maximum velocity (V).
- (2) Maximum A/B for free-surface flow corresponding to the depth y being less than or equal to 0.82 time of the channel diameter.

## Chapter VII

EFFECTS OF HYDRAULIC PARAMETERS ON  
THE COMPUTED HYDROGRAPHRoughness coefficient

The evaluation of the friction slope  $S_f$  in equation (20) depends on an assumption of the energy loss rate. For the case of steady-uniform flow, this term has been well established. For unsteady flow, the general assumption has been that the energy loss rate is the same as that for steady uniform flow. Although many semi empirical relations are available, the Darcy-Weisbach was chosen for this study as being the most appropriate. This relationship may be stated as:

$$S_f = \frac{f}{4R} \frac{v^2}{2g} \quad (92)$$

For the experimental channel it was found that the Prandtl-von Karman equation for hydraulically smooth boundary was applicable for a steady flow with fully developed boundary layer flowing partly full. This equation is

$$\frac{1}{\sqrt{f}} = 2 \log (R_e \sqrt{f}) + 0.4 \quad (93)$$

where  $f$  is the Darcy-Weisbach coefficient,  $R_e$  is the Reynolds number and is defined as

$$R_e = \frac{VR}{v} \quad (94)$$

in which  $V$  is the mean velocity,  $R$  is the hydraulic radius of partly-full flow, and  $\nu$  is the kinematic viscosity of the fluid.

The purpose of this section is to present the effect of the friction coefficient  $f$  on the shape of computed hydrographs along the channel. Two conditions of the Darcy-Weisbach coefficient  $f$  being used in the computation were studied.

- (1) Single value of  $f$  was used for all conditions.
- (2) Values of  $f$  as the function of Reynolds number from Prandtl von Karman equation for hydraulically smooth boundary were used.

It was found that the Reynolds numbers of the free-surface flow for this particular channel with slopes ranging from 0.00003 to 0.00100, range from 30,000 to 360,000. According to Prandtl-von Karman equation for hydraulically smooth boundary, the Darcy-Weisbach coefficient  $f$  ranges from 0.010 to 0.016.

#### Single value of $f$ for all conditions

By investigating the shape of Prandtl-von Karman equation for the range of the Reynolds number for this particular channel, it was found that the probable values of  $f$  lie between 0.010 to 0.014. Therefore three values of  $f$ , 0.010, 0.012 and 0.014 were studied. Figure 20 shows the computed depth-hydrographs at three positions along the channel with different values of  $f$ . The upper portion of figure 20 is at 50.0 feet from the upstream inlet for the

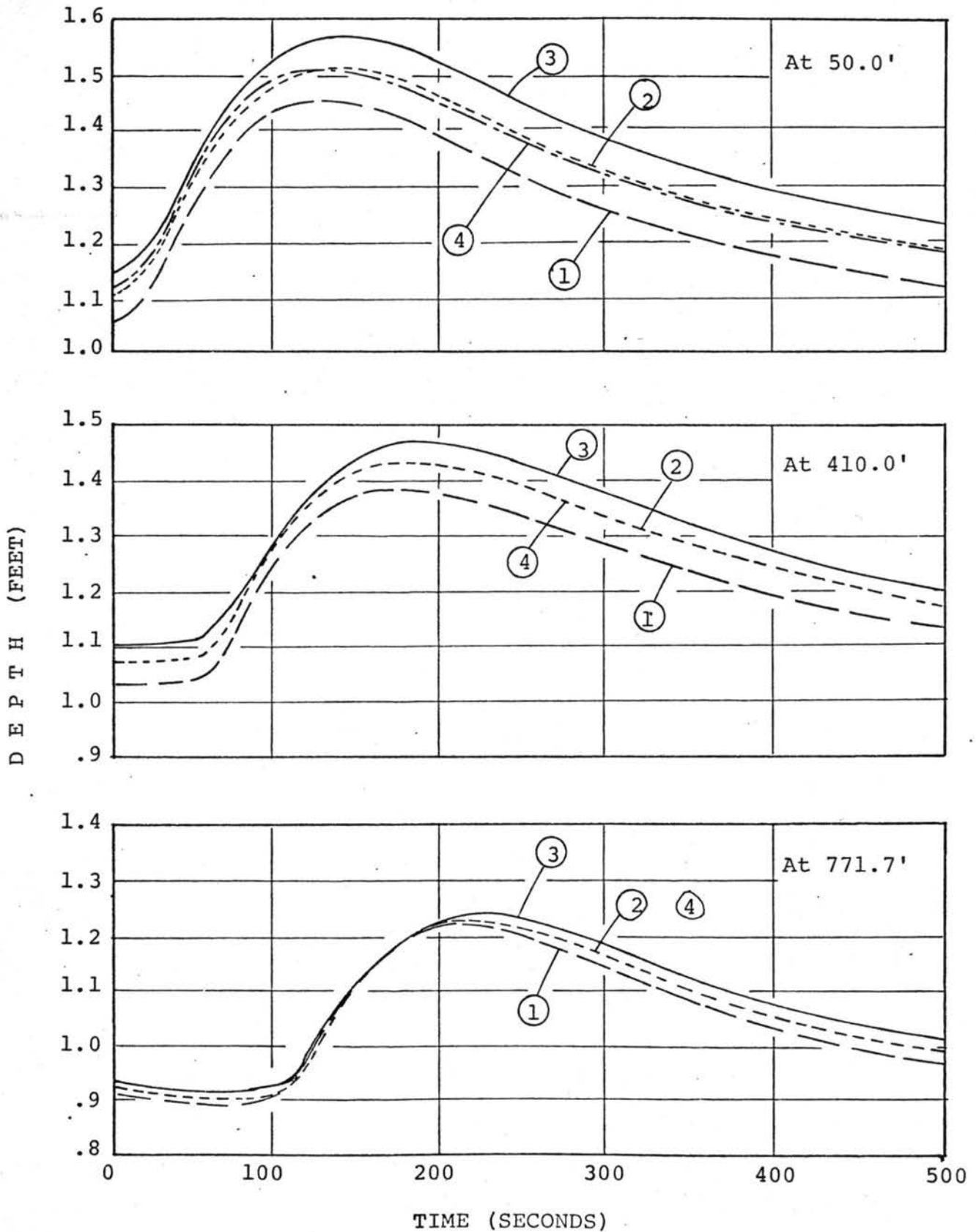


Fig. 20 - Effect of friction coefficient,  $f$ , at various positions along the channel (1)  $f = 0.010$ , (2)  $f = 0.012$ , (3)  $f = 0.014$ , (4)  $f = f(R_e)$

values of  $f$  being 0.010, 0.012 and 0.014, the middle and lower portions are at 410.0 and 771.7 feet respectively. By comparison of these three computed depth-hydrographs with  $f$  being 0.010, 0.012 and 0.014, it was found that:

(1) There are significant differences of the depth-hydrographs at 50.0 feet from the inlet on the order of 5 percent of the channel diameter between roughness values of 0.010 and 0.014. These differences decrease toward downstream due to the downstream boundary conditions being at critical flow depth, and the initial conditions being an M2 curve. This can be seen from the comparison of the differences of depths, which were computed from  $f$  of 0.010 and 0.014, at  $t = 0$  and at any time  $t$ . The differences are not the same at various times but they are proportional. Therefore it is clear that the only factor which caused these proportional differences at various times is the unsteadiness.

(2) Larger values of  $f$  produce higher values of peak depths  $D_{PK}$  along the channel. The differences of the percentages of  $D_{PK}$  to the channel diameter are 4.0 at the upstream, 3.0 at the middle and 0.1 at the downstream of the channel. Table 6 shows the ratios of  $D_{PK}$  to the channel diameter in percent at various distances along the channel with  $f$  being 0.010, 0.012 and 0.014.

(3) Smaller value of  $f$  produce earlier peak depths. The differences of the time at peak depth  $T_{PK}$  between the use of the low and high values of  $f$  are

TABLE 6.  $D_{PK}$ /CHANNEL DIAMETER, IN PERCENT ALONG THE CHANNEL  
WITH VARIOUS VALUES OF  $f$

	DISTANCE (Feet)																	
	0	50	100	150	200	250	300	350	400	450	500	550	600	650	700	750	800	
0.010	49.95	49.62	49.28	48.94	48.59	48.23	47.86	47.48	47.07	46.64	46.16	45.63	45.03	44.36	43.56	42.39	39.76	
0.012	52.11	51.72	51.32	50.91	50.50	50.08	49.64	49.19	48.70	48.18	47.61	46.99	46.29	45.50	44.51	42.99	39.81	
0.014	54.01	43.56	53.11	42.65	52.18	51.70	51.20	50.68	50.12	49.52	48.88	48.17	47.38	46.47	45.29	43.48	39.86	
$f(R_e)$	52.00	51.66	51.30	50.94	50.56	50.17	49.76	49.32	48.86	48.35	47.79	47.16	46.47	45.67	44.70	43.27	40.21	



approximately 3 percent of the inflow hydrograph parameter  $t$  at the upstream, 6 percent at the middle, and 7 percent at the downstream.

(4) There is no regular change in peak depths  $D_{PK}$  and the time at peak depth  $T_{PK}$  along the downstream portion of the channel within 100 feet from the outlet. This is due to the downstream boundary conditions being a free fall at the outlet and it was assumed that the critical depths for the unsteady flow always occur at the distance  $4.5 d_c$  from the end of the channel, in which  $d_c$  is the critical depth for the steady stage corresponding to the discharge  $Q_b$ . Table 7 shows the ratios of  $T_{PK}$  to  $t_p$  in percent at various distances along the channel with  $f$  being 0.010, 0.012 and 0.014.

$f$  as the function of Reynolds number

This section considered the Darcy-Weisbach coefficient  $f$  as the function of Reynolds number  $R_e$ . Its relationship was given by Prandtl-von Karman equation for hydraulically smooth channel, equation (93). Figure Tables 8 and 9 show respectively the comparison of the depth-hydrographs, the ratios of  $D_{PK}$  to the channel diameter, and the ratios  $T_{PK}$  to  $t_p$  with  $f$  being 0.010, 0.012, 0.014, and the function of the Reynolds number. By comparison of these figures and tables it was found that:

(1) There is no significant difference between the depth-hydrographs computed by using  $f$  equals to 0.012

TABLE 7.  $T_{PK}/t_p$  IN PERCENT ALONG THE CHANNEL  
WITH VARIOUS VALUES OF  $f$

f	DISTANCE (Feet)							
	0	50	100	150	200	250	300	350
0.010	124.03	130.47	136.90	142.78	149.29	155.89	162.63	169.05
0.012	126.21	132.55	139.51	145.26	152.38	159.07	166.14	173.19
0.014	128.20	135.06	141.31	148.00	154.87	162.16	169.38	176.23
f (R)	123.03	128.65	134.89	141.24	147.57	153.91	160.24	166.59

f	DISTANCE (Feet)							
	400	450	500	550	600	650	700	750
175.48	182.74	189.18	196.44	203.70	211.78	222.39	216.93	208.00
180.16	186.51	194.37	202.23	210.09	217.95	221.07	218.11	211.86
183.10	190.74	198.39	206.82	214.45	220.89	222.45	219.40	215.58
172.92	180.07	186.42	193.74	201.50	209.50	215.47	213.21	206.59

TABLE 8. DIFFERENCE IN  $D_{PK}$  COMPUTED FROM  $f$  AS THE FUNCTION OF REYNOLDS NUMBER AND VARIOUS VALUES OF  $f$  (in percent of channel diameter)

	DISTANCE (Feet)																
	0	50	100	150	200	250	300	350	400	450	500	550	600	650	700	750	800
0.010	-2.05	-2.04	-2.02	-2.00	-1.97	-1.94	-1.90	-1.84	-1.79	-1.71	-1.63	-1.53	-1.44	-1.31	-1.14	-0.88	-0.45
0.012	0.11	0.06	0.02	-0.03	-0.06	-0.09	-0.12	-0.13	-0.16	-0.17	-0.18	-0.17	-0.18	-0.17	-0.19	-0.28	-0.40
0.014	2.01	1.90	1.81	1.71	1.62	1.53	1.44	1.36	1.26	1.17	1.09	1.01	0.91	0.80	0.59	0.21	-0.35

TABLE 9. DIFFERENCE IN  $T_{PK}$  COMPUTED FROM  $f$  AS THE FUNCTION OF REYNOLDS NUMBER AND VARIOUS VALUES OF  $f$  (in percent of  $t_p$ )

	DISTANCE (Feet)																
	0	50	100	150	200	250	300	350	400	450	500	550	600	650	700	750	800
0.010	1.00	1.82	2.01	1.54	1.72	1.91	2.39	2.46	2.56	2.67	2.76	2.70	2.18	2.28	6.92	3.72	1.41
0.012	4.68	3.90	4.62	4.02	4.81	5.16	5.90	6.60	7.24	6.44	7.95	8.49	8.57	8.45	5.60	4.90	5.27
0.014	5.17	6.41	6.42	6.76	7.30	8.25	9.14	9.64	10.18	10.67	11.97	13.08	12.93	11.39	6.98	6.19	8.99

and  $f$  as the function of  $R_e$  in the order of 0.3 percent of the channel diameter.

(2) The differences in peak depth  $D_{PK}$  computed by using  $f$  equals to 0.012 and  $f$  as the function of  $R_e$  are less than 0.4 percent of the channel diameter at all distances along the channel and they are shown in Table 8.

(3) The differences in the time at peak depth  $T_{PK}$  computed by using  $f$  equal to 0.012 and  $f$  as the function of  $R_e$  range from 3.9 to 8.5 percent of  $t_p$  along the channel. These differences at various distances along the channel are shown in Table 9.

(4) A single value of  $f$  being 0.012 gives the smallest differences in depth-hydrographs comparing with  $f$  being as the function of  $R_e$ .

TA7 ~~copy 2~~

C6

CER69/70-1B

COPY 2

C. E. - R. R. COPY

UNSTEADY FLOW IN A STORM  
DRAINAGE SYSTEM

Part B  
HYDRAULIC PARAMETERS, BOUNDARY,  
AND INITIAL CONDITIONS

A. H. Barnes  
U. S. Bureau of Public Roads  
Contract No. CPR-11-3584

ENGINEERING RESEARCH  
AUG 18 '70  
FOOTHILLS RESEARCH ROOM

Colorado State University  
Engineering Research Center  
January 1970

CER69-70AB1B

UNSTEADY FLOW IN A STORM  
DRAINAGE SYSTEM

Part B

HYDRAULIC PARAMETERS, BOUNDARY,  
AND INITIAL CONDITIONS

A. H. Barnes

U. S. Bureau of Public Roads  
Contract No. CPR-11-3584

Colorado State University  
Engineering Research Center  
January 1970

CER69-70AB1



U18401 0575324

## Chapter VIII

## EXPERIMENTAL EVALUATION OF THE HYDRAULIC PARAMETERS

A. General

The St. Venant equations of unsteady flow relate the dependent variables of depth and velocity to the dependent variables of space and time through the geometric and hydraulic parameters of the system. The geometric characteristics of the system were presented in Chapter III. The discussion to follow presents an evaluation of the hydraulic parameters of the experimental system.

The governing equations (19) and (20) are repeated for ease of reference:

$$\text{Continuity: } \frac{A}{VB} \frac{\partial V}{\partial x} + \frac{\partial y}{\partial x} + \frac{1}{V} \frac{\partial y}{\partial t} = 0$$

$$\text{Momentum: } \frac{V}{g} \frac{\partial V}{\partial x} + \frac{1}{g} \frac{\partial V}{\partial t} + \frac{\partial y}{\partial x} = S_o - S_f$$

This mathematical form of the phenomena includes only one term ( $S_f$ ) which involves the hydraulic characteristics of the system.

The assumptions leading to this form includes the simplification of uniform velocity distributions. If the non-uniformity of velocity distribution is considered, the momentum equation would be written as

$$\alpha \frac{V}{g} \frac{\partial V}{\partial x} + \frac{\beta}{g} \frac{\partial V}{\partial t} + \frac{\partial y}{\partial x} = S_o - S_f \quad (95)$$

in which  $\alpha$  and  $\beta$  are velocity distribution factors defined as

$$\beta = \frac{\int v^2 dA}{V^2 A} \quad (96)$$

and

$$\alpha = \frac{\int v^3 dA}{V^3 A} \quad (97)$$

These coefficients are commonly referred to as the Boussinesq and Coriolis coefficients respectively.

Considerable experimental effort was devoted in this study to define as accurately as possible the hydraulic parameters of  $S_f$ ,  $\beta$  and  $\alpha$ .

## B. Hydraulic Resistance

### 1. Introduction

The resistance to motion of open channel flow is expressible in numerous forms. Foremost among those commonly in use are the Chezy, Manning, Colebrook-White, Hazen-Williams, and Darcy-Weisbach equations.

The committee for Hydromechanics of the Hydraulics Division of the American Society of Civil Engineers (6) recommended the use of the Darcy-Weisbach expression for future normalization of resistance data. Thus, this study has evaluated and expressed boundary resistance in terms of the Darcy-Weisbach equation

$$S_f = \frac{f}{D} \frac{V^2}{2g} \quad (98)$$



in which  $S_f$  is the slope of the energy gradient,  $f$  is the Darcy-Weisbach friction factor,  $V$  is the mean velocity, and  $D$  is the diameter of the equivalent pipe. For channel cross-sections other than circular the diameter ( $D$ ) is customarily replaced by four times the hydraulic radius ( $4R$ ). The validity of this replacement may be questioned for open-channel flow. However, for lack of a better length parameter describing the velocity gradients and hence the shear stresses, the hydraulic radius is commonly used. Equation (98) is thus rewritten as

$$S_f = \frac{f}{R} \frac{V^2}{8g} \quad (99)$$

in which  $R$  is the hydraulic radius defined as the cross-section area divided by the wetted perimeter ( $A/P$ ).

The Darcy-Weisbach friction factor  $f$ , has been demonstrated to be a function of the Reynolds number, relative roughness, and channel shape:

$$f = (R_e, k/d, \text{shape}) \quad (100)$$

The form of this equation depends in turn on the range of the Reynolds number, the relative roughness and of course, the shape of the channel cross-section. For hydraulically smooth boundaries and for Reynolds number greater than 25,000 the Prandtl-Von Karman equation,

$$\frac{1}{\sqrt{f}} = a \log_{10} (R_e \sqrt{f}) + b \quad (100)$$

relates the friction factor to Reynolds number. The constants "a" and "b" may be determined experimentally. Their values will depend on the form of the Reynolds number length parameter. For open channel applications, it is convenient to express the Reynolds number as

$$R_e = \frac{VR}{v} \quad (101)$$

in which  $R$  is the hydraulic radius of the given cross-section. Equation (100) then becomes:

$$\frac{1}{\sqrt{f}} = 2 \log_{10} (R_e \sqrt{f}) + 0.4 \quad (102)$$

In the case of a circular cross-section flowing full, the appropriate length dimension in the Reynolds number is the diameter. In this case equation (100) takes the familiar form

$$\frac{1}{\sqrt{f}} = 2 \log_{10} (R'_e \sqrt{f}) - 0.8 \quad (103)$$

Within practical limits of Reynolds numbers for specific applications it is convenient to use a simplified form of the  $f:R_e$  relationship. The evaluation of  $f$  given  $R_e$  from equation (100) introduces unnecessarily excessive computations. Thus, it was desirable to develop a simplified relationship of the form:

$$f = c R_e^d \quad (104)$$

in which "c" and "d" are experimentally determined constant.

The purpose of this study was a) to confirm the hydraulically smooth nature of the experimental pipe, b) develop a simplified expression for the friction factor and c) determine the effect of an assumed constant friction factor as compared to a Reynolds number related values.

## 2. Experimental Facilities and Observations

The experimental facility on which the studies were conducted consisted of a nominal 3-foot diameter, 822 ft.-long circular conduit. The pipe material was 1/2" thick rolled-steel plate with a longitudinal weld, which was located at the crown. The approximate 20' lengths of the pipe were welded except at three positions where bolted connections were made. Extreme care was taken to insure that all inside welds and joints were carefully ground and the depressions filled with a plastic material and subsequently smoothed to insure a uniformly smooth surface. The inside surface was sand blasted and painted with two coats of a rust preventative paint. The entire 822 ft. of pipe was supported on inclined rails at approximately 20 foot intervals which permit the pipe to be moved along an inclined plane to any slope between 0 and approximately 4 per cent. A transition from the supply line to the movable 3'-diameter pipe permitted changes from one slope to another. The discharge was controlled by a 26" diameter motor-operated ball-valve. The flow was

indicated by means of orifice plates with opening-diameter to pipe-diameter ratios of either 0.35, 0.50, or 0.70. The outlet end of the pipe either discharged freely or was controlled by means of a gate with needles whose number and position determined the depth of flow at the downstream end.

Water surface elevations were determined by means of hook gage readings taken in gage wells located at 16 positions along the pipe. These wells were connected to the invert of the pipe through a flexible hose. The piezometer openings were 1/16" diameter. At each position there were a sufficient number of openings to insure a reasonable response time for each well.

The invert slope of the pipe was carefully determined by means of a precise self-leveling level with an optical micrometer which permitted measurements to the invert to approximately the nearest 1/1000 of an inch. Readings were taken approximately every 20 feet and a least-square determination of the mean slope was computed. If the maximum deviations at any point exceeded approximately 3/100 of a foot, from the mean line, adjustments to the pipe invert were made.

The discharge corresponding to the desired depth of flow was estimated from previous observations and established at the orifice. The downstream control gate was adjusted to produce that type of a backwater or drawdown curve as desired. Due to the length of time required for steady state conditions to develop, it was not practical to adjust the downstream

control until a constant depth developed throughout the length of the pipe. Thus, several conditions of non-uniform flow were established both above and below the normal depth. Hook gage readings at the various piezometer locations were made at approximately 15 minute intervals until such time as the readings reproduced themselves.

The hook gage readings, gage zeros, and invert elevations were then transferred to punch cards along with the steady discharge rate and pipe slope. All data was then analyzed by means of a digital computer and is described hereafter.

### 3. Experimental Analysis

Calculation of f. The total energy per unit weight flowing for a channel partially full is defined as:

Total energy = Invert elevation + Depth of flow + Velocity head. The difference in successive values of total energy divided by the distance between conduit stations represents the energy loss rate. This loss rate with the average hydraulic radius and average of the velocity heads at the ends of the reach were then substituted into the resistance equation to evaluate the friction factor  $f$ . Stated mathematically

$$f = \frac{8g R_{av.}}{(V^2/2g)_{av.}} \frac{E_2 - E_1}{\Delta x}$$

The Darcy-Weisbach friction factor  $f$  was computed initially by considering the slope of the energy gradient between the successive piezometer locations shown in

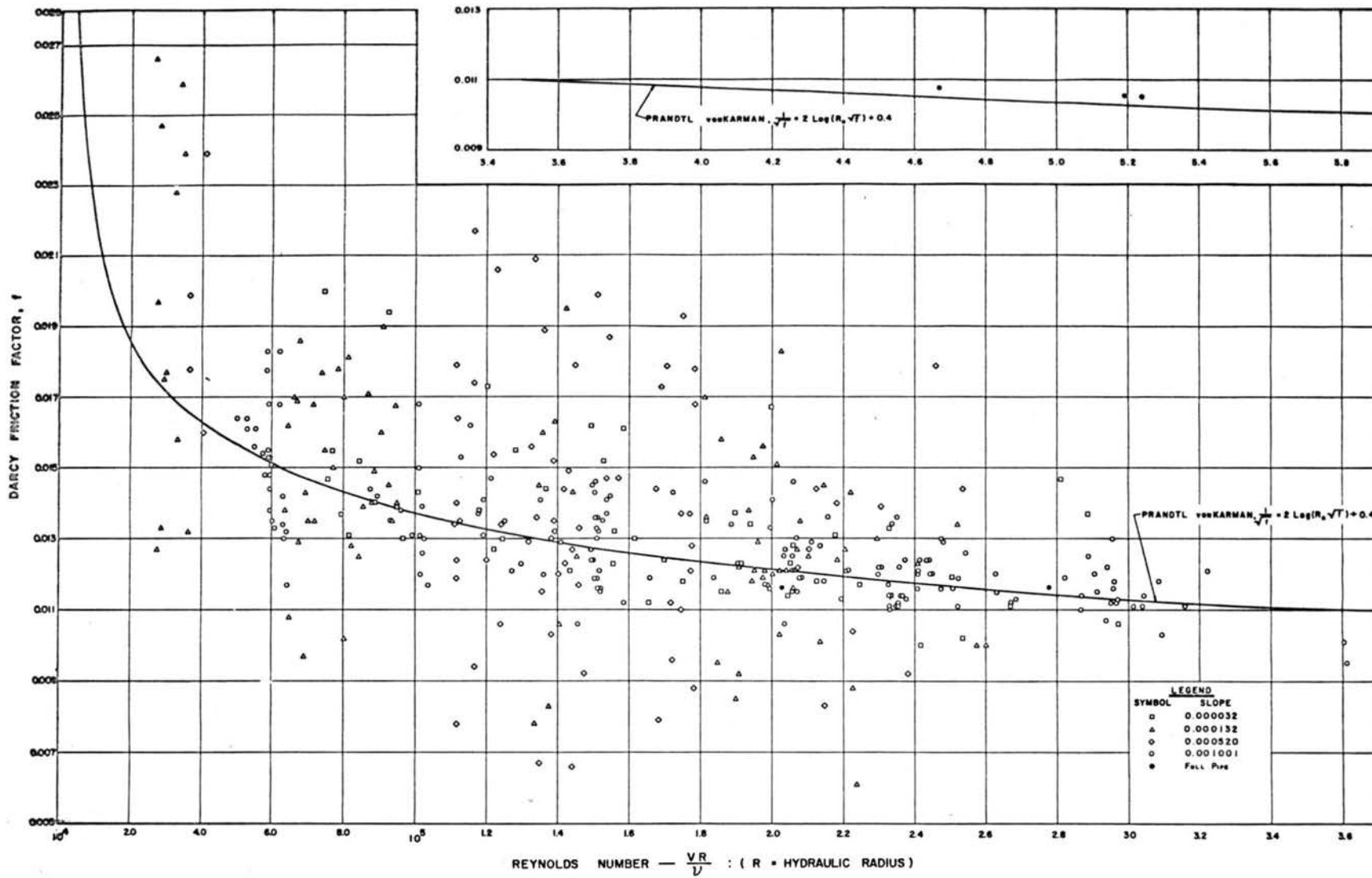
Table 11. The computations were performed by means of the digital computer thus eliminating any personal bias in establishing slope of the gradient. A plot of these  $f$  values versus Reynolds number, however, indicated a wide scatter of values as shown in Figure 21. This was largely due to experimental errors in observation of depth and the influence of the unavoidable bottom irregularity on the surface water profile, which produced excessive variation in the energy slopes. It was apparent that a mean slope throughout a longer reach was necessary to define the friction factor. Therefore, the values of energy at specific peizometer locations were plotted and the best estimate to the slope was graphically determined. A least square fit of these data would not produce the desired results, in as much as in those regions of high curvature of the water surface, the slope of the energy gradient did not remain constant. This is due to the fact that the friction factor varies with Reynolds number and thus with depth. The slope of the energy gradient was taken as that slope most representative of the particular flow conditions. In order to determine the average value of the hydraulic radius and the average velocity head, the following procedure was used. The depth of flow at the limits of the reach were computed, based on the energy indicated by the uniform gradient. These two depths were then averaged from which the average area, average hydraulic radius, average velocity and the average velocity head were computed.

TABLE 11

PIEZOMETER LOCATIONS

<u>No.</u>	<u>Distance From Upstream End</u>	<u>Incremental Distance</u>
1	20.00	
2	100.00	80.00
3	197.00	97.00
4	308.40	111.40
5	406.10	97.70
6	509.60	103.50
7	613.20	105.60
8	707.20	94.00
9	772.20	65.00
10	802.20	30.00
11	807.25	5.05
12	812.25	5.00
13	816.25	4.00
14	819.10	3.00
15	820.70	1.60
16	821.70	1.00

---



VARIATION OF FRICTION FACTOR  $f$  WITH REYNOLDS NUMBER

FIG. 21



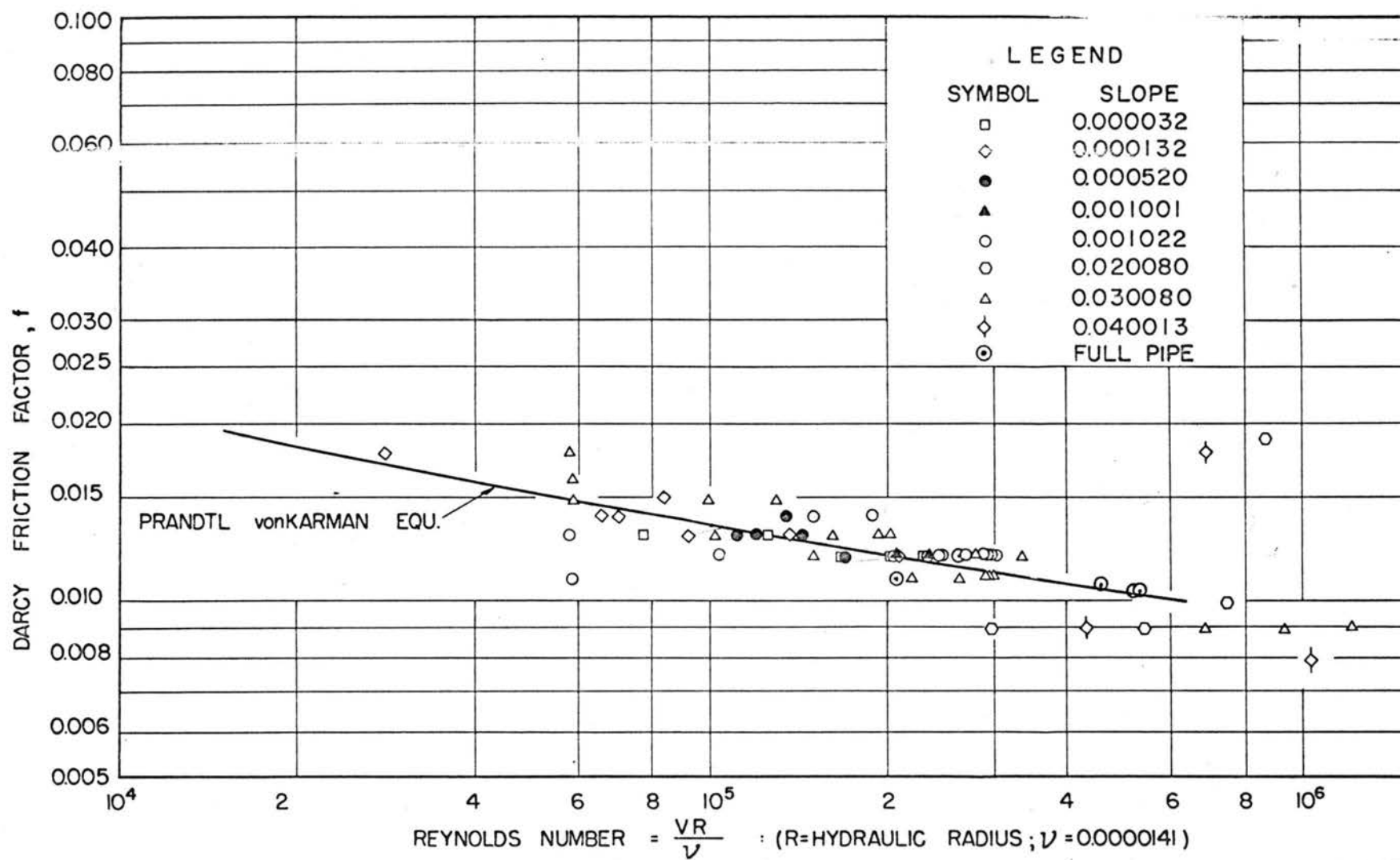
The results of these computations is presented in Figure 22. It is apparent that the experimental points computed from average energy slopes demonstrate a improved correlation with Reynolds number. The points tend to cluster around the Prandtl-von Karman smooth boundary equation.

The plotted points represent the results of experimental ranges of depth from 0.56 to 2.6 feet or depth-to-diameter ratios of 0.19 to 0.89. The discharges varied from 2.25 to 72.0 cfs. The corresponding Reynolds number range is from approximately  $3 \times 10^4$  to  $1 \times 10^6$ .

For the data as shown in Figure 22, the values of the constants "a" and "b" in the equation (100) were determined to be 0.1434 and 2.075 respectively. These are to be compared with the Prandtl-von Karman equation constants of 0.4 and 2.0 for free-surface smooth boundary flow. The mean deviation of the roughness values for this data was 0.00167 with a standard deviation of 0.0024.

For economization of computing time, constants in the equation (104) were evaluated and used in subsequent computer programs. These constants "c" and "d" were 0.10939 and -0.17944 respectively.

It should be noted that the refinement of expressing the friction factor as a function of Reynolds number does not significantly affect the results. A representative constant value may be used with no appreciable differences in results.



VARIATION OF FRICTION FACTOR  $f$  WITH REYNOLDS NUMBER BASED ON THE  
SLOPE REPRESENTATIVE OF THE ENTIRE LENGTH

FIG. 22

### 3. Effect of Depth on f

The Darcy-Weisbach friction factor has been demonstrated to be a function of Reynolds number as well as geometry. Although, it is not possible to separate the effects of velocity and geometry there have been attempts in the past<sup>1</sup> to demonstrate the effect of depth alone on friction factors.

A similar attempt was made in this study to compare results with previously published results.

The procedure is as follows. The Darcy-Weisbach equation relates friction factor, depth, velocity and slope in the general form

$$F_1(f, y, V, S) = 0$$

The Prandtl-von Karman equation relates the variables of friction factor, depth, velocity, and properties of the fluid. This may be generalized as

$$F_2(f, y, V, \nu) = 0 \quad .$$

By eliminating the velocity  $V$  between these two expressions,

$$F_3(f, y, S, \nu) = 0 \quad ,$$

---

<sup>1</sup>"Design of Sewers to Facilitate Flow," by Thomas R. Camp, Sewage Works Journal, Vol. 18, No. 1., January, 1946.

thus for a given slope (S), kinematic viscosity ( $\nu$ ), and depth of flow ( $y$ ), the friction factor ( $f$ ) may be computed.

A plot of the results of this computation for two extremes of slope and two representative equations relating to Reynolds number is shown in Figure 23.

It is significant to note that the theoretical as well as experimentally observed values lie appreciably below the curve proposed by Camp.

Based on Figure 23, it may be seen that the friction factor expressed by the Darcy-Weisbach ( $f$ ) for various depths does not differ from that for full pipe by more than  $\pm 10\%$  percent. Thus, it may be seen that the variation of  $f$  with depth is less than the error of estimation of  $f$  for flow within approximately the upper  $2/3$  of the pipe. Within the lower  $1/3$  an increased friction factor would be appropriate.

#### 4. Effect of Measurement Errors on Calculation of the Friction Factor

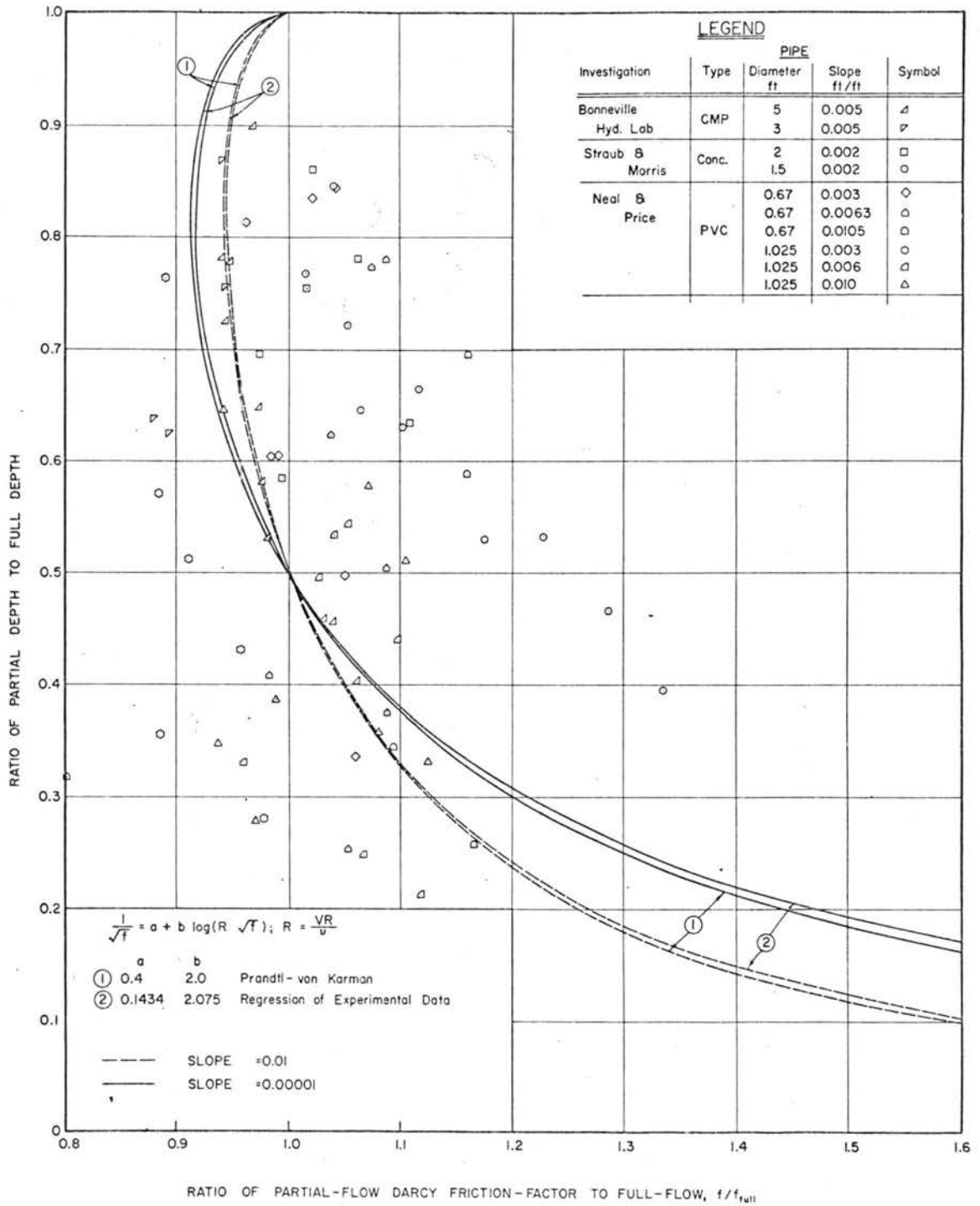
In order to estimate the effect of observational errors on the computed value of roughness factor, certain assumptions are required. For the ensuing analysis the following assumptions will be made:

Diameter ( $D$ ) = 3 feet

Depth ( $y$ ) = 1.5 feet  $\pm$  0.005 ft.

Slope ( $S$ ) = 0.001  $\pm$  .00001

Discharge ( $Q$ ) = 30 cfs  $\pm$  0.3



VARIATION OF FRICTION FACTOR WITH DEPTH OF FLOW  
IN A CIRCULAR CROSS - SECTION

FIG. 23

for the equation of the friction factor,

$$f = \frac{8gSRA^2}{Q^2}$$

the error equation for independent errors will be:

$$\sigma_f^2 = \left( \frac{\partial f}{\partial S} \sigma_S \right)^2 + \left( \frac{\partial f}{\partial (RA^2)} \sigma_{RA^2} \right)^2 + \left( \frac{\partial f}{\partial Q} \sigma_Q \right)^2$$

in which  $\sigma$  (sigma) is the random error in the corresponding quantity. The section factor term is evaluated by means of Figure 5. Substitution of the indicated values:

$$\sigma_f^2 = (2.681 \times 0.00001)^2 + (0.000286 \times 0.01)^2 + (.0001787 \times 0.3)^2$$

$$\sigma_f = \pm 6 \times 10^{-5}$$

For the nominal friction factor of 0.012 for this conduit, this estimated absolute error  $6 \times 10^{-5}$  represents a 0.5 percent error.

From the above it will be noted that the largest contribution to error in the friction factor is due to error in discharge. Whereas an error in section factor ( $RA^2$ ) resulting from an error in the depth determination has the least effect. The error in friction factor of  $\pm 6 \times 10^{-5}$  is substantially less than the standard error determined from the data plotted in Figure 22. The error of  $\pm 6 \times 10^{-5}$  in the friction factor may then represent a lower limit for practical evaluations.

## 5. Conclusions

From theoretical and analytical consideration of the experimental data it can be concluded that:

- (1) The conduit boundary used in this study is hydraulically smooth.
- (2) Estimations of friction factors from short reaches may result in significant error.
- (3) The friction factor may be represented by the equation:

$$f = 0.10939 R_e^{-0.17944}$$

in a Reynolds number range of  $3 \times 10^4$  to  $10^6$ .

- (4) A Darcy-Weisbach friction factor of 0.012 is representation of this boundary.
- (5) Roughness values for any depth in a circular cross-section can be estimated based on the full pipe roughness.
- (6) The assumption of constant roughness values may be in error by a maximum of  $\pm 10$  percent for depths in excess of one-third in diameter.
- (7) The roughness for full-pipe flow is not representative of roughness for depths less than one-third full.
- (8) The relative error in determining the Darcy-Weisbach friction factor may be in error by as much as 0.5 for variations in depth of .33% at one-half full-pipe flow.

## C. Velocity Distribution Coefficients

### 1. Introduction

Equations (96) and (97) define the velocity distribution coefficients based on momentum and energy consideration respectively. This may be demonstrated as follows:

Momentum due to a motion of an incompressible fluid may be expressed as

$$M = \int_A \rho v |v| dA \quad .$$

One-dimensional considerations permit

$$M = \int_A v^2 dA \quad .$$

An approximation to this evaluation of one-dimensional momentum flux is to represent it in terms of the mean velocity  $V$  as,

$$M = (\text{constant}) V^2 A \quad .$$

The constant is then defined as

$$\beta = \frac{\int_A v^2 dA}{V^2 A} \quad (105)$$

The kinetic energy per unit weight may be correspondingly developed into the form:

$$\alpha = \frac{\int v^3 dA}{V^3 A} \quad (106)$$



Thus the general form of a velocity distribution factor may be represented by

$$\phi = \frac{\int v^n dA}{V_A^n} \quad (107)$$

where  $n$  takes on integer values. For  $n$  equal to one,  $\phi$  is of course, one, by the definition of mean velocity. Values of  $n$  and 2 and 3,  $\phi$  is the momentum ( $\beta$ ) and energy ( $\alpha$ ) velocity coefficients.

The above form permits the evaluation of the effect of velocity distributions and the interrelation of  $\alpha$  and  $\beta$ .

Consider the time average velocity at a point as represented by

$$v = (1+k) V \quad (108)$$

where  $V$  is the mean time-average-velocity in the cross-section and  $k$  is plus or minus depending on position. Since  $V$  is defined as

$$V = \frac{1}{A} \int v dA = \frac{1}{A} \int (1+k)V dA = \frac{V}{A} \int dA + \frac{V}{A} \int k dA ,$$

$k dA$  must be zero.

Then expressing beta and alpha in terms of  $k$

$$\beta = \frac{\int v^2 (1+k)^2 dA}{V_A^2} = 1 + \frac{1}{A} \int k^2 dA$$

and

$$\alpha = \frac{\int V^3 (1+k)^3 dA}{V_A^3} = 1 + \frac{3}{A} \int k dA + \frac{3}{A} \int k^2 dA + \frac{1}{A} \int k^3 dA$$

Since  $\int k dA$  is zero;

$$\alpha = 1 + \frac{3}{A} \int k^2 dA + \frac{1}{A} \int k^3 dA \quad (11)$$

Thus from equations (109) and 110) the following conclusions may be noted:

- a. The larger the deviation of the point velocities from the mean, the larger will be the values of the coefficients.
- b. For the cases where the maximum velocity is less than twice the mean velocity the absolute value of  $k$  will be less than one and thus

$$0 < \left| \int k^3 dA \right| < \int k^2 dA$$

- c. As the value of  $k$  approaches zero, the  $k^3$  will become less significant compared with the  $k^2$  term and hence as an approximation

$$\frac{\alpha-1}{\beta-1} \approx 3 \quad (111)$$

The values of alpha and beta determined experimentally in this study tend to demonstrate this relationship.

## 2. Evaluation of the Velocity Distribution Coefficients

Equation (107) suggests several methods of evaluating  $\phi$ . One method would be a direct integration of a given velocity distribution function, the other two are the graphical method and the numerical method of integration by using point velocities as observed in a specific flow through a replacement of integrals by summations.

a. Direct Integration Method - The direct integration of equation (107) depends upon a knowledge of the explicit function of velocity as related to position. Such equations for fully developed turbulent flow are available for only certain limiting cases of boundary configuration.

For the case of an infinitely wide open-channel with two-dimensional flow the following equation<sup>1</sup> has been determined experimentally for velocity distributions outside the boundary layer:

$$\frac{(v-V)}{V\sqrt{f}} = 2 \log_{10} \frac{y}{y_0} + 0.88 \quad (112)$$

in which

$v$  is the point velocity at position  $y$  ,  
 $V$  is the mean velocity in the depth  $y_0$  and  
 $f$  is the Darcy-Weisbach roughness factor in the Darcy-Weisbach equation. Substituting the value of  $v$  from equation (112) into equation (107), and integrating

---

<sup>1</sup> Rouse, H. Elementary Mechanics of Fluids, John Wiley and Sons.

in the limits to  $y_0$ ,  $\phi$  for values of  $n$  equal to 2 and 3 become, respectively,

$$\phi_2 = \beta = 1.0 + 0.755 f + 0.023 \sqrt{f} + \delta_1 (f) \quad (113)$$

$$\phi_3 = \alpha = 1.0 + 2.263 f + 0.035 \sqrt{f} - 1.284 f \sqrt{f} + \delta_2 (f) \quad (114)$$

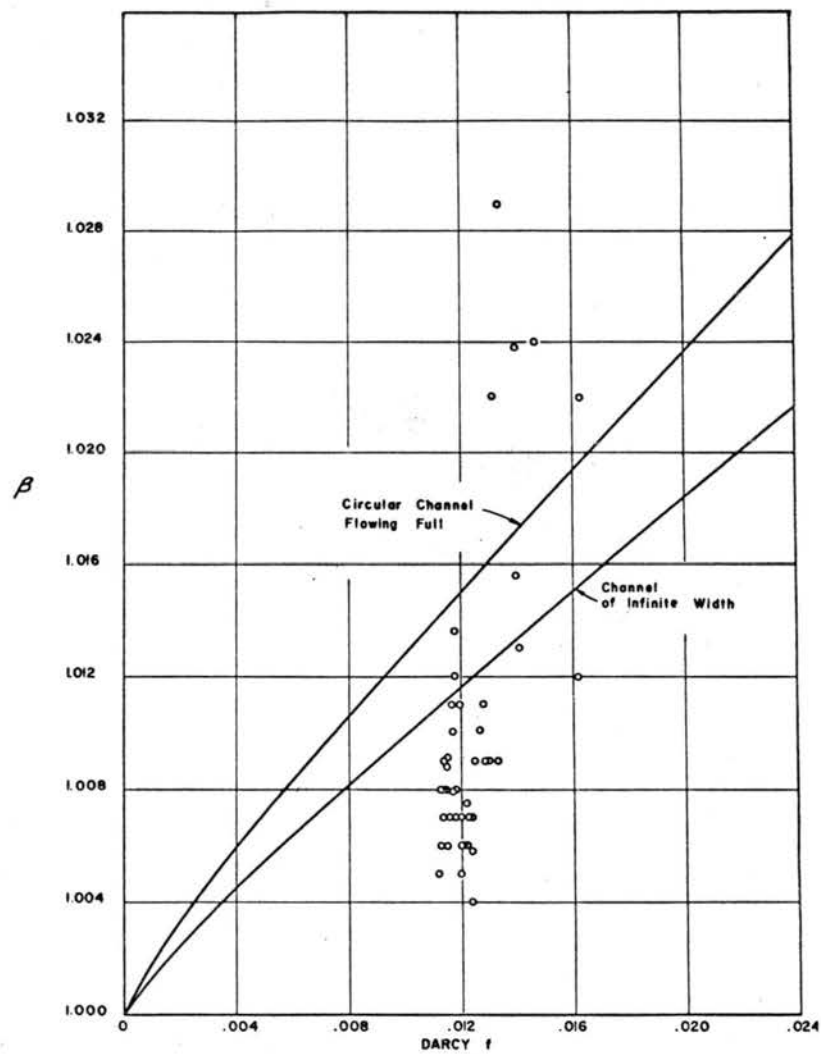
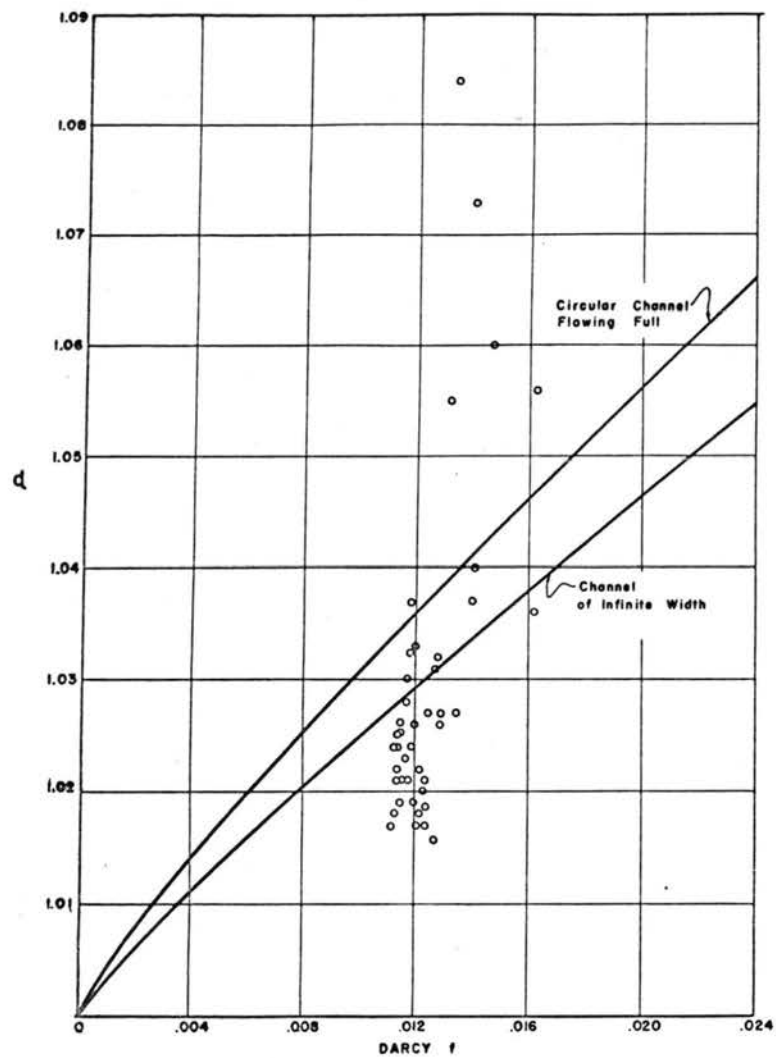
In which the  $\delta$  functions are the result of integrating from the limit of the boundary layer rather than from the solid boundary. In each case, however, these functions are negligible in their effect on the respective distribution factors. The plots of these equations are shown in Figure 21 as well as the observed values. Within this range of friction factors, the  $\alpha$  and  $\beta$  coefficients are approximately linear for values of  $f$  greater than 0.004.

It is interesting to note that the ratio of  $(\alpha-1)/(\beta-1)$  lies approximately between 2.5 and 2.6 as shown in Figure 24. The fact that the factor 3 of equation (111) does not agree with the range 2.4 - 2.5 as developed for the logarithmic velocity distribution in infinitely wide channel indicates that for that case at least, the integral of the  $K^3$  term must be significant as well as negative. This point will be discussed later.

For the case of a full circular-pipe flow, the following equation<sup>2</sup> has been determined experimentally as the velocity distribution function:

---

<sup>2</sup> Elementary Fluid Mechanics-Rouse-Wiley Publishing Co.



VELOCITY DISTRIBUTION COEFFICIENTS VERSUS FRICTION FACTOR  $f$

FIG. 24

$$\frac{v-V}{V\sqrt{f}} = 2 \log_{10} \left( \frac{y}{r_0} \right) + 1.32 \quad (115)$$

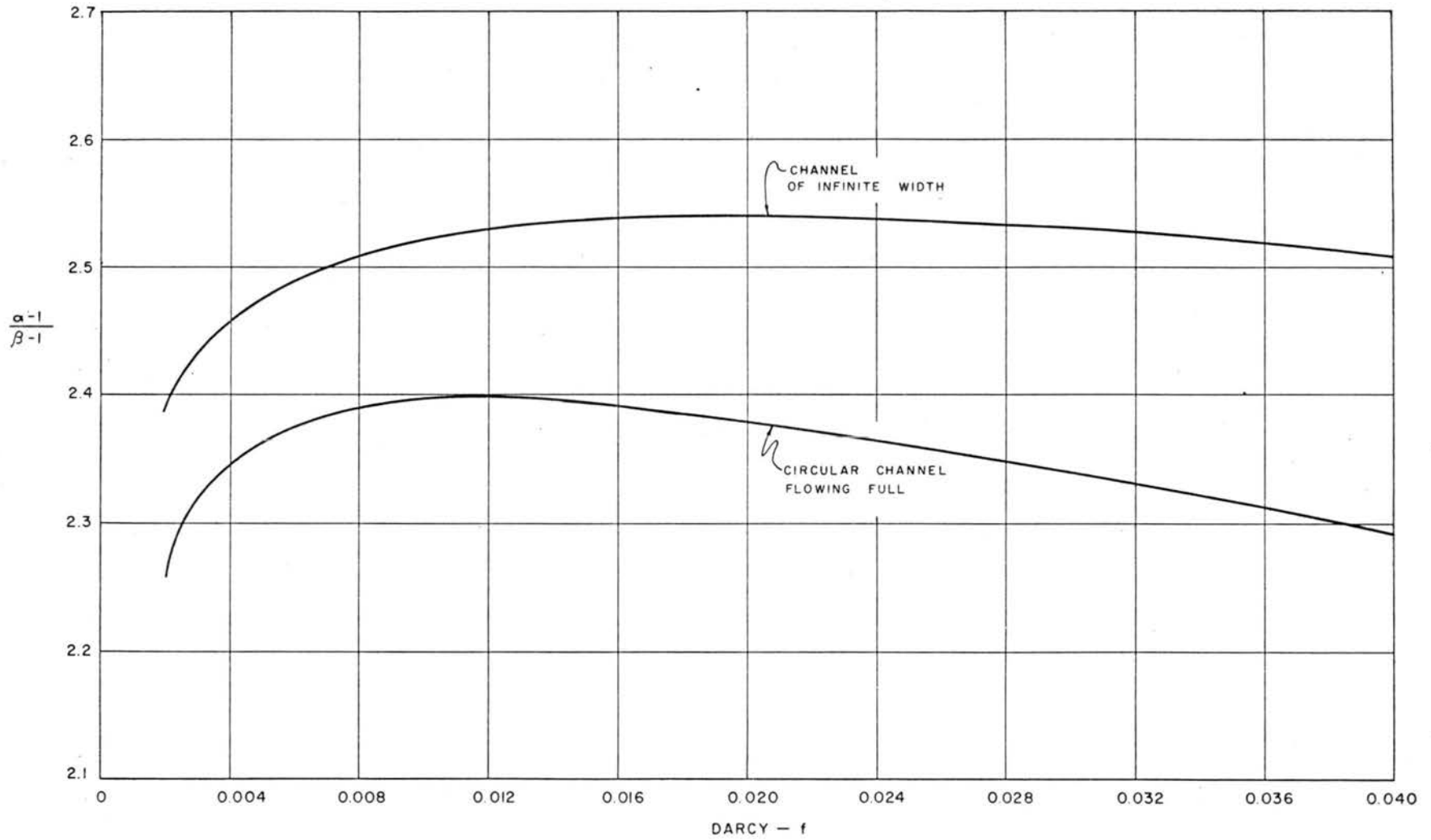
in which the variables are defined, and  $r_0$  is the radius of the conduit. Substituting the value of  $v$  from equation (115) into equation (107) and solving for  $\phi$  within the limits of boundary thickness ( $\delta$ ) and  $r_0$  one obtains, respectively.

$$\beta = \phi_2 = 1 + 0.034 \sqrt{f} + 0.941 f \quad (116)$$

$$\alpha = \phi_3 = 1 + 0.051 \sqrt{f} + 2.828 f - 2.685 f \sqrt{f} \quad (117)$$

The values of alpha and beta from equations (116) and (117) are also plotted in Figure 24. These curves approach straight lines for large  $f$ -values. Similarly as in the case of an infinitely wide open-channel, the alpha and beta coefficients only depend on the friction factor. In this case the ratio  $(\alpha-1)/(\beta-1)$  lies also approximately between 2.3 and 2.4 (see Fig. 25).

As the velocity distributions are not symmetrical around the mean velocity, the integral  $\int k^3 dA$  may be negative if the absolute values of the negative  $k$  are much greater than the positive  $k$  values. This is the case for the velocity distributions of both the infinitely wide open-channel and the full pipe flow as given by equations (112) and (115) while using the lower limit zero. Therefore, the fact that  $(\alpha-1)/(\beta-1)$  is smaller than three should be expected.



RELATIONSHIP OF  $\alpha$  AND  $\beta$  VERSUS FRICTION FACTOR  $f$

FIG. 25

The comparison of curves of equations (116) and (117) with the corresponding curves for beta and alpha of equations (113) and (114) in Figure 24, indicates that for channels in which the side walls affect substantially the velocity distributions (or when the height of sides is of the same order of magnitude as the width of the bottom of channel), the  $k$  values on the average are greater than the  $k$  values for infinitely wide open-channels. Hence, the alpha and beta coefficients are greater for full circular channel flow.

As the velocity distributions of partly-full flows through the circular conduits can be considered as the cases which are between the velocity distributions of an infinitely wide open channel and a full flow circular conduit, the above equations (113), (114), (116), and (117) give an indication or a range of the expected velocity coefficients for the partly full pipes as they change with the friction factor  $f$ .

b. Graphical Integration Method - The classical method for computing the velocity distribution coefficients from observed data is to plot the position of observed velocities along with the velocity at that point. The lines of equal velocity (isovels) are then drawn by interpolation between the known velocities. The area between successive incremental velocities is then determined, for example, by planimeter. The summation of the individual areas times the mean velocity in the area taken to the



appropriate power (2 or 3), provides the numerical integration of the numerator of beta and alpha.

c. Numerical Integration Method- A numerical integration method was developed around the point velocity measurement equipment.

Time average point velocities were measured by Ott laboratory current meters. Five meters were mounted on a rod which was supported at the center of the rod. The rod support was at the pipe centerline and could rotate to place the meters in any angular position. The meters were spaced along the rod to sample equal circumferential areas. The meters were placed at the minimum recommended spacing distance from the pipe wall. The meter support rod was positioned at angular intervals of 10 degrees. Thus the point velocities were observed at five radial positions and as many 10 degree intervals as required to sample the circular segment.

The numerical data processing was based on the observations that the velocity distributions along radial directions were smooth (in general) and could be approximated by third degree polynomials. Velocity distributions along circumferential arcs of constant radius were also smooth and could be approximated by third degree polynomials.

The computer procedure was:

1. Fit a third degree polynomial to the observed velocities at a fixed radius of the form:

$$v_r = a_r + b_r \theta + c_r \theta^2 + d_r \theta^3$$

2. For a given angular position, fit a third degree polynomial to the computed velocities along the radial direction of the form:

$$v_{\theta} = a_{\theta} + b_{\theta}r + c_{\theta}r^2 + d_{\theta}r^3$$

3. For the velocity expression at a given angular position, the integrals of  $v_{\theta}dA$ ,  $v_{\theta}^2dA$  and  $v_{\theta}^3dA$  could easily be developed in which  $dA$  was the area represented by a 10-degree sector to the free water surface.

4. The results of step 3 divided by the appropriate relation of mean velocity and total area resulted in the alpha and beta factors.

The root-mean-square difference between the observed velocities and the computed velocities based on the polynomial fitting procedure was computed for each cross section. These values are reported for the early runs.

The calibration equations for each current meter and propeller were written into the program so that the velocity was computed from the given data before the fitting was begun.

### 3. Results

Several comparisons of test conditions and observational procedures were made to identify these effects on the computed velocity distributions.

These considerations were reproducibility; and effect of depth, location along the conduit, number of point velocities, and length of time for observing the mean

velocity. The results of these evaluations are presented in Table 12. The table presents in the following order, the run identification (RUN NO.), discharge in cfs as measured by the inflow orifice (DISCH), the depth of flow in ft. at the measurement cross-section (DEPTH), the cross-sectional area in  $\text{ft}^2$  (AREA), the mean-velocity in ft per sec, based on the measured discharge (VEL), the number of point velocity observations (N), the average number of point observations per square foot. (N/A), the ratio of the mean velocity based on the measured discharge to the mean velocity obtained by integrating the observed velocities (GAMMA), the momentum velocity factor (BETA), the energy velocity factor (ALPHA), the root-mean-square difference between the observed velocities and the velocities in ft per sec. computed from the polynomial fits (STDDEV), and the time interval in sec. for observing the mean velocity.

These results are not intended to be conclusive. They do provide however, a measure of respective effect and possible reliability of the overall results.

The following general observations should be pointed out.

- a. The root-mean-square (STDDEV) as a percent of the mean velocity is of the order of 1 percent.
- b. The computed mean velocity compared with the measured mean is larger in general by less than 3 percent.
- c. The relationship between the alpha and beta coefficients conforms to eq. (111).

Table 12

## EFFECTS ON VELOCITY DISTRIBUTION COEFFICIENTS

1	2	3	4	5	6	7	8	9	10	11	12
RUN NO	DISCH	DEPTH	AREA	VEL	N	N/A	GAMMA	BETA	ALPHA	STDDEV	TIME
REPRODUCIBILITY											
X7MH2A	26.340	2.210	5.449	4.834	146	26.79	1.006	1.006	1.018	0.051	
X7MH2B	26.340	2.139	5.268	5.000	144	27.34	1.008	1.005	1.017	0.081	
X10M2A	16.130	1.612	3.797	4.248	91	23.96	1.025	1.011	1.030	0.041	
X10M2B	16.130	1.597	3.754	4.297	91	24.24	1.028	1.011	1.029	0.035	
EFFECT OF DEPTH											
X12M2A	8.260	1.064	2.209	3.739	33	14.94	0.920	1.066	1.123	0.037	
X6MH2A	13.450	1.442	3.301	4.075	70	21.21	1.037	1.005	1.019	0.037	
X10M2A	16.130	1.612	3.797	4.248	91	23.96	1.025	1.011	1.030	0.041	
X9MH2C	20.520	1.888	4.588	4.472	122	26.59	1.025	1.006	1.019	0.047	
X8MH2X	24.240	2.079	5.110	4.744	140	27.40	1.002	1.009	1.027	0.042	
X7MH2A	26.340	2.210	5.449	4.834	146	26.79	1.006	1.006	1.018	0.051	
EFFECT OF POSITION IN DIRECTION OF FLOW											
X8MH1A	23.930	2.110	5.192	4.609	148	28.51	1.011	1.009	1.025	0.058	
X8MH2X	24.240	2.079	5.110	4.744	140	27.40	1.002	1.009	1.027	0.042	
X8MH3A	24.240	2.063	5.067	4.783	144	28.42	1.007	1.007	1.021	0.048	
X9MH1C	20.520	1.909	4.647	4.416	123	26.47	1.014	1.006	1.019	0.094	
X9MH2C	20.520	1.888	4.588	4.472	122	26.59	1.025	1.006	1.019	0.047	
X9MH3C	20.520	1.880	4.566	4.494	121	26.50	1.024	1.008	1.024	0.046	
X10M1A	16.130	1.617	3.812	4.231	94	24.66	1.006	1.010	1.028	0.044	
X10M2A	16.130	1.612	3.797	4.248	91	23.96	1.025	1.011	1.030	0.041	
X10M3A	16.130	1.611	3.795	4.251	91	23.98	1.017	1.011	1.030	0.045	
EFFECT OF NUMBER OF POINT VELOCITIES											
X8MH2X	24.240	2.079	5.110	4.744	140	27.40	0.999	1.010	1.028	0.029	
X8MH2Y	24.240	2.094	5.150	4.707	73	14.18	1.012	1.008	1.022	0.049	
EFFECT OF LENGTH OF TIME OF OBSERVATIONS											
X6MH2A	13.450	1.442	3.301	4.075	70	21.21	1.037	1.005	1.019	0.037	30
X6MH2A	13.450	1.442	3.301	4.075	70	21.21	1.034	1.005	1.020	0.028	60
X6MH2A	13.450	1.442	3.301	4.075	70	21.21	1.032	1.005	1.019	0.021	90
X6MH2A	13.450	1.442	3.301	4.075	70	21.21	1.031	1.005	1.020	0.018	120
X6MH2A	13.450	1.442	3.301	4.075	70	21.21	1.031	1.005	1.019	0.018	150
X6MH2A	13.450	1.442	3.301	4.075	70	21.21	1.032	1.006	1.020	0.101	180
X8MH2X	24.240	2.079	5.110	4.744	140	27.40	1.002	1.009	1.027	0.042	30
X8MH2X	24.240	2.079	5.110	4.744	140	27.40	0.999	1.010	1.028	0.029	60
X8MH2X	24.240	2.079	5.110	4.744	140	27.40	0.999	1.009	1.027	0.029	90
X8MH2X	24.240	2.079	5.110	4.744	140	27.40	0.999	1.009	1.027	0.030	120
X8MH2X	24.240	2.079	5.110	4.744	140	27.40	0.998	1.009	1.027	0.030	150
X8MH2X	24.240	2.079	5.110	4.744	139	27.20	0.996	1.009	1.027	0.030	180
X8MH2Y	24.240	2.094	5.150	4.707	73	14.18	1.012	1.008	1.022	0.049	30
X8MH2Y	24.240	2.094	5.150	4.707	74	14.37	1.013	1.008	1.022	0.039	60
X8MH2Y	24.240	2.094	5.150	4.707	73	14.18	1.011	1.008	1.023	0.032	90
X8MH2Y	24.240	2.094	5.150	4.707	73	14.18	1.010	1.008	1.024	0.029	120
X8MH2Y	24.240	2.094	5.150	4.707	73	14.18	1.010	1.008	1.024	0.030	150
X8MH2Y	24.240	2.094	5.150	4.707	73	14.18	1.010	1.008	1.024	0.026	180

- d. The variation of the velocity distributions coefficients within any one of five effect categories is insufficient to detect the effect for the sample size. This is to say that the experimental and computational errors overshadow the effect of varying the experimental conditions.

Based on the above preliminary results, an extended series of observations were made to relate the distribution coefficients to depth and mean velocity. The observations were made at mid-position along the 822 ft. conduit. Each point velocity was averaged over a 60-second period.

The results of these observations are presented in Table 13. The discussion of the results in the following section.

#### 4. Discussion of Results

It is to be expected that the velocity distribution coefficients would differ with changes in those parameters which determine the velocity profiles. Those parameters which have primary effect on the velocity profile are the geometric form of the cross section, the properties of the fluid, the condition of the boundary surface (resistance) and the mean velocity. All of these variables are encompassed in Reynolds number ( $VR/\nu$ ) and the Darcy-Weisbach roughness factor ( $f$ ).

The Darcy-Weisbach roughness factor is related to the Reynolds number; hence one would expect to be able to predict alpha and beta having the relationship of the beta

Table 13. Velocity distribution factors

Designation	Slope	Depth* ft	Hydraulic Radius ft	Q cfs	Mean Velocity fps	$Re = \frac{VR}{\nu}$ $\times 10^5$	$\alpha$	$\beta$	Friction Factor f
S1-4	0.000032	2.926	0.732	5.610	0.834	0.4	1.036	1.012	0.0162
S1-7		1.547	0.757	11.980	3.320	1.653	1.017	1.004	0.0124
S1-8		1.779	0.818	16.040	3.748	2.017	1.019	1.006	0.0120
S1-9		1.984	0.857	19.620	4.042	2.278	1.021	1.007	0.0118
S2-2	0.000132	1.749	0.811	10.080	2.404	1.283	1.026	1.009	0.0129
S2-3		2.064	0.869	15.340	3.026	1.736	1.020	1.007	0.0123
S2-4		2.371	0.890	18.940	3.245	1.900	1.017	1.006	0.0121
S2-5		2.630	0.873	19.570	3.073	1.765	1.018	1.006	0.0122
S2-6		1.152	0.620	4.710	1.915	0.781	1.040	1.013	0.0141
S2-9		0.903	0.512	3.260	1.848	0.622	1.060	1.024	0.0147
S2-10		1.785	0.819	16.640	3.873	2.087	1.024	1.008	0.0119
S2-10		1.936	0.849	16.640	3.524	1.968	1.021	1.007	0.0120
S3-1	0.000520	2.644	0.870	18.350	2.870	1.643	1.021	1.007	0.0124
S3-2		2.309	0.889	12.270	2.156	1.261	1.027	1.009	0.0130
S3-3		2.079	0.870	14.100	2.756	1.577	1.027	1.009	0.0125
S3-4		1.740	0.809	10.410	2.498	1.330	1.032	1.011	0.0128
S3-5		1.497	0.742	7.960	2.299	1.122	1.055	1.022	0.0132
S3-6		1.154	0.620	6.210	2.519	1.028	1.084	1.029	0.0134
S3-7		0.871	0.497	2.040	1.215	0.397	1.056	1.022	0.0163
S3-10		1.771	0.816	15.970	3.752	2.014	1.033	1.011	0.0120
D2A	0.001022	0.810	0.468	4.000	2.637	0.812	1.073	1.024	0.0140
D2B		0.817	0.471	4.000	2.605	0.807	1.037	1.016	0.0140
D3C		1.964	0.854	8.220	1.713	0.962	1.027	1.009	0.0135
D7A		1.989	0.858	23.380	4.803	2.711	1.024	1.008	0.0114
D7C		2.357	0.890	23.380	4.028	2.358	1.021	1.007	0.0116
D8B		2.166	0.880	25.620	4.800	2.779	1.024	1.008	0.0113

\* Pipe diameter = 2.926 ft.

Table 13. Cont. Velocity distribution factors

Designation	Slope	Depth* ft	Hydraulic Radius ft	Q cfs	Mean Velocity fps	Re = $\frac{VR}{\nu}$ $\times 10^5$	$\alpha$	$\beta$	Friction Factor f
X6MH2A	0.001001	1.442	0.725	13.450	4.075	1.944	1.019	1.005	0.0120
X7MH2A		2.210	0.884	26.340	4.835	2.812	1.018	1.006	0.0113
X7MH2B		2.139	0.878	26.340	5.000	2.888	1.017	1.005	0.0112
X8MH1A		2.110	0.874	23.930	4.609	2.650	1.025	1.009	0.0114
X8MH2X		2.079	0.871	24.240	4.744	2.718	1.027	1.009	0.0114
X8MH24		2.094	0.873	24.240	4.707	2.703	1.022	1.008	0.0114
X8MH3A		2.063	0.869	24.240	4.783	2.734	1.021	1.007	0.0114
X9MH1C		1.909	0.844	20.520	4.416	2.452	1.019	1.006	0.0115
X9MH2C		1.888	0.841	20.520	4.472	2.474	1.019	1.006	0.0115
X9MH3C		1.880	0.839	20.520	4.494	2.481	1.024	1.008	0.0115
X10M1A		1.617	0.777	16.130	4.231	2.163	1.028	1.010	0.0117
X10M2A		1.612	0.776	16.130	4.248	2.169	1.030	1.011	0.0117
X10M3A		1.611	0.775	16.130	4.251	2.167	1.030	1.011	0.0117
X10M2B		1.597	0.772	16.130	4.297	2.182	1.030	1.011	0.0117
X12M1A		1.090	0.843	8.260	3.618	2.006	1.035	1.007	
D3A	0.001022	1.057	0.580	8.220	3.754	1.432	1.031	1.010	0.0127
D3B		1.078	0.589	8.220	3.655	1.416	1.016	0.983	0.0127
D4C		1.903	0.843	12.920	2.790	1.666	1.019	1.006	0.0124
D5A		1.605	0.774	16.000	4.236	2.157	1.032	1.012	0.0118
D5B		1.601	0.772	16.000	4.249	2.159	1.037	1.014	0.0118
D5C		2.187	0.882	16.000	2.968	1.718	1.022	1.008	0.0122
D6A		1.855	0.834	20.510	4.562	2.503	1.025	1.009	0.0115
D6B		1.868	0.837	20.510	4.526	2.492	1.026	1.009	0.0115
D6C		2.198	0.883	20.510	3.785	2.199	1.023	1.008	0.0117

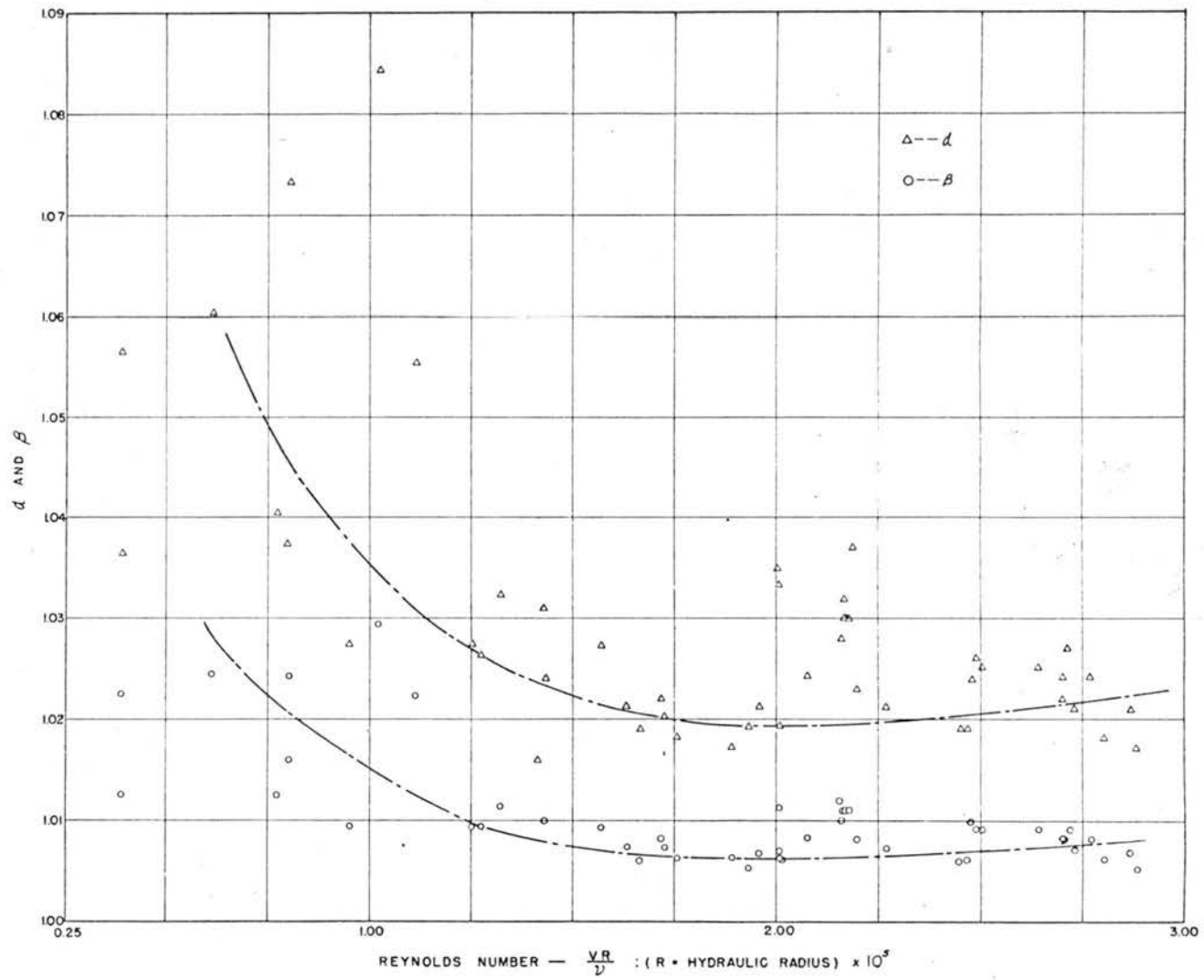
and alpha coefficients to the friction factor ( $f$ ). Since the range of the Darcy-Weisbach factor is small for this series of data, and because the Reynolds number fluctuates within a small range, the spread of results is apparently due to other causes.

Figure 26 displays the relationship of alpha and beta with Reynolds number. These results, generally indicate an increase of the velocity distribution coefficients with a decrease of Reynolds number. The apparent scatter around a functional relationship is due to observational and computational errors.

For the observed velocity distribution coefficients, the following parameters remained essentially constant; the circular form of the section, the fluid properties (water at approximately 45°F) and roughness factor because the Reynolds number varied over a narrow range. It would follow, therefore, that the variation in alpha and beta could be represented as a function of depth and mean velocity or slope, as a first approximation. As the effect of depth and mean velocity are incorporated through their product into the Reynolds number (assuming an approximate proportionality of depth and hydraulic radius), the main relationship should be between the velocity distribution coefficients and Reynolds number.

The effect of depth on the velocity distribution factors is presented in Table 14 and Figure 27. The values in Table 14 are grouped in ascending order of the



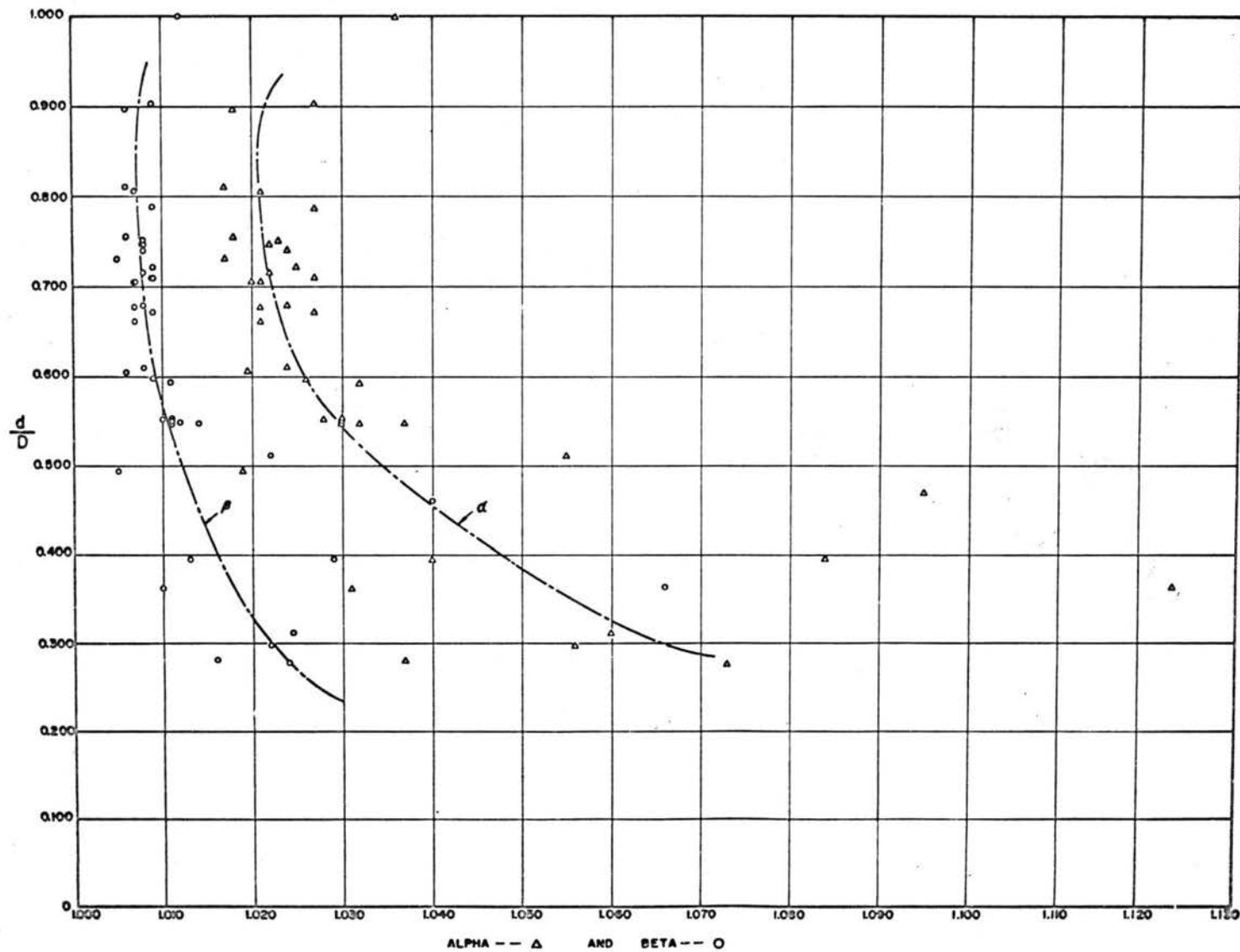


VELOCITY DISTRIBUTION COEFFICIENTS VERSUS REYNOLDS NUMBER

FIG. 26

Table 14. Velocity distribution factors as a function of depth

Range of Depth	Run No.	d/Dia.	Depth-d ft	Velocity fps	$\alpha$	$\beta$
0-1.0	D2A	0.276	0.810	2.637	1.073	1.024
	D2B	0.279	0.817	2.605	1.037	1.016
	S3-7	0.297	0.871	1.215	1.056	1.022
	S2-9	0.310	0.903	1.848	1.060	1.024
1.0-1.5	D3	0.360	1.057	3.754	1.031	1.010
	X12M2A	0.363	1.064	3.739	1.123	1.066
	S2-6	0.393	1.152	1.915	1.040	1.013
	S3-6	0.394	1.154	2.519	1.084	1.029
	X12M2B	0.468	1.372	2.668	1.095	1.040
	X6MH2A	0.492	1.442	4.075	1.019	1.005
	S3-5	0.510	1.497	2.299	1.055	1.022
1.5-1.8	S1-7	0.528	1.547	3.320	1.017	1.004
	X10M2B	0.545	1.597	4.297	1.030	1.011
	D5B	0.546	1.601	4.249	1.037	1.014
	D5A	0.547	1.605	4.236	1.032	1.012
	X10M3A	0.549	1.611	4.251	1.030	1.011
	X10M2A	0.550	1.612	4.248	1.030	1.011
	X10M1A	0.551	1.617	4.231	1.028	1.010
	S3-4	0.593	1.740	2.498	1.032	1.011
	S2-2	0.596	1.749	2.404	1.026	1.009
	S1-8	0.604	1.779	3.748	1.019	1.006
	S2-103	0.609	1.785	3.873	1.024	1.008
	1.8-2.1	D6A	.634	1.855	4.562	1.025
D6B		.638	1.868	4.526	1.026	1.009
X9MH3C		.642	1.880	4.494	1.024	1.008
X9MH2C		.645	1.888	4.472	1.019	1.006
D4C		.650	1.903	2.790	1.019	1.006
X9MH1C		.652	1.909	4.416	1.019	1.006
1.8-2.1	S2-10	0.660	1.936	3.524	1.021	1.007
	D3C	0.670	1.964	1.713	1.027	1.009
	S1-9	0.677	1.984	4.042	1.021	1.007
	D7A	0.678	1.989	4.803	1.024	1.008
	X8MH3A	0.704	2.063	4.783	1.021	1.007
	S2-3	0.704	2.064	3.026	1.020	1.007
	S3-3	0.709	2.079	2.756	1.027	1.009
	X8MH2X	0.709	2.079	4.744	1.027	1.009
	X8MH27	0.714	2.094	4.707	1.022	1.008
	2.1-2.5	X8MH1A	0.720	2.110	4.609	1.025
X7MH2B		0.729	2.139	5.000	1.017	1.005
D8B		0.739	2.166	4.800	1.024	1.008
D5C		0.746	2.187	2.968	1.022	1.008
D6C		0.750	1.198	3.785	1.023	1.008
X7MH2A		0.754	2.210	4.835	1.018	1.006
S3-2		0.787	2.309	2.156	1.027	1.009
D7C		0.804	2.357	4.028	1.021	1.007
S2-4		0.809	2.371	3.245	1.017	1.006
2.5-		S2-5	0.897	2.630	3.073	1.018
	S3-1	0.902	2.644	2.870	1.027	1.009
	S1-4	0.998	2.926	2.210	1.036	1.012



VELOCITY DISTRIBUTION COEFFICIENTS VERSUS DEPTH  
OF FLOW IN A CIRCULAR CROSS - SECTION

FIG. 27

depth-diameter ratio. The corresponding mean velocities which are also listed do not arrange themselves in any discernable manner. This is probably due to the fact that the mean velocity increases with the depth for a given slope and roughness, and the depth has already accounted for the effects of the mean velocity. Figure 27 indicates slightly increasing values of both beta and alpha for lowering depths. This would be expected as the deviation from the mean velocity becomes greater and the friction factor becomes effectively larger at the smaller depths.

At the half pipe diameter depth the beta factor has a value of approximately 1.01 and alpha value of approximately 1.03. At greater depths the beta factor reduces to approximately 1.007 and the alpha factor reduces to approximately 1.022. For depths less than half full, both factors appear to increase. Data was not available for depths less than one-fourth of a diameter; hence, the limit values cannot be estimated.

An attempt was made to identify any relationship between the mean velocity and the velocity distribution coefficients. It may be seen from Table 15 that for modest range of depth, the variation of mean velocity does not result in a consistent variation in beta or alpha.

Considering the limited range of Darcy-Weisbach factor, the mean velocity, the variation in beta and alpha can be identified primarily with Reynolds number and secondarily with depth of flow.

Table 15. Velocity distribution factors as a function of velocity

Run No.	Velocity fps	Depth ft	$\alpha$	$\beta$
S3-7	1.215	0.871	1.056	1.022
D3-C	1.713	1.964	1.027	1.009
S2-9	1.848	0.903	1.060	1.024
S2-6	1.915	1.152	1.040	1.013
S3-2	2.156	2.309	1.027	1.009
S1-4	2.210	2.926	1.036	1.012
S3-5	2.299	1.497	1.055	1.022
S2-2	2.404	1.749	1.026	1.009
S3-4	2.498	1.740	1.032	1.011
S3-6	2.519	1.154	1.084	1.029
D2B	2.605	0.817	1.037	1.016
D2A	2.637	0.810	1.073	1.024
X12M2B	2.668	1.372	1.095	1.040
S3-3	2.756	2.079	1.027	1.009
S3-1	2.870	2.644	1.027	1.009
D5C	2.968	2.187	1.022	1.008
S2-3	3.026	2.064	1.020	1.007
S2-5	3.073	2.630	1.018	1.006
S2-4	3.245	2.371	1.017	1.006
S1-7	3.320	1.547	1.017	1.004
S2-10	3.524	1.936	1.021	1.007
X12M2A	3.739	1.064	1.123	1.066
S1-8	3.748	1.779	1.019	1.006
S3-10	3.752	1.771	1.033	1.011
D6-C	3.785	2.198	1.023	1.008
S2-10	3.873	1.785	1.024	1.008
D7-C	4.028	2.357	1.021	1.007
S1-9	4.042	1.984	1.021	1.007
X6MH2A	4.075	1.442	1.019	1.005
X10M1A	4.237	1.617	1.028	1.010
D5A	4.236	1.605	1.032	1.012
X10M2A	4.248	1.612	1.030	1.011
D5B	4.249	1.601	1.037	1.014
X10M3A	4.251	1.611	1.030	1.011
X10M2B	4.279	1.597	1.030	1.011
X8MH1A	4.609	2.110	1.025	1.009
X8MH27	4.707	2.094	1.022	1.008
X8MH2X	4.744	2.079	1.027	1.009
X8MH3A	4.783	2.063	1.021	1.007
D8B	4.800	2.166	1.024	1.008
D7A	4.803	1.989	1.024	1.008
X7MH2A	4.835	2.210	1.018	1.006
X7MH2B	5.000	2.139	1.017	1.005

## 5. Conclusions

The results of this study are applicable to hydraulically smooth circular cross-sections flowing partially full with Reynolds number between  $0.4 \times 10^5$  and  $3.00 \times 10^5$ .

In the lower range of Reynolds numbers, the observed velocity distribution factors are greater and display greater dispersion. At the larger Reynolds numbers, the values trend toward invariance with less dispersion.

The relationship between alpha and beta has been demonstrated both theoretically and experimentally to be expressible as  $(\alpha-1)/(\beta-1) = 2.3$  to  $3.0$ . The value of  $3.0$  is representative of the experimental results.

A representative value of alpha for the experimental conditions is  $1.03$ . A representative value of beta would be  $1.01$  for the observed data.

## D. Boundary Conditions

### 1. Introduction

The solution of the unsteady flow equations require a definition of two boundary conditions. These boundary conditions are independent of the solution procedure and must be defined physically and mathematically.

In this study these two boundary conditions are (a) the inflow hydrograph and (b) a depth-time or depth-discharge relationship at either the upstream or downstream end of the reach. The location of this latter condition depends on whether the base flow is super- or sub-critical. The following discussion will relate to sub-critical flow in which case the latter boundary condition is downstream.

In the case of sub-critical flow with the resulting downstream boundary condition, the physical condition may best be expressed as a depth versus discharge relationship.

For a free outfall the depth was assumed as critical. Thus the initial water surface was that of a drawdown profile. The location of critical depth as normally computed does not occur at the end of the physical channel but some distance upstream. The section to follow describes the procedure used to evaluate this distance.

The second experimental condition imposed at the downstream end was that of a restricted opening. This insured that the depth of flow was always greater than normal. This resulted in an initial condition of a

backwater surface profile. The detailed discussion of this condition follows that for critical depth.

## 2. Free-outfall Condition

### a. General

The free-outfall at the downstream of a prismatic channel may be physically considered as that as condition for which the total energy of flow is a minimum for the discharge. Mathematically this condition may be expressed by;

$$\frac{Q^2 B}{gA^3} = 1 \quad (118)$$

in which;

- Q is the volume discharge rate
- B is the surface width
- A is the cross-sectional area
- g is the acceleration due to gravity.

This expression is based on two assumptions. The first is that the pressure distribution is hydrostatic. The second is that the kinetic energy may be expressed through the mean velocity.

The first assumption is violated in the vicinity of the free-outfall because of the significant curvature of the streamlines. Furthermore at the end, the pressure at the bottom must be atmospheric or zero relative. Thus, the potential portion of the total energy relative to the channel bottom is actually less than that assumed in the development of equation (118)



The second assumption depends on a uniform velocity distribution in the cross-section. The greater the velocity distribution differs from the uniform, for the same mean velocity, the larger will be the true kinetic energy as compared with the assumed. Based on the previous evaluation of the alpha velocity distribution factor, being close to one, it may be assumed that this assumption is reasonable.

b. Experimental observations and results.

The purpose of these experimental measurements was to determine the location of critical depth as computed from equation (118). This position then served as the location of the downstream boundary. Water-surface profiles were measured for a range of discharges from 2.10 to 16.62 cfs. The channel slope ranged from 0.000032 to 0.001022 feet per foot.

Table 16 presents the fourteen conditions of discharge and slope, and the corresponding ratio of end depth of the compute critical depth. Figure (28) presents the water-surface profiles for the same conditions along with the locations of the computed critical depth.

c. Conclusions

Within the range of observed end depths, the mean ratio of end-depth to critical depth was 0.750. The ratio tended to be smaller than the mean for the lower depths.

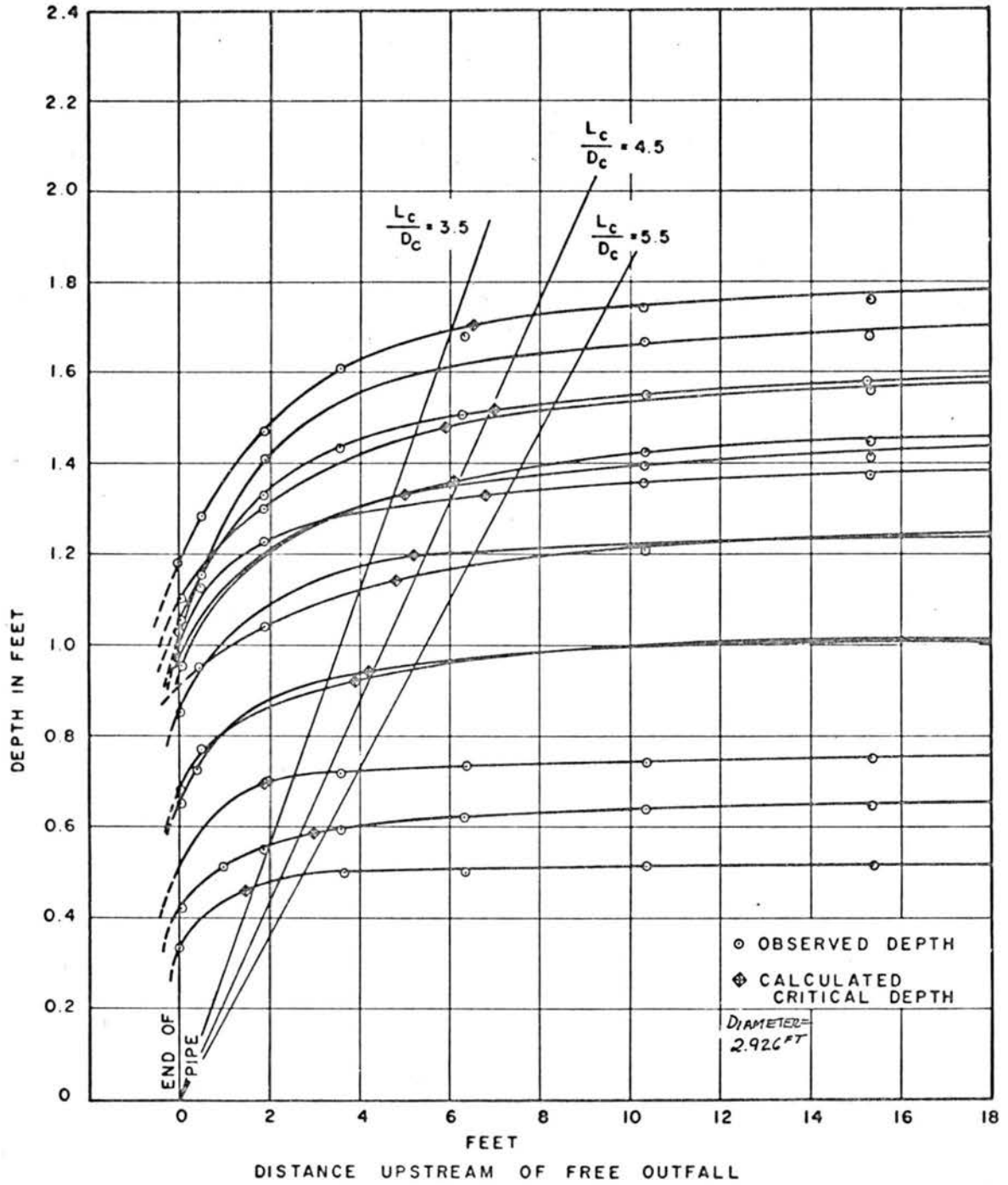
The location of computed critical depth from the channel end varied from less than 3.5 times critical depth to almost

Table 16. Free outfall data values

Diameter - 2.926 ft

Run No.	Slope	Discharge	$D_e/D_c$
D1A	.001022	2.10	0.731
S2-9	.000132	3.26	0.746
S1-5	.000032	4.14	0.758
D2A	.001022	4.58	0.749
S1-6	.000032	7.96	0.776
S3-9	.000520	7.98	0.764
D3A	.001022	8.26	0.751
S1-7	.000032	11.98	0.761
D4A	.001022	12.92	0.740
S3-10	.000520	15.97	0.739
D5A	.001022	16.02	0.752
S1-8	.000032	16.04	0.726
S2-10	.000132	16.64	0.753
S1-9	.000032	19.62	0.761

Mean - 0.750



LOCATION OF CRITICAL DEPTH AT A CIRCULAR CROSS - SECTION  
 FREE OUTFALL  
 FIG. 28

5.5 times critical depth. A location of 4.5 times critical depth was considered as typical and used in subsequent computations. This reduction in length of the integration length for the numerical solution of unsteady flow is probably insignificant and could safely be ignored in other applications.

### 3. Controlled Outfall Conditions

#### a. General

The mathematical simulation of the downstream boundary condition for controlled outflow required the calibration of an end restriction. Any geometric configuration was acceptable providing it satisfied the following criteria.

1. The discharge as a function of depth could be expressed simply such as  $Q = my^n$  in which "m" and "n" are constants and "y" is the depth of flow upstream of the restrictions.

2. The restriction was not so great as to cause the pipe to flow full under the maximum anticipated hydrograph discharge.

3. The approach-velocity distribution was symmetrical and did not differ appreciably from the undisturbed flow.

These criteria were satisfied by a restriction consisting of five 7-inch vertical wooden slats held in position by 2-1/2 inch wide vertical aluminum H-sections. The clear opening was 5 inches between supports. The discharge could thus be controlled by varying the vertical position or removal of one or more slats.

b. Results

Calibration of various combinations of openings was made by measuring the water surface elevation approximately 20 feet upstream of the control, and the corresponding discharge. For the range of discharges anticipated in the unsteady flow runs, it was concluded that the best combinations of openings was with the center three slats removed.

For this condition the relationship between discharge and depth was determined to be

$$Q = 4.84 y^{1.35}$$

This relationship applied for depths between approximately one-third and eight-tens of full diameter.

This gate configuration and relationship was used for all subsequent boundary condition evaluations in which backwater profiles were the initial condition. No attempt was made to modify this steady state relationship for unsteady flows.

## Chapter IX

## INITIAL CONDITIONS

A. General

The integration of the governing equations of unsteady flow (19) and (20) require initial values of velocity and depth at given locations in time and space. These values are independent of the ensuing solution and may be arbitrarily established. Realistically the conditions should be the result of a physical condition.

For the subject study the initial condition was that of nonuniform steady flow at the hydrograph base discharge. A mathematical expression for this condition is the ordinary differential equation,

$$\frac{dy}{dx} = \frac{S_o - S_f}{1 + \frac{d}{dx} \left( \frac{\alpha Q^2}{2gA} \right)} \quad (119)$$

in which;

- y is the depth at position x
- x is the distant along the channel
- $S_o$  is the bed slope
- $S_f$  is the friction slope
- $\alpha$  is the energy velocity distribution factor
- Q is the steady discharge
- A is the cross-sectional area
- g is the acceleration due to gravity.

The slope of the energy gradient  $S_f$  was evaluated by the Darcy-Weisbach equation. The friction factor evaluation was described earlier.

A comparison of computed versus observed water-surface profiles for non-uniform steady flow was made. These comparisons were made to test the validity of the theoretical and numerical determination of initial conditions.

#### B. Computational Procedure and Results

The determination of depth at specified positions along the pipe was accomplished by a Newton-Raphson iteration of equation (119) to a tolerance of 0.001 ft. of the depth. Given information included: (1) discharge  $Q$ ; (2) channel slope -  $S_o$ ; (3) friction factor -  $f$ ; (4) velocity distribution factor -  $\alpha$  (5) position along the pipe of points of observed depth -  $x$ ; and (6) observed or critical depth at the extreme downstream position.

The depth of flow was observed at the following eight positions with respect to the upstream end of the pipe: 20.00 ft., 197.92 ft., 406.07 ft., 509.64 ft., 613.20 ft., 707.71 ft., 772.71 ft., and 821.00 ft.

The boundary conditions for the steady non-uniform flow were established as follows:

(a) for the mild slope profiles at depths greater than normal depth (M-1 type curves) the observed depth at the 802.71 ft. station was used;

(b) for the mild slope profiles at depths between critical and normal depth (M-2 type curves) the computed

critical depth at a position of 4.5 times critical depth upstream of the pipe end (821.00 ft.) was used.

The root-mean-square (rms) deviation between the observed and computed depths was computed for three different value of alpha (1.00, 1.02 and 1.05), and three values of  $f$  (.011, .012 and .013). The values of alpha were selected based on,

- (1) the usually assumed value of 1.00 in lieu of better knowledge as to its true value;
- (2) the value of 1.02 as most representative of the values within the expected depth range; and
- (3) the value of 1.05 as being an extreme for the flow in a uniform channel.

The roughness values were selected based on the most reasonable constant value throughout the expected ranges of depth and velocity, and approximately 10 percent more and less. It is to be expected that these values would include an engineering estimate of the best value for this channel. The results of these computations are tabulated in Tables (17) and (18).

The invert of the physical pipe deviated from a mathematically uniform slope as indicated in Table (19). Since the actual depth of flow above this slightly irregular invert may not be expected to agree with the computed depth, an adjusted depth was computed at each position. The adjusted depth was based on the depth which would have occurred with the same total energy but with the invert



Table 17. RMS deviations for M-1 type backwater curves (normal depth &lt; initial depth)

Run No.	Q cfs	Normal Depth	Initial Depth	Alpha = 1.00			Alpha = 1.02			Alpha = 1.05			f	Slope
				Critical Depth	RMS Dev.		Critical Depth	RMS Dev.		Critical Depth	RMS Dev.			
					Actual	Adjusted		Actual	Adjusted		Actual	Adjusted		
S3-3	14.10	1.834	2.074	1.205	0.075	0.077	1.211	0.074	0.074	1.220	0.075	0.074	0.011	0.000520
S3-5	7.96	1.269	1.554	0.896	0.034	0.034	0.900	0.034	0.034	0.907	0.034	0.034	0.011	
S3-6	6.21	1.097	1.107	0.788	0.034	0.034	0.792	0.034	0.034	0.798	0.034	0.034	0.011	
S3-7	2.04	0.594	1.028	0.446	0.016	0.014	0.448	0.019	0.016	0.452	0.019	0.016	0.011	
S3-8	1.42	0.490	0.621	0.371	0.025	0.024	0.373	0.025	0.025	0.376	0.025	0.025	0.011	
S3-3	14.10	1.893	2.074	1.205	0.066	0.065	1.211	0.067	0.065	1.220	0.066	0.065	0.012	
S3-5	7.96	1.303	1.554	0.896	0.027	0.026	0.900	0.021	0.026	0.907	0.027	0.025	0.012	
S3-7	2.04	0.508	1.028	0.446	0.017	0.016	0.448	0.017	0.016	0.452	0.018	0.016	0.012	
S3-8	1.42	0.501	0.621	0.371	0.022	0.029	0.373	0.023	0.023	0.376	0.022	0.023	0.012	
S3-3	14.10	1.950	2.074	1.205	0.061	0.058	1.211	0.059	0.058	1.220	0.060	0.058	0.013	
S3-5	7.96	1.335	1.554	0.896	0.022	0.021	0.900	0.022	0.021	0.907	0.022	0.020	0.013	
S3-7	2.04	0.621	1.028	0.446	0.018	0.015	0.448	0.018	0.015	0.452	0.018	0.015	0.013	
S3-8	1.42	0.512	0.621	0.371	0.020	0.020	0.373	0.020	0.020	0.376	0.020	0.020	0.013	
X5A	13.20	1.415	1.441	1.164	0.027	0.040	1.170	0.029	0.040	1.179	0.029	0.040	0.011	0.001001
X5B	13.20	1.415	1.757	1.164	0.016	0.032	1.170	0.017	0.032	1.179	0.016	0.033	0.011	
X5C	13.20	1.415	2.379	1.164	0.021	0.020	1.170	0.021	0.020	1.179	0.021	0.020	0.011	
X9A	20.30	1.884	2.341	1.457	0.062	0.060	1.465	0.067	0.062	1.476	0.067	0.062	0.011	
X10B	16.00	1.599	1.990	1.287	0.042	0.039	1.293	0.041	0.039	-----	-----	-----	0.011	
X12A	8.20	1.066	1.697	0.909	0.022	0.024	0.914	0.023	0.024	-----	-----	-----	0.011	
X12B	8.20	1.066	1.104	0.909	0.014	0.012	0.914	0.014	0.035	-----	-----	-----	0.011	
X5B	13.20	1.415	1.757	1.164	0.023	0.020	1.170	0.022	0.020	1.179	0.022	0.020	0.012	
X5C	13.20	1.415	2.379	1.164	0.021	0.018	1.170	0.021	0.017	0.179	0.020	0.018	0.012	
X9A	20.30	1.945	2.341	1.457	0.023	0.020	1.465	0.077	0.064	1.476	0.071	0.073	0.012	
X10B	16.00	1.646	1.990	1.287	0.050	0.042	1.293	0.048	0.042	1.303	0.047	0.041	0.012	
X12A	8.20	1.093	1.697	0.909	0.019	0.017	0.914	0.019	0.018	0.921	0.019	0.018	0.012	
X12B	8.20	1.093	1.104	0.909	0.018	0.026	0.914	0.018	0.026	0.921	0.015	0.026	0.012	
X12C	8.20	1.093	1.109	0.909	0.015	0.028	0.914	0.015	0.028	-----	-----	-----	0.012	
X13A	4.68	0.798	0.833	0.681	0.018	0.030	-----	-----	-----	-----	-----	-----	0.012	
X13B	4.68	0.798	1.079	0.681	0.013	0.022	-----	-----	-----	-----	-----	-----	0.012	
X12C	8.20	1.093	1.109	-----	-----	-----	0.914	0.015	0.028	-----	-----	-----	0.012	
X12D	8.21	1.093	1.053	-----	-----	-----	0.915	0.044	0.040	-----	-----	-----	0.012	
X5B	13.20	1.491	1.757	1.164	0.033	0.026	1.170	0.035	0.026	1.179	0.032	0.026	0.013	
X5C	13.20	1.491	2.379	1.164	0.026	0.022	1.170	0.026	0.022	0.179	0.026	0.022	0.013	
X9A	20.30	2.006	2.341	1.457	0.044	0.045	1.465	0.046	0.045	1.476	0.091	0.080	0.013	
X10B	16.00	1.690	1.990	1.287	0.060	0.054	1.293	0.060	0.053	1.303	0.059	0.053	0.013	
X12A	8.20	1.119	1.697	0.909	0.0024	0.021	0.914	0.023	0.020	0.921	0.022	0.018	0.013	
D4C	12.92	1.388	2.225	1.151	0.026	0.026	1.157	0.027	0.027	1.166	0.028	0.028	0.011	
D5C	20.51	1.883	2.253	1.465	0.040	0.040	1.473	0.040	0.040	1.484	0.041	0.042	0.011	
D1C	2.10	0.516	1.417	0.453	0.020	0.023	-----	-----	-----	0.458	0.021	0.023	0.012	
D2C	4.58	0.724	2.293	0.674	0.011	0.010	-----	-----	-----	-----	-----	-----	0.012	
D4C	12.92	1.425	2.225	1.151	0.016	0.016	-----	-----	-----	1.166	0.017	0.017	0.012	
D5C	20.51	1.945	2.253	1.465	0.025	0.024	1.473	0.025	0.024	1.484	0.025	0.023	0.012	
D1C	2.10	0.527	1.417	0.453	0.019	0.022	0.455	0.020	0.022	-----	-----	-----	0.013	
D2C	4.58	0.801	2.293	0.674	0.011	0.010	0.677	0.011	0.012	0.682	0.011	0.010	0.013	
D4C	12.92	1.462	2.225	1.151	0.012	0.011	1.157	0.012	0.011	1.166	0.011	0.011	0.013	
D5C	20.51	2.006	2.253	1.465	0.027	0.026	1.473	0.027	0.026	1.484	0.027	0.025	0.013	
D1C	2.10	0.504	1.417	-----	-----	-----	0.455	0.021	0.024	-----	-----	-----	0.011	
D2C	4.58	0.766	2.293	-----	-----	-----	0.677	0.012	0.011	-----	-----	-----	0.011	



Table 19. Physical pipe invert deviations

Slope	Max. Deviation - ft.	Root-Mean-Square Deviation - ft.
.0000052	+.0188	.0116
.0000157	+.0182	.0135
.0000303	+.0214	.0099
.0001325	+.195	.0099
.0005197	+.0347	.0117
.0010101	+.0279	.0119
.0074578	-.0240	.0133
.0200690	+.0375	.0141

on the mean slope. The rms deviations for the adjusted depths are also tabulated in Tables (20) and (21).

### C. Discussion of Results of Comparison of Backwater

#### Calculations

The data tabulated in Tables (17) and (18) were analyzed in terms of the mean values of the rms deviations for each friction and alpha factor. The consolidated results are presented in Tables (20) and Table (21). These results do not indicate any strong tendency for a smaller rms deviation for the friction and alpha factors previously estimated for this pipe, i.e., 0.012 and 1.02. A representative rms deviation for the conditions observed is approximately 0.025 feet for both the M-1 and M-2 type surface profiles. There is a larger spread of deviations for changes in the roughness value than for changes in the velocity distribution factor  $\alpha$ .

### D. Conclusions

Based on the preceding results, it was concluded that a steady non-uniform water surface profile could be computed as the initial condition for the unsteady solution.

It was also concluded that the friction factor evaluation was more important than the velocity distribution coefficient. Subsequent computations utilized the variation of the friction factor with Reynolds number.

Table 20. Steady non uniform water surface profiles  
Median RMS values - feet

Velocity distribution factor $\alpha$	<u>Unadjusted Depth</u>			<u>Composite</u>
	<u>Friction factor f</u>			
	<u>.011</u>	<u>.012</u>	<u>.013</u>	
1.00	.026	.020	.023	.022
1.02	.024	.024	.023	.023
1.05	.024	.022	.024	.022
Composite	.026	.021	.023	
	<u>Adjusted Depth</u>			
1.00	.033	.023	.022	.024
1.02	.033	.026	.022	.026
1.05	.031	.023	.021	.023
Composite	.033	.024	.022	

Table 21. Median RMS values for M-2 type curves

Velocity distribution factor $\alpha$	<u>Unadjusted Depth</u>			<u>Composite</u>
	<u>Friction factor f</u>			
	<u>.011</u>	<u>.012</u>	<u>.013</u>	
1.00	.035	.026	.0305	.030
1.02	.034	.025	.0305	.031
1.05	.036	.026	.036	.032
Composite	.034	.027	.032	
	<u>Adjusted Depth</u>			
1.00	.037	.030	.034	.034
1.02	.040	.0255	.031	.034
1.05	.041	.0265	.037	.035
Composite	.039	.026	.034	

Since the velocity distribution coefficient variation did not produce significant differences, subsequent computations utilized an alpha value of one.